Universidad Pública de Navarra

Electrical and Electronic Engineering Department

OPTICAL FIBER SENSORS BASED ON NANOSTRUCTURED MATERIALS FOR ENVIRONMENTAL APPLICATIONS

PhD dissertation by

Adolfo Josué Rodríguez Rodríguez

Advisors:

Dr. Ignacio Raúl Matías Maestro

Dr. Carlos Ruiz Zamarreño

Dr. Daniel Alberto May-Arrioja

Dr. René Fernando Domínguez Cruz

Pamplona, September 2014

Universidad Pública de Navarra

Departamento de Ingeniería Eléctrica y Electrónica

SENSORES DE FIBRA ÓPTICA BASADOS EN MATERIALES NANOESTRUCTURADOS PARA LA DETECCIÓN DE PARÁMETROS MEDIOAMBIENTALES

Memoria de la tesis doctoral realizada por

Adolfo Josué Rodríguez Rodríguez

Directores:

Dr. Ignacio Raúl Matías Maestro

Dr. Carlos Ruíz Zamarreño

Dr. Daniel Alberto May-Arrioja

Dr. René Fernando Domínguez Cruz

Pamplona, Septiembre 2014

TESIS DOCTORAL: **“OPTICAL FIBER SENSORS BASED ON NANOSTRUCTURED MATERIALS FOR ENVIRONMENTAL APPLICATIONS”**

Autor: Adolfo Josué Rodríguez Rodríguez

Directores: Dr. Ignacio R. Matías Maestro
Dr. Carlos Ruiz Zamarreño
Dr. Daniel Alberto-May Arrioja
Dr. René Fernando Domínguez Cruz

Tribunal nombrado para evaluar la citada Tesis Doctoral:

Presidente: _____

Secretario: _____

Vocal: _____

Revisores externos:

_____

_____

Acuerda otorgar la calificación de:

_____

En Pamplona, a _____ de _____ de 20___

“Libre, y para mi sagrado, es el derecho de pensar…. La educación es fundamental para la felicidad social; es el principio en el que descansan la libertad y el engrandecimiento de los pueblos.”

Benito Juárez

RECONOCIMIENTOS

La realización de esta tesis ha sido posible gracias al apoyo recibido por parte del Consejo Nacional de Ciencia y Tecnología (CONACYT) bajo el contrato CB-2010/157866 y CB-2010/156529, así como de la Comisión Interministerial de Ciencia y Tecnología a través de la financiación de los proyectos CICYT fondos FEDER TEC2010-17805.

AGRADECIMIENTOS

Dedico y agradezco este trabajo de investigación:

A Dios principalmente por darme fortaleza, paciencia e iniciativa para elaborar correctamente cada paso de esta investigación y por poner en mi camino amigos y maestros que me brindaron conocimientos y consejos cuando más los necesite. Dedico este trabajo a mi madre Ana Rosa Rodríguez Salas, a mi hermano Wenceslao Eduardo Rodríguez Rodríguez, así como a mi abuelita María Serafina Salas Zapata (Q.E.P.D.) por apoyarme en todo momento, motivándome para realizar con éxito esta investigación.

A mis maestros que durante el transcurso de este Doctorado me instruyeron con sus conocimientos. A mis directores de tesis: los Drs. Ignacio Raúl Matías Maestro, Carlos Ruíz Zamarreño, Daniel Alberto May-Arrioja y René Fernando Domínguez Cruz, a quienes admiro y aprecio profundamente, por depositar en mi persona su paciencia, confianza e invaluables conocimientos, que gracias a estos, me fue posible la realización de este trabajo. Agradezco también a los Drs. Francisco Javier Arregui San Martín, Javier Goicoechea Fernández, Victor Iván Ruíz-Pérez por sus recomendaciones, sugerencias y comentarios que fueron de gran valor para mí al momento de realizar las pruebas necesarias para obtener resultados satisfactorios necesarios en este trabajo de investigación.

A la Universidad Autónoma de Tamaulipas (UAT), en particular la Unidad Académica Multidisciplinaria Reynosa Rodhe (UAMRR) por brindarme la oportunidad de realizar mi formación académica a nivel de Ingeniería y de Maestría, así como el honor de formar parte de su cuerpo docente.

A la Universidad Pública de Navarra (UPNA) por brindarme la oportunidad de realizar mis estudios Doctorales en el área de las Telecomunicaciones, por brindarme su confianza para el aprovechamiento del equipo y materiales en mi estancia de estudios en el laboratorio de Sensores ubicado en el edificio Los Tejos.

Agradezco también, a mis alumnos y amigos del equipo de investigación y desarrollo tecnológico “Diseño, Automatización y Programación (DAP)” por el empeño y dedicación para la realización de cada uno de sus estudios de tesis y seminario de investigación.

RESUMEN

La contaminación ambiental es la presencia de agentes físicos, químicos o biológicos presentes en el agua, suelo y aire; siendo perjudiciales para la salud de las personas, así como para la vida vegetal y animal. Las actividades económicas son esenciales para el desarrollo de la sociedad, sin embargo, muchas de estas actividades son una fuente de contaminación constante. Por ejemplo, la fuga de fluidos y gases en plantas industriales afectan negativamente a la salud e higiene para la elaboración de alimentos, bebidas, aditivos y materias primas causando un impacto ambiental y económico negativo en la industria. La búsqueda continua de métodos para el desarrollo de sistemas de medición es una característica de la evolución tecnológica de la humanidad. Las fibras ópticas presentan varias ventajas para ser empleadas en sistemas sensores; tales ventajas son: inmunidad a la interferencia electromagnética, dimensiones reducidas, ligeras, bajas pérdidas, fácil multiplexación y resistencias a la corrosión, entre otras. En general, podemos encontrar una amplia gama de aplicaciones en la industria para el desarrollo de sensores en fibra óptica. Sin embargo, en esta tesis se han seleccionado tres aplicaciones industriales de interés relevante: detección de gas amoniaco a bajas concentraciones, detección de adulteración en bebidas alcohólicas y detección de adulteración de combustibles. Se caracterizan los parámetros de los sensores desarrollados tales como la sensitividad, reversibilidad, reproducibilidad y precisión para la medición de cada tipo de sensor. Los resultados obtenidos en esta tesis serán útiles en el estudio de nuevos materiales aplicables a sensores ópticos, permitiendo la apertura a nuevas vías de investigación en el campo de los sensores en fibra óptica para aplicaciones industriales.

ABSTRACT

Environmental pollution is the presence of physical, chemical or biological agents in water, soil and air which are harmful to our health, safety and welfare of the people as well as plant and animal life. Economic activities are essential to the development of society; however, many of these activities are a constant source of contamination. For example, leakage of fluids and gases in industrial plants adversely affect the health and hygiene for food processing, beverages, additives and raw materials causing serious environmental and economic impact on the general industry. The continual search for methods for developing measurement systems is a feature in the technological evolution of humankind. Optical fibers exhibit several advantages such as being immune to electromagnetic interferences, reduced dimensions, lightweight, low losses, easy multiplexation and resistant to corrosion for the development of optical fibers sensors. However, we selected three applications were the principle of operation of our sensor provides an advantage over other reported sensors: gaseous ammonia detection for low concentrations, adulteration of alcoholic beverages detection and combustibles quality control. The overall objective of this research is to design, fabricate, deploy and verify the correct operation of optical fiber structures for the identification of interesting liquid and gaseous environmental pollutants. The sensors parameters such as its sensitivity, reversibility, reproducibility and accuracy of measurement for each type of sensor are also characterized. These results obtained from this thesis would be a useful work in the study of new materials applicable to optical sensors, while opening new avenues of research in the field of optical fiber sensors for industrial applications.

CONTENTS

CHAPTER I. INTRODUCTION 3

1.1. General Introduction 3

1.2. Background 4

1.3. Objectives of the thesis 9

1.4. Organization of the thesis 10

REFERENCES 13

CHAPTER II. FUNDAMENTALS OF SENSORS 18

Abstract 18

2.1. Introduction 18

2.2. Optical fibers 19

2.3. Types of optical fibers 22

2.4. Optical fiber sensors 23

2.5. Optical fiber sensors based on the measurement of the evanescent field. 27

2.6. Optical fiber sensors based on the multimodal interference (MMI) effects. 30

REFERENCES 38

CHAPTER III. OPTICAL FIBER SENSORS FOR THE DETECTION OF AMMONIA GAS 43

Abstract 43

3.1. Introduction 44

3.2. Principle of operation 44

3.3. Experimental procedure 49

3.4. Experimental results 53

3.5. Conclusions 66

REFERENCES 69

CHAPTER IV. FIBER OPTIC SENSOR APPLIED IN ETHANOL INDUSTRY 74

Abstract 74

4.1. Introduction ... 75

4.2. Principle of operation ... 78

4.3. Rum adulteration detection using an optical fiber sensor based on multimodal interference effect (MMI) ... 79

4.4. Gasohol quality control for real time applications by means of multimode interference (MMI) fiber sensor. ... 89

4.5. Conclusions ... 97

REFERENCES ... 99

CHAPTER V. SENSITIVITY OPTIMIZATION OF MULTIMODAL INTERFEROMETERS (MMI) BY MEANS OF THIN INDIUM TIN OXIDE (ITO) COATINGS ... 103

Abstract ... 103

5.1. Introduction ... 103

5.2. Principle of operation ... 106

5.3. Experimental procedure ... 107

5.4. Results and discussion ... 110

5.5. Conclusions. ... 115

REFERENCES ... 116

CHAPTER VI. CONCLUDING REMARKS. ... 122

ANNEXES ... 125

ANNEX A. Publications from research ... 126

ANNEX B. Images taken during the manufacturing of the optical fiber sensor based on multimode interference (mmi) effects. ... 127

ANNEX C. Images taken during the manufacturing of the optical fiber sensor based on coatings by sputtering. ... 128

ANNEX D. Images taken during lectures about optical fibers sensors in industry. ... 129

CHAPTER I. INTRODUCTION

1.1. GENERAL INTRODUCTION

The continual search for methods for developing measurement systems is a feature in the technological evolution of humankind. Over the years different approaches have been implemented such as mechanical transducer mechanisms, the implementation of electric-electronic components and quite recently using optical devices.

In the past four decades optical fibers have been an important factor in the development of optical communication systems, as well as in the development of measurements systems. This is due to the fact that optical fibers exhibit several advantages such as being immune to electromagnetic interferences, reduced dimensions, lightweight, low losses, easy multiplexation and resistant to corrosion and temperature changes [1-3]. Therefore, optical fiber sensors have been used to monitor a wide range of parameters such as pH, humidity, concentrations of gases, volatile organic compounds, voltage, temperature, pressure, humidity, vibration, specialty chemicals, acoustic emission and fracture [4-12]. For these reasons, it is necessary to continue the development of sensing technologies that incorporate optical fibers using low cost materials, efficient transduction mechanisms, simple interrogation and reading mechanisms, a straightforward fabrication process, and adaptability to different environmental areas. They should also meet satisfactorily the main parameters that define the quality of an optical sensor: high sensitivity, selectivity, reversibility, fast response time, long lifetime and reproducibility [12].

1.2. BACKGROUND

Environmental pollution is the presence of physical, chemical or biological agents in water, soil and air which are harmful to our health, safety and welfare of the people as well as plant and animal life. These agents may be solid, liquid, gaseous or a mixture of them. The presence of these agents comes from natural sources (volcanoes, forest fires, windstorms, living and decaying plants, etc.) or anthropogenic sources that make the activities of daily life [13, 14]. Economic activities are essential to the development of society; however, many of these activities are a constant source of contamination. For example, leakage of fluids and gases in industrial plants adversely affect the health and hygiene for food processing, beverages, additives and raw materials causing serious environmental and economic impact on the general industry [15, 16].

In general, we can find a wide range of applications for the development of optical fiber sensors. However, we selected three applications were the principle of operation of our sensor provides an advantage over other reported sensors.

***Gaseous Ammonia detection*:** One of the toxic gases commonly present in the industry is ammonia, which is a natural gas employed in the automotive and chemical industry and medical analysis [16]. Due to its potential hazard to human beings, even at small concentrations, real time environmental monitoring of ammonia is a critical issue in closed environments. Ammonia has a strong smell that can be perceived at concentrations close to 50 ppm and which induces irritation in the upper respiratory tract and chronic cough [17]. On the other hand, prolonged exposure to ammonia concentrations below 25 ppm has no significant influence on pulmonary functions [18]. In fact, the American Conference of Industrial Hygienists (ACGIH) has set a limit to the ammonia concentration in air of 25 ppm in the workplace during a daily working period of 8 hours, and a

concentration of only 35 ppm for a short-term exposure time of 15 min [19, 20]. Prolonged exposure between 25 ppm to 100 ppm influence the generation of asthma and bronchitis, chronic eye irritation and may cause dermatitis [17]. Concentrations above 100 ppm can produce eye burning, tearing, swollen eyelids, corneal abrasion, blurred vision and even permanent blindness [17-20]. Therefore, the design of novel techniques and sensors that allow the accurate detection of low ammonia concentrations with real time monitoring is quite important [16]. Among the different approaches to detect ammonia it is possible to find those based on the use of Nessler's reagent [21], photoionization detectors [22], semiconductor thin films [23], potentiometric electrodes [24], commercial infrared gas analyzers [25] and sensors based on absorption FET (ASPFET) [26]. Although these sensors can detect gaseous ammonia, they exhibit some disadvantages. For instance, Nessler's reagent is a chemical reagent used to detect small amounts of ammonia. However, this reagent is toxic when inhaled, swallowed or absorbed through the skin, and is also a carcinogenic substance. Sensors based on semiconductor thin films exhibit a low selective drift for a particular gas, low reproducibility, weak stability, poor sensitivity and a short sensor active life time. Photoionization detectors exhibit high sensitivity and fast response time, but they need to be calibrated very often to provide accurate measurements. Sensors based on a potentiometric electrodes have the advantage of being sensitive and selective, but they have significant limitations such as relative high power consumption, expensive and requiring the presence of an experienced operator. Regarding sensors operating on APSFET they are susceptible to electromagnetic interferences. In the case of commercial infrared gas analyzers they are usually expensive and bulky. Due to the high toxicity of this gas in industry there is a constant need to develop sensors that provide reliable measurements and can also be used in harsh environments.

Adulteration of Alcoholic Beverages: Food technology is the science that deals with study and ensures microbiological, physical and chemical quality of foodstuffs in all parts of the manufacturing process, responsible for the development of new products through the application of new technologies and the use of traditional and non-traditional raw materials, depending on the characteristics of the country and its population.

Throughout history, traditional alcoholic beverages of each country or region have been produced since many of them are representative of the country of origin. A standard practice in most countries, which is required by law, is to specify how much alcohol (ethanol) is contained in the alcoholic beverage. This is typically done by displaying on the bottle label the percentage of alcohol by volume. Based on the type of beverage this percentage can range from 7% up to more than 50%. The key objective of such regulations is to maintain the quality of the beverage, but mainly to prevent harm to human beings due to alcohol intoxication. In the last decade, the adulteration of alcoholic beverages has been a common malpractice in order to increase the revenues of businesses dealing with their commercialization. Adulterated alcoholic beverages are legal alcoholic products that have been illicitly tampered with, for instance, by criminally diluting them with water, purposely putting them into new containers to conceal their true origin or adding toxic substances to manipulate the quality of alcoholic beverages. Regardless of the quality degradation, the main issue is related to poisoning or death due to such malpractice. Ethanol (EtOH) has been widely used to manipulate alcoholic beverages and although the mortality associated with acute ethanol intoxication is rare, it can be an important factor when combined with other drugs. It is also directly responsible for more than half of traffic accidents. Meanwhile, ethylene glycol (EG) is used in the adulteration of alcoholic beverages as a solvent and antifreeze, and the toxicity is due to the accumulation of metabolites [27, 28]. Among the variety of commercial alcoholic beverages, rum is the most consumed

worldwide [29], which makes it an easy target for adulteration. In Mexico, for instance, six out of ten bottles are either adulterated or counterfeited with ethanol and EG. As a result, instruments that can accurately detect contaminants in alcoholic beverages are highly desirable. Electronic methods have been previously proposed to recognize and detect impurities in alcoholic beverages [30-32]. Although these electronic sensors have efficient results for the measurement of liquid impurities, they may be sensitive to electromagnetic interference, expensive, and unsuitable for remote operation. On the other hand, optical technologies are well suited for this task. Raman spectrometry [33], Fourier Transform (FT) near infrared and Raman spectrometry [34], NIR Raman analysis [35], and gas-chromatography methods [36] have been also used to detect the presence of methanol and ethanol dissolved in alcoholic beverages. For instance similar methods have been applied to detect adulteration in tequilas [37, 38]. The main issue with such techniques is that the equipment in very expensive. Other technique based on surface plasmon resonance (SPR) [39] has been also reported. However, the system tends to be bulky and susceptible to external disturbances that can misalign the system.

Gasohol Quality Control: In the last two decades there has been a growing interest to develop renewable fuels that could replace or reduce the use of gasoline. As a consequence of the growing demand of petroleum and green combustibles, some alternatives have been proposed as renewable fuel sources. In this sense, methanol and ethanol are also used as fuel, especially when mixed with gasoline. Methanol emerges as an alternative fuel due to the toxicity of the emissions from gasoline and the destruction of the ozone layer. In addition, the calorific value of gasoline is approximately twice the calorific value of methanol, thus making it more rentable. Some advantages of methanol as diesel combustible to vehicles are: it can be produced from renewable sources and grass waste, bagasse sugar or litter among others; generates less environmental pollution than

fossil fuels and ordinary vehicles can use this combustible by only replacing the plastic parts of the fuel system [40, 41]. However, methanol has received less attention than ethanol because it is highly toxic, extremely volatile and therefore would increase the risk of fire or explosion [42]. Ethanol has become a very popular choice as fuel (E100) in markets such as Brazil, USA, Sweden, Thailand and others, with the advantage that combustion is less polluting and highly oxygenated. This combustible comes from sugar cane and corn, as well as cellulosic biomass, trees and grasses. It should be noted that the maximum permissible exposure in United States of America in air (40 h/ week) is 1,900 mg/m^3 for ethanol, 900 mg/m^3 for gasoline and 260 mg/m^3 for methanol. Ethanol is also employed as additive in gasoline to replace the Methyl Tert-Butyl Ether (MTBE), responsible for significant contamination of soil and groundwater. The resulting fuel mixture of ethanol and gasoline is called gasohol [43, 44]. Two common blends are E10 and E85, with ethanol content of 10% and 85%, respectively. Since alcohol has corrosive properties, special adaptations to conventional engine vehicles that employ ordinary gasoline are required; otherwise the engine is at risk of degradation in some component materials as well in the fuel system [45]. Therefore, the design of novel techniques and sensors that allow the accurate detection and identification of combustible with real time monitoring is quite important. Among the different approaches to detect combustible and hydrocarbons it is possible to find those based on the use of chemiresistors [46], piezoresonance sensors systems [47], photoacoustic sensor system [48], electronic fuel analyzers [49] and infrared fuel concentration analyzers [50, 51]. Although these electronic sensors have efficient results for the measurement of liquid combustibles, oils and hydrocarbons, they may be sensitive to electromagnetic interference, exhibit a low selective drift for a particular hydrocarbon, relative high power consumption, some are expensive and requiring the presence of an experienced operator, they are usually bulky and unsuitable for remote operation.

A common feature during the adulteration of alcoholic beverages and the preparation of gasohol mixtures is that the refractive index of the original liquid is modified when is mixed with other liquid. Therefore, refractive index optical fiber sensor can be used to monitor when a liquid has been contaminated.

1.3. OBJECTIVES OF THE THESIS

The overall objective of this research is to design, fabricate, deploy and verify the correct operation of optical fiber structures for the identification of interesting liquid and gaseous environmental pollutants. The sensors parameters such as its sensitivity, reversibility, reproducibility and accuracy of measurement for each type of sensor are also characterized. To carry out this, the following specific objectives are proposed:

- Theoretical study of the measurement process with optical fiber sensors and classification according to the measurement environment.

- Design, fabrication and characterization of an intrinsic optical fiber sensor incorporating coatings with sensitive materials for the detection of gaseous ammonia. Ammonia is detected via interaction of the evanescent optical field with the sensitive coating.

- Design, fabrication and testing of an intrinsic optical fiber sensor based on Multimode Interference (MMI) effects in optical fibers. The sensor allows us to measure refractive index of a liquid, which is used to determine the ethanol concentration of a binary mixture. The sensor is applied to determine the quality of alcoholic beverages and combustibles (gasohol).

- Identification and selection of a suitable material for the manufacture of a sensitive coating. The coating is applied on the surface of the MMI device in order to enhance the sensitivity of the MMI sensor.

The results obtained from this thesis would be a useful work in the study of new materials applicable to optical sensors, while opening new avenues of research in the field of optical fiber sensors for industrial applications.

1.4. ORGANIZATION OF THE THESIS

The content of this thesis is divided into six chapters briefly described below:

Chapter I is a general introduction to the subject of the research that will be developed. We briefly describe the importance of efficient sensor devices for monitoring environmental parameters for industrial applications. An overview of sensors developed using traditional technologies is also described, which provides a good starting point for the development of this thesis. At the end of the work we develop new optical fiber sensors that form the basis for future developments. The main objectives of this work are also presented.

In Chapter 2 we provide an overview of optical fiber sensors including a review of the theoretical foundations of single-mode fiber (SMF) and multi-mode fiber (MMF). We also explain the concept of evanescent field in MMF and the formation of self-images observed in MMI fiber devices. A brief introduction to the study of optical fiber sensors is also included, which demonstrates the advantages with respect to traditional sensor systems, their classification and their main applications today.

In Chapter 3, an optical fiber ammonia sensor employing a universal pH indicator is proposed and demonstrated. The key concept for employing this optical

fiber sensor is to take advantage of the basicity of ammonia. Therefore, by employing a BCG pH indicator and a pH universal indicator, which undergoes a suitable colour change when exposed to ammonium ions, ammonia can be measured by tracking absorption changes. The advantage of these pH indicators is that they exhibit sensitivity to ammonia over a broad wavelength range. In addition, these indicators are embedded in a hydrophobic and gas permeable polyurethane film named Tecoflex®. This film provides additional advantages to the sensor, such as operation in dry environments, efficient transport of the element to be measured to the sensitive area of the sensor, and prevent leakage or detachment of the indicator.

In Chapter 4, the fabrication of an optical fiber sensor based on MMI effects is presented and demonstrated for Ethanol identification and employed to the quality control of rum and combustibles. The operation of the sensor relies on the fact that when the sample is adulterated, the refractive index (RI) of the adulterated sample will be different as compared to the original sample. Therefore, considering that the MMI sensor exhibits a sensitivity of 258.06 nm/RIU for liquids with RI ranging from 1.318 to 1.4203, we can accurately determine if a sample of rum or combustible is free of contaminants or adulterated with other liquid. Although the sensor cannot determine which kind of liquid is altering the pure sample, it can easily detect when the original sample has been adulterated, even with small amounts of liquid. The sensor also provides high repeatability and reversibility while using a fast and simple fabrication process.

In Chapter 5, the sensitivity optimization of MMI refractometers is studied as a function of the Indium Tin Oxide coatings thickness. Recently, MMI structures in optical fibers have been used to develop novel refractometers. In addition, high RI films coatings have been used as a way to enhance the sensitivity of fibers sensors that operate via evanescent field. Therefore, the utilization of ITO coatings in MMI

allows us to control the sensitivity by adjusting the ITO coating thickness. More specifically, the sensitivity of these devices has been raised from 188.7 nm/Refractive Index Unit (RIU) for an uncoated MMI sensor to 308.211 nm/RIU and 559.81 nm/RIU for devices with ITO coating thicknesses of approximately 18 nm and 36 nm respectively.

Chapter 6 provides some final concluding remarks of the results, recommendations and future research directions.

REFERENCES

1. B. Lee, “Review of the present status of optical fiber sensors”, Opt Fiber Technol, vol.9, pp. 57-59, 2003.
2. M.D. Marazuela, M.C. Moreno-Bondi, “Fiber-optic biosensors-an overview”, Anal. Bioanal, Chem., vol. 372, pp. 664-682, 2002.
3. P.E.Tippens, Física.Conceptos y aplicaciones. Ed. McGraw Hill, séptima edición, USA, 2007.
4. I.R. Matias, F.J. Arregui, R.O. Claus, Optical Fiber Sensors, Encyclopedia of SENSORS, vol. X, pp.1-19, 2006.
5. G.F. Fernando, D.J. Webb, P. Ferdinand, Optical-Fiber Sensors, MRS BULLETIN, 2012.
6. Y.Shizhuo, P.B. Ruffin, F.T.S. Yu, Fiber optic sensors Second edition, Taylor & Francis Group, USA, 2008.
7. J. Dakin and B. Culshaw, Optical Fiber Sensors: Principals and Components, Vol. 1, Artech, Boston, Mass, USA, 1988.
8. B. Culshaw and J. Dakin, Optical Fiber Sensors: Systems and Applications, Vol.2, Artech, Norwood, Mass, USA, 1989.
9. A. Krohn, Fiber Optic Sensors: Fundamental and Applications, Instrument Society of America, Research Triangle Park, NC, USA, 1988.
10. B. Culshaw, Optical Fibre Sensing and Signal Processing, P. Pergrnus, London, UK, 1984.
11. G.D. Pitt, P. Extance, R.C. Near et al., “Optical-fibre sensors”, IEEE Technical Review, vol.3, no.8, pp. 379-417, 1986.
12. C. Pérez Conde, Sensores ópticos, Servei de Publicacions Universitat de València, 1996.
13. Bonet, Sanchez Antonio, Gran enciclopedia educativa. Ediciones Zamora Ltda. México, Panamá, Colombia, España, 1991.

14. E. Enkerlin, R. Garza, G. Cano, E. Vogel, Ciencia Ambiental y Desarrollo Sostenible, Internacional Thomson Editores, México, 1997.
15. D. Elsom, La contaminación atmosférica, Ediciones Cátedra SA, 1990.
16. Timmer, B., Olthuis, W., van den Berg, A. Ammonia sensors and their applications–A review. Sen. Actuators B Chem., vol. 107, pp. 666–677, 2005.
17. Ammonia (NH3) CAS 7664–7; UN 2672 (Between 12% and 44% solution), UN 2073 (>44% solution), UN 1005 (anhydrous gas or >50% solution). Available online: http://www.atsdr.cdc.gov/ MHMI/mmg126.pdf (accessed on 20 October 2013).
18. Toxicological Profile for Ammonia. Available online: http://www.atsdr.cdc.gov/toxprofiles/ tp126.pdf (accessed on 20 October 2013).
19. Public Health Statement. Ammonia. Available online: http://www.atsdr.cdc.gov/ToxProfiles/ tp126-c1-b.pdf (accessed on 20 October 2013).
20. International Programme on Chemical Safety. Environmental Health Criteria 54. Ammonia. Available online: http://www.inchem.org/documents/ehc/ehc/ehc54.htm (accessed on 20 October 2013).
21. F.C. Koch, T.L. McMeekin, “A new Nesslerization micro-Kjeldahl method and a modification of the Nessler–Folin reagent for ammonia”, J. Am. Chem. Soc. vol. 46, pp. 2066–2069, 1924.
22. J.N. Davenport, E.R. Adlard, “Photoionization detectors for gas chromatography”, J. Chromatogr, vol. 290, pp. 13–32, 1984.
23. A.K. Prasad, P.I. Gouma, D.J. Kubinski, J.H. Visser, R.E. Soltis, P.J. Schmitz, “Reactively sputtered MoO3 films for ammonia sensing”, Thin Solid Films, vol. 436, pp. 46–51, 2003.

24. M.E. Meyerhoff, “Polymer membrane electrode based potentiometric ammonia gas sensor”, Anal. Chem., vol. *52*, pp. 1532–1534, 1980.
25. S. Christie, E. Scorsone, K. Persaud, F. Kvasnik, “Remote detection of gaseous ammonia using the near infrared transmission properties of polyaniline”, Sens. Actuators B Chem., vol.90, pp. 163–169, 2003.
26. G. Barillaro, A. Nannini, F. Pieri, “APSFET: A new, porous silicon-based gas sensing device”, Sens. Actuators B Chem., vol. *93*, pp. 263–270, 2003.
27. J. Roldan, C. Frauca, A. Duenas, “Intoxicación por alcoholes”, Anales Sis. San Navarra, vol. 26, pp.129-139, 2003.
28. J. Brent, “Current management of ethylene glycol poisoning”, Drugs, vol. 61, pp. 979-988, 2001.
29. A. Smith, “Spice keeps rum moving in Europe”, The International Wine & Spirit Research Magazine, pp.10-12, 2012.
30. R. C. Young, W. J. Buttner, B. R. Linnell, R. Ramesham, “Electronic nose for space program applications”, Sens. Actuators B Chem., vol. 93, pp. 7–16, 2003.
31. A. Branca, P. Simonian, M. Ferrante, E. Novas, R. Martin Negric, “Electronic nose based discrimination of a perfumery compound in a fragrance”, Sens. Actuators B Chem., Vol. 92, pp. 222–227, 2003.
32. S. Ampuero, J. O. Bosset, “The electronic nose applied to dairy products: A review”, Sens. Actuators B Chem., vol. 94, pp. 1–12, 2003.
33. N. Duyen, E. Wu, “Determination of Low Concentration Methanol in Alcohol by Affordable High Sensitivity Raman Instrument”, Spectroscopy, vol. 25, p. 15, 2010.
34. L. S. Mendes, F. C. C. Oliveira, P. A. Z. Suarez, J. C. Rubim, “Determination of ethanol in fuel ethanol and beverages by Fourier transform (FT)-near infrared and FT-Raman spectrometries”, Anal. Chim. Acta, vol. 493, pp. 219–231, 2003.

35. R. Y. Sato-Berrú, J. Medina-Valtierra, C. Medina-Gutiérrez, C. Frausto-Reyes, “Quantitative NIR Ramananalysis in liquid mixtures”, Spectrochim. Acta A, vol. 60, pp. 2225–2229, 2004.
36. I. Heberle, A. Liebminger, U. Weimar, W. Gopel, “Optimised sensor arrays with chromatographic preseparation: Characterisation of alcoholic beverages”, Sens. Actuators B Chem., vol. 68, pp. 53–57, 2004.
37. O. Barbosa-García, G. Ramos-Ortíz, J. L. Maldonado, J. L. Pichardo-Molina, M. A. Meneses-Nava, J. E. A. Landgrave, J. Cervantes-Martínez, “UV–VIS absorptionspectroscopy and multivariateanalysis as a method to discriminate tequila”, Spectrochim. Acta A,vol. 66, pp.129–134, 2007.
38. U. Contreras, O. Barbosa-García, J. L. Pichardo-Molina, G. Ramos-Ortíz, J. L. Maldonado, M. A. Meneses-Nava, N. E. Ornelas-Soto, P. L. López-de-Alba, “Screeningmethodforidentification of adulterate and fake tequilas byusing UV-VIS spectroscopy and chemometrics”, Food Res. Int. vol.43, pp. 2356–2362, 2010.
39. G. Martínez-López, D. Luna-Moreno, D. Monzón-Hernández, R. Valdivia-Hernández, “Opticalmethod to differentiate tequilas basedon angular modulationsurfaceplasmonresonance”, Opt. Lasers Eng., vol. 49, pp. 675–679, 2011.
40. T.B. Reed, R.M. Lerner, Methanol: A Versatile Fuel for Immediate Use. Science, vol. 182, 1973.
41. G. Olah, A. Goeppert, G.K. Surya Prakas, Beyond Oil and Gas: The Metanol Economy, Willey VchVerlagGmbh, second edition, 2009.
42. Frequently Asked Questions about Methanol. Available online: http://www.methanex.com/products/faqs.html (Accessed on 25 May 2014).
43. Fuel Economy and Emissions of the Ethanol Optimized Saab 9-5 Biopower. Available online:https://www1.eere.energy.gov/bioenergy/pdfs/analysis_saab2007.pdf (Accessed on 25 May 2014).

44. The Brazilian biofuels industry. Available online:http://www.biotechnologyforbiofuels.com/content/1/1/6 (Accessed 25 May 2014).
45. Ethanol fuel and cars. Available online: http://interestingenergyfacts.blogspot.mx/2008/09/ethanol-fuel-and-cars.html. (Accessed on 25 May 2014).
46. K. Clifford, H. Hughes, R.C. Hughes, In Situ Chemiresistor Sensor Package For Real Time Detection of Volatile Organic Compounds in Soil and Groundwater, *Sensors,* vol.2, pp. 23-24, 2002.
47. A.V. Kalach, V.F. Selemenev, A piezoresonance sensor system for rapid evaluation of the quality of gasolines. Chem Tech Fuels Oil+, vol. 43, pp.60-61, 2007.
48. S.S. Freborn, J. Hannigan, F. Greig et al, A pulsed Photoacustic Instrument for the Detection of Crude Oil Concentrations in Produced Water. American Institute of Physics, Review of Scientific Instruments, vol. 69, pp. 3948-3952, 1998.
49. Testing Kits-PetroFLAG-Analizador cuantificación de hidrocarburos en el suelo. Available online: http://www.ambicare.com/es/productos/testes-rapidos/petroflag-analizador-cuantificacion-de-hidrocarburos-en-el-suelo (Accessed 26 May 2014).
50. Control Instruments Corporation. Infrared Analyzers. Available online: http://www.controlinstruments.com/technologies/infrared-analyzers(Accessed 27 May 2014).
51. Zeltex® ZX-440-XL Near Infrared Gasoline/Diesel Fuel Analyzer. Available online:http://www.zeltex.com/desktop/zx-440xl.pdf(Accessed 27 May 2014).

CHAPTER II. FUNDAMENTALS OF SENSORS

ABSTRACT

In this chapter we provide an overview of optical fiber sensors. The theoretical foundations of single-mode fibers (SMF) and multi-mode fibers (MMF) are described, as well as a theoretical description of the evancescent field in MMF. The basic concepts behind the self-image formation in multimode interference devices (MMI) are also covered. A brief introduction to the study of optical fiber sensors is also provided, their classification and their main applications as well as their advantages with respect to traditional sensor systems.

2.1. INTRODUCTION

In industry it is common to use electrochemical sensors to detect and measure chemical and biological variables for diverse applications such as environmental monitoring, detection of pollutants, biomedical analysis and processing controls among others. However, these sensors have several limitations such as short lifetime, large size, the necessity of high level technical knowledge for proper operation, etc. Optical fibers have played a key role in the expansion of optical communications in the last four decades because they exhibit several intrinsic advantages: immunity to electromagnetic interference, efficient data protection, low cost, low losses, faster transmission of information and increased bandwidth of the signal [1, 2]. Therefore, a multitude of optical fiber sensors have been developed for a wide range of applications during the last decades. These sensors can be developed using commercial optical fibers, and fibers with structures specifically designed for a specific target. In the following

sections we review the basic principles behind the operation of optical fibers. We also provide a description of the principle of operation for the evanescent field and MMI sensors. Both effects constitute the basis for the sensors developed in the following chapters for the detection of toxic substances.

2.2. OPTICAL FIBERS

The optical fiber is a cylindrical dielectric waveguide, highly flexible and capable of guiding electromagnetic waves in the range of optical communications (175 THZ-375 THZ) [3, 4]. The optical fiber has two regions (concentric cylinders), a concentric core inside and the cladding that protects it. The core of the fiber is used as the transmission medium, while the cladding serves to contain the signal, transmitted through the phenomenon of total internal reflection (TIR). This means that the core has a higher refractive index that the cladding [5]. The entire structure of an optical fiber is shown in Fig.1.

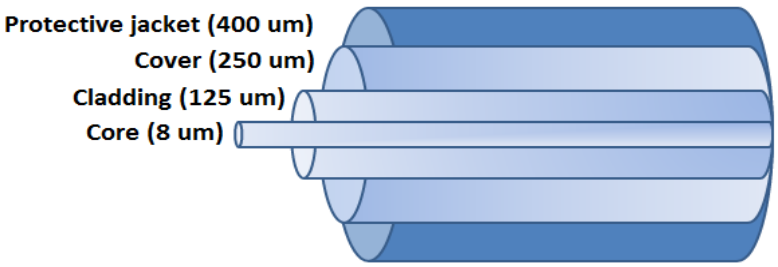

Figure 1. Basic structure of a typical optical fiber.

Based on their optical properties, optical fibers can be classified according to the material of fabrication, the number of propagation modes and the distribution of the refractive index of the core as shown in Table 1 [5-8].

Classification	Optical fiber type
Material of fabrication	• Silica fiber • Multicomponent glass fiber
Number of modes of propagation	• Single-mode fiber (SMF) • Multi-mode fiber (MMF)
Distribution of the RI of the core	• Step-index fiber (SIF) • Gradual-index fiber (GIF)

Table 1. Optical fiber classification

Considering that light is being guided in silica (fiber core), the use of optical fibers in communication systems has several benefits, such as [5-8]:

- Immunity to electromagnetic interference
- Low crosstalk
- They are more lightweight than traditional copper wires
- Low attenuation losses
- More efficient data protection
- Faster transmission and higher bandwith than copper
- High resistance to heat, cold and corrosion
- Easy to locate cuts through a process based on telemetry

These advantages make the optical fiber as the ideal transmission medium required for future communication systems. Nevertheless, it is necessary to mention some disadvantages of optical fibers, which are the subject of research such as [5-8]:

- Fragility
- Use of expensive transmitters and receivers
- Electricity cannot be transmitted via the optical fiber to power intermediate repeaters

- The need of Optical-Electrical-Optical (OEO) conversions
- High power transmission is limited

While optical communications is the predominant application for optical fibers, this technology has many other applications, some of them are shown in Table 2 [5-8].

Aplication	Description
Telephony	• Links without repeaters. • Intercity links with repeaters. • Transoceanic submarine optical cable links. • Distribution of large capacity subscribers of telephone, videophone and data transmission.
TV	• Distribution by cable. • Camera studio links. • Teleconferences. • Security systems.
Computing	• Links between computers. • Links between computers and peripherals. • Connection of office supplies. • Internal links for computer equipment.
Process control and instrumentation	• Operation in flammable environments. • Nuclear controls. • Measurement and control intrumentation.
Sensing	• Sensing for industrial application. • Sensing in concrete structures. • Sensing in medical applications. • Sensing for identifying toxic substances.

Table 2. Some optical fibers applications.

Among the different applications, optical fiber sensors have received a great deal of interest due to its advantages for certain niche applications.

2.3. TYPES OF OPTICAL FIBERS

According to the characteristics of the propagation modes we have three possible configurations for commercial optical fibers: step index multi-mode fiber (MMF), graded index multi-mode fiber (GI-MMF) and single-mode fiber (SMF) as shown in Fig. 2.

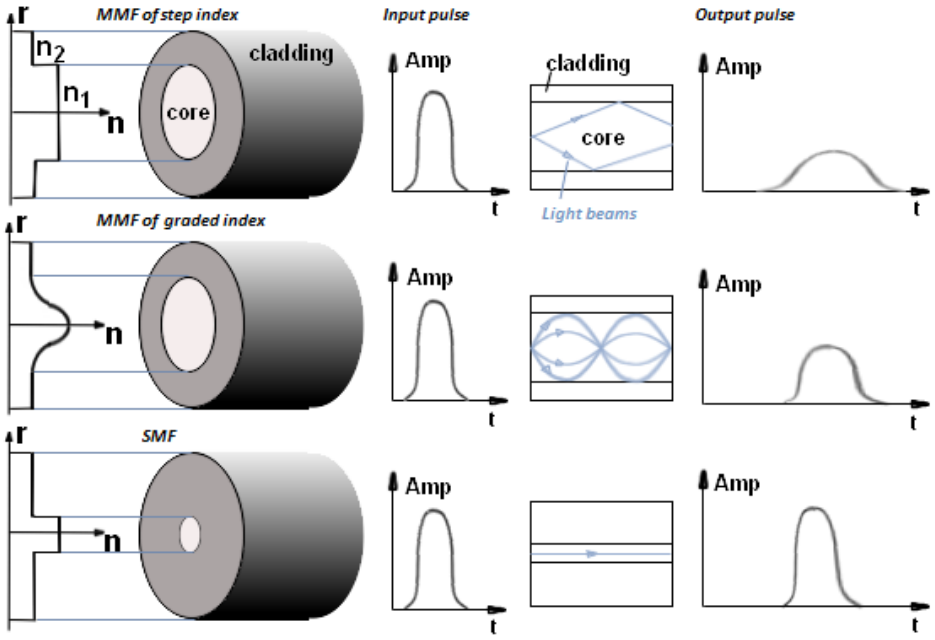

Fig. 2. Optical fibers configurations.

In the step index MMF configuration the core is homogeneous between 50 and 150 μm with a cladding diameter ranging between 100 y 250 μm. The refractive index of the core and cladding are constant along the optical fiber, and its numerical aperture is around 0.3. This kind of optical fiber can support hundreds of modes, which correspond to different propagation angles inside the fiber and also

to slightly different transit time. This is known as intermodal *dispersion or modal dispersion* [9-12]. Intermodal dispersion will induce temporal broadening when optical pulses propagate through the fiber, and this limits the use of step index MMF for short distance optical communications. A way to reduce this effect is by gradually reducing the core refractive index as we move away from the optical axis to the edge of the core. The fibers having this configuration are called *graded index MMF* [9-12]. Since the refractive index is higher along the center and smaller at the edges, light traveling at large angles will travel faster than those rays with smaller angles moving close to the optical axis. In fact, light rays follow sinusoidal paths down the fiber converging periodically at the same point. Graded index MMF usually have a core diameter between 20-90 μm and a numerical aperture of 0.2. Although model dispersion can be considerably reduced using a graded index MMF, the best solution to the problem of *intermodal dispersion* is to fabricate a small core (less than 10 μm) such that there is only one mode propagating along the fiber. These *single-mode fibers* (SMF) provide the best performance for use in Telecommunication [9-12].

2.4. OPTICAL FIBER SENSORS

In general, optical fiber sensors use electromagnetic radiation as a way to interrogate the fiber sensor head. These sensors cover different portions of the electromagnetic spectrum, i.e., UV (200 nm to 400 nm), visible region (400 nm to 780 nm), near-infrared (780 nm to 3000 nm) and the infrared (3000 to 5000 nm) [1-5]. Optical fiber sensors systems based on fiber optic technology carry a light signal that is modulated according to the physical parameter being measured. This light is finally recorded using either a photodetector or an optical spectrum analyzer. Fig. 3 shows the generic block diagram of an optical fiber sensor system [1-5].

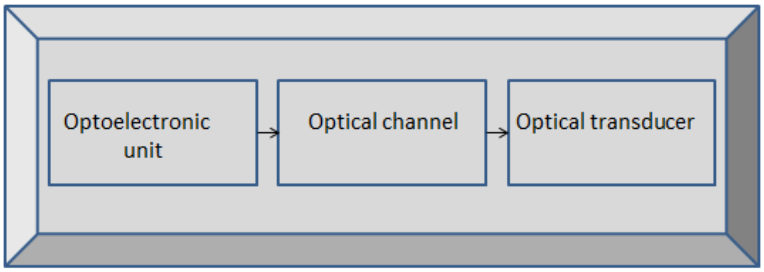

Fig. 3. Optical fiber sensor generic block diagram.

The growing interest in optical fiber sensor can be attributed to the advantages of optical fibers mentioned before, and have been employed to monitor a wide range of parameters as shown in Table 3.

Parameter	**Technique**
Tension [13-15]	Raman Interferometry (Michaelson and *Fabry-Perot)*
Temperature [16,17]	Fluorescence Bragg gratings
Flow [18]	Doppler
Pressure [19]	Interferometry
Chemical concentration [20]	IR spectroscopy (average, near and evanescent wave)

Table 3. -Selective parameters that can be monitored by means of optical fiber sensors.

The use of these techniques among others has created a new generation of sensors offering significant opportunities and great potential in several applications. Some areas of application are shown in Table 4.

Area	Aplication
Large metal buildings and concrete [24]	Bridges, dams, sea and air vehicles.
Electric power industry [25]	Monitoring of load power transmission lines, measurement of winding temperature and current measuring.
Medical science [26]	Temperature and ultrasound.
Chemical sensing [27]	Detection of toxic gases, liquids identifying contaminants in products of certified quality.

Table 4. Optical fiber sensors application areas.

Based on the optical structure, transduction mechanism, and parameter being measured, optical fiber sensors can be classified as it is presented in Table 5.

Classification	Parameter
Type of modulation	Intensity, interferometric, polarimetric, spectroscopic.
Nature transduction	Extrinsic, intrinsic.
Spatial distribution	Point, distributed, quasi-distributed
Measuring parameters	Voltage/current, temperature, radiation, moisture, chemicals, electromagnetic fields, tension, rotation, mechanical.

Table 5. Optical fiber sensors classification.

Extrinsic optical fiber sensors (Fig. 4) are sensors in which the light guided by the optical fiber is modulated by an external device which is perturbed under the action of the measured variable of the phenomenon being detected. This type of sensor is used in measurements of voltage/current, temperature, radiation, biomedical, chemical/gas, electromagnetic fields, power and Telecommunications to monitor the status and performance of the optical fibers within a network [1-5].

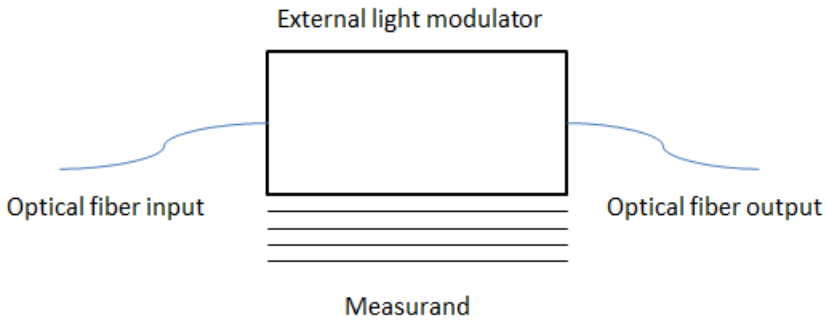

Fig. 4. General scheme of an optical fiber sensor extrinsic modulation.

In the case of intrinsic sensors (Fig. 5) the optical fiber not only transmits the light but also acts as the transducer. In this kind of sensors some of the properties of the fiber are modified by the action of the environment, for example, the refractive index, the absorption or fluorescence characteristics of the fiber [1-5]. The variation of such parameters modifies the transmission of radiation through the optical fiber and this is correlated with the physical parameter being measured.

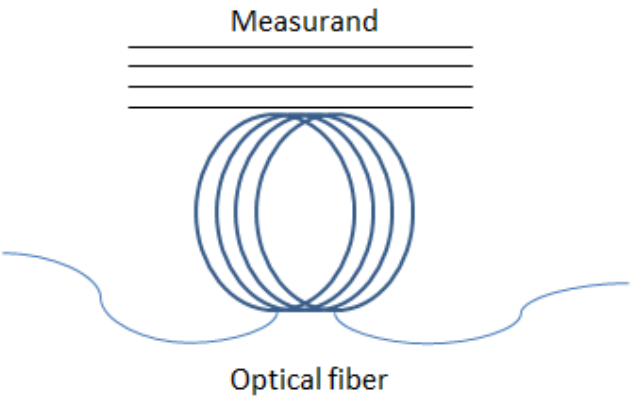

Fig. 5. General scheme of an optical fiber sensor intrinsic modulation.

A simple way make an optical fiber sensible to the external medium is to remove its cladding. Since the cladding has been removed any liquid that makes

contact with the fiber will alter the transmission characteristics through the fiber and, by measuring the transmitted intensity or the spectrum we can measure the refractive index of the liquid. Optical fiber refractive index sensors are a traditional method for measuring concentrations of compounds and even determine percentages of binary mixtures [5-10]. Intrinsic sensors are mainly used in medicine, defense, and aerospace applications, and also to measure temperature, pressure, humidity, acceleration and voltage [5-10].

2.5. OPTICAL FIBER SENSORS BASED ON THE MEASUREMENT OF THE EVANESCENT FIELD.

The evanescent field refers to the electromagnetic field present in the interface between the core and the cladding of the optical fiber, wherein the thin area where TIR takes place in any type of optical fiber [25]. In evanescent field sensors based on the interaction with the external environment or with a coating on the fiber surface via the evanescent field, the disturbances of the external medium might cause a change in the transmitted spectrum or variation in the transmitted power [26]. For example, in the case of the ammonia sensor that is presented in Chapter 3 of this work, the evanescent field interacts with a section of the fiber structure formed by a sensitive material that change its absorption characteristics depending on the moisture content or pH value of the environment [27]. Therefore, the transmitted intensity will decrease exponentially and this provides information of the parameter being measured. On the other hand, changes in the refractive index of the external medium introduce variations in the light propagating in the fiber core, and this also allow us to measure certain variables [38-32]. In the following paragraphs, a theoretical description of the principle of operation of this type of sensors is provided [29-36].

If we start from the wave equation for the incident at the interface of the medium, we have:

$$\nabla^2\vec{E} + n^2k_0^2\vec{E} = 0 \quad (1)$$

where $\vec{E}$ is the electric field, and where the Laplacian is given by:

$$\nabla^2 = \frac{\partial^2}{\partial x^2} + \frac{\partial^2}{\partial y^2} + \frac{\partial^2}{\partial z^2}$$

with n as the RI of the propagating medium and k_0 is the wavevector of the incident wave in vacumm. If the electric field is parallel to the interface between the media, then only have components in the longitudinal axis, so that the vector wave equation reduces to a scalar equation:

$$\frac{\partial^2 E_y}{\partial x^2} + \frac{\partial^2 E_y}{\partial z^2} + n^2k_0^2E_y = 0 \quad (2)$$

This equation is exponentially into the less dense solution medium, for the case in which $\theta_i \gg \theta_c$, that is, when the TIR is met:

$$E_{y^2} = E_T.exp(-jk_0n_1z.sen\,\theta).exp\left(k_0n_2x\sqrt{\left(\frac{n_1}{n_2}\right)^2 sen^2\theta_1 - 1}\right)(V/m) \quad (3)$$

where n_1 and n_2 are the refractive index of the core and cladding of the optical fiber respectively. The second exponential term in equation (3) represents an exponential decay of the field in the cladding (external medium) in the direction perpendicular to the interface, that is, away from the core fiber. This electromagnetic field which penetrates the external medium is the *evanescent field,* as illustrated in Fig. 6.

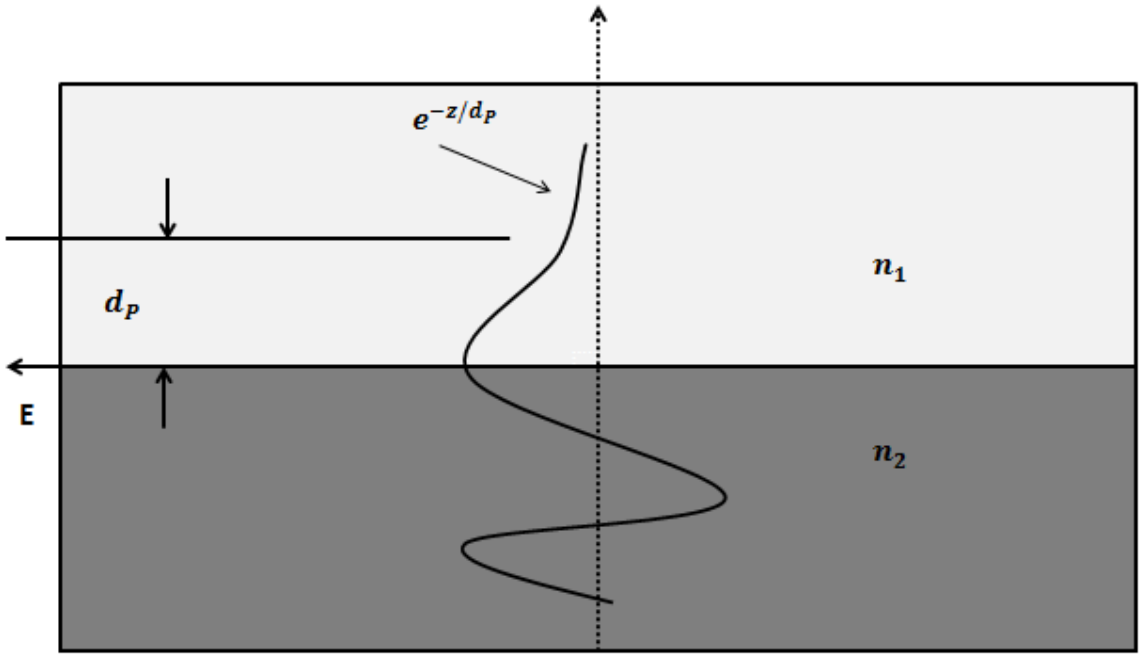

Fig. 6. An illustration of exponential of evanescent field.

The penetration length for this electromagnetic field to fall to $\frac{1}{e(0.37)}$ of its value at the interface, which is a function of both the wavelength of the light and the angle of incidence, can be mathematically defined by:

$$d_p = \frac{\lambda}{4\pi\sqrt{(n_1^2 sin^2\theta - n_2^2)}} \quad (m) \tag{4}$$

where λ is the wavelength of the transmitted light, θ is the incident angle at the core/cladding interface and n_1 and n_2 are the refractive index of the core and cladding of the optical fiber respectively. As shown in Eq. (4), the depth of the field depends largely on the refractive indices of the media and the light wavelength. Penetration depth is a very important parameter that needs to be considered when designing evanescent wave-based bio and chemical sensors, to be discussed in detail in chapter III.

2.6. OPTICAL FIBER SENSORS BASED ON THE MULTIMODAL INTERFERENCE (MMI) EFFECTS.

As shown in Fig. 7, a MMI fiber structure is fabricated by just splicing a section of multimode fiber (MMF) between two single mode fibers (SMF).

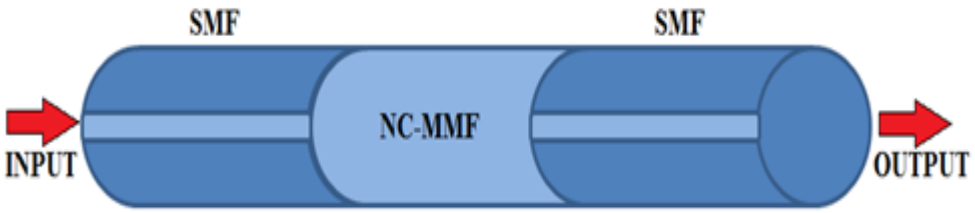

Fig 7. Schematic of MMI structure.

The basic physical principle of the MMI sensors is that when an optical signal is launched into the MMF it excites the supported modes of the MMF, and as the modes propagate along the MMF their interference gives rise to an interference carpet that is highly dependent with the phase relationship between the modes [37]. Due to the MMI effect both transmission and attenuation bands are obtained in the transmitted optical spectrum. At certain lengths, where the phase difference is a multiple of 2π, we have the formation of self-images which are an exact replica of the input field. Particularly, the transmission bands obtained by the self-imaging effect exhibit minimum losses and its central wavelength can be controlled as a function of the MMF segment dimensions. Therefore, by carefully selecting the length and diameter of the MMF, light coupled trough the input SMF will be imaged with small losses to the output SMF [37].

In order to determine the reimaging locations inside a MMF, with an input field provided from a SMF fusion spliced directly to the MMF (Fig. 7), it is

necessary to first determine which modes are excited in the MMF. Using the linearly polarized mode approximation, the input field provided from the SMF $\overline{E_s}(r)$ can be approximated as a Gaussian beam.

$$\bar{E}(r) = e^{-(r/w)^2} e^{-i\beta_o z_{\hat{x}}} \tag{5}$$

where β_o is the longitudinal propagation constant for the SMF guided mode LP_{01}. The half-width at half-maximum (HWHM) spot size $\bar{\omega}$ of the Gaussian beam can be determined empirically based on the radius of the SMF a_0, and the normalized frequency V given by

$$\bar{\omega} = \frac{a_0}{\sqrt{\ln 2}}(0.65 + 1.619V^{-1.5} + 2.879V^{-6}) \tag{6}$$

where n_{core} and n_{clad} are the core and cladding refractive indexes, respectively, and the normalized V frequency is defined as

$$V = a_0 k\sqrt{n_{core}^2 - n_{clad}^2} \tag{7}$$

This input field excites a specific number of guided modes inside the MMF. By neglecting the radiation modes the field distribution at any point along the MMF can be calculated using

$$E_M\,(r,\theta,z) = \sum_{m=-M}^{M}\sum_{v=1}^{N}\Psi_{v,m}(r,\theta,\mathrm{z}) \tag{8}$$

where the suffixes v and m are the indices for the guided radial and azimuthal components respectively. N and $2M+1$ are the local number of radial and azimuthal guided modes respectively. The term $\Psi_{v,m}(r,\theta,\mathrm{z})$ represents the complex field amplitude of the guided modes. Solving Maxwell equations inside the MMF for linearly polarized modes, this field can be written as follows:

$$\Psi_{v,m}(r,\theta,\mathrm{z}) = \begin{cases} c_{v,m}J_m\left(u_{v,m}\frac{r}{a}\right)\cos(m\theta)e^{-iz\beta_{v,m^z}}\hat{x} & r \le a \\ d_{v,m}K_m\left(w_{v,m}\frac{r}{a}\right)\cos(m\theta)e^{-iz\beta_{v,m^z}}\hat{x} & r > a \end{cases} \tag{9}$$

where $u_{v,m}, w_{v,m}, \beta_{v,m}$, and a are the normalized transverse propagation constant inside the core, in the cladding, longitudinal propagation constant for this mode and the radius of the MMF, respectively. The normalized transverse wavenumber $u_{v,m}$ and $w_{v,m}$ are defined as

$$u_{v,m} = a\sqrt{k_0^2 n_{core}^2 - \beta_{v,m}^2} \quad \text{and} \quad w_{v,m} = a\sqrt{\beta_{v,m}^2 - k_0^2 n_{clad}^2} \tag{10}$$

where n_{core} and n_{clad} are the core and cladding refractive indices, k_0 is the wavenumber in free space and the subindices v and m correspond to the radial and azimuthal components. A direct relation between field excitation coefficients $c_{v,m}$ and $d_{v,m}$ is also obtained by applying the continuity of the tangential field components as the core cladding interference, and given as

$$d_{v,m} = \frac{J_m(U_{v,m})}{K_m(w_{v,m})} \tag{11}$$

The Eq. (9) can be incorporated into Eq. (8) to represent the radial and azimuthal modes within the MMF. At $z = 0$, the left hand side of Eq. (8) should equal the input field, $E_s(r)$, as shown in Fig. 8. In other words, at this position the input field is projected onto an orthogonal set of the transverse field components of the guided and leaky modes inside the MMF with different weights. These weights are referred to as the mode excitation coefficients of these modes. Here, we will neglect the influence of the leaky modes inside the MMF, and hence in Eq. (8) the constant $c_{v,m}$ is the field excitation coefficient of the $LP_{v,m}$ mode. Since the input field defined by $E_s(r)$ does not include any azimuthal components, the field distribution inside the MMF should be radially symmetric. Therefore, the excitation coefficient vanishes for values of m greater than 0. This constraint simplifies the field representation within the MMF into a sum of radial modes as follows

$$E_M(r,0) = \begin{cases} \sum_{v=1}^{N} c_{v,0} J_0\left(u_{v,0}\frac{r}{a}\right)\hat{x} & r \le a \\ \sum_{v=1}^{N} d_{v,0} K_0\left(w_{v,0}\frac{r}{a}\right)\hat{x} & r > a \end{cases} \tag{12}$$

For simplicity we will omit the suffix for the azimuthal modes and write the excitation coefficients, the normalized traverse propagation constant and the longitudinal propagation constant as $c_v, d_v, u_{v,}$ and β_v respectively. Because of the circular symmetry of the input field and assuming perfect alignment of the central axes of the cores between the SMF and MMF, only LP_{0m} modes can be excited. It is important to note that a reduction in the number of modes is an advantage as it reduces the computational complexity and computational time.

Now the input field right at the MMF input can be written as:

$$E_M(r,0) = \sum_{v=0}^{m-1} c_v \Psi_v(r,0) \tag{13}$$

where c_v is the excitation coefficient for each mode, and this coefficient can be calculated by an overlap integral between $E_M(r)$ and $\Psi_v(r)$ given by:

$$c_v = \frac{\int_0^\infty E_M(r,0)\Psi_v(r,0)dr}{\int_0^\infty \Psi_v(r,0)\Psi_v(r,0)dr} \tag{14}$$

As the light propagates in the MMF section, the field at a propagation distance z can be calculated by

$$E_M(r,z) = \sum_{v=0}^{m-1} c_v \Psi_v(r,0)\, e^{-(j\beta_v z)} \tag{15}$$

where β_v is the propagation constant of each eigenmode of the MMF. The propagation constant can be calculated from the eigenvalues of the MMF. The analytical formulation for the location of the self-images is developed using the fact the power coupling efficiency is maximum for a specific mode number. Under the asymptotic formulation and using the suggestion for the coupling efficiency shown in [41-47], the difference in the longitudinal propagation constants between two radials modes, v_1 and v_2, can be expressed as follows.

$$(\beta_{v1} - \beta_{v2}) = \frac{u_{v2}^2 - u_{v1}^2}{2k_0 a^2 n_{core}} \tag{16}$$

where u_{v1} and u_{v2} are provided by

$$u_{v,m} = a\sqrt{k_0^2 n_{core}^2 - \beta_{v,m}^2} \quad \text{and} \quad w_{v,m} = a\sqrt{\beta_{v,m}^2 - k_0^2 n_{clad}^2} \tag{17}$$

where n_{core} and n_{clad} are the core and cladding refractive indices, and the subindices v and m correspond to the radial and azimuthal components. The normalized transverse propagation constant u_v can also write as:

$$u_v = \left(2v - \frac{1}{2}\right)\frac{\pi}{2} \tag{18}$$

In order to form a self-imaging the modes inside the MMF have to interfere constructively along the axial plane. For the modes within the MMF to interfere constructively on the axial plane the phase difference between the modes should be an integer multiple of 2π. We can then take the most dominant radial mode and the adjacent mode for any numerical estimation. Combining Eq. (17) and (18), and also considering the two modes v_p and v_{p-1}, the phase difference between these two modes can thus be expressed as in the following equation.

$$\left(\beta_{v_{p-1}} - \beta_{v_p}\right) z = \left(\frac{u_{v_p}^2 - u_{v_{p-1}}^2}{2k_0 a^2 n_{core}}\right) z = \left(\frac{\pi^2(4v_p - 3)}{4k_0 a^2 n_{core}}\right) z \tag{19}$$

At the following longitudinal location inside the MMF along the optical axis, z_m, the phase difference becomes an integer multiple of 2π when,

$$z_m = \frac{8ka^2 n_{core}}{\pi(4v_p - 3)} m = L_p m, \qquad m = 1,2,3 \ldots \tag{20}$$

$$L_p = \frac{8ka^2 n_{core}}{\pi(4_{vp} - 3)} \tag{21}$$

where L_p corresponds to the location where the phase difference between the two modes equals 2π. The explicit self-imaging position where the input field is reproduced is derived from the representation of the given in Eq. 8. Looking at the complex field vector contained in this formulation, the phase term can be

manipulated by factoring out the phase term characteristic of the radial mode that has a maximum coupling associated to it, $e^{-i\beta_{v_p}z}$. By doing so, the self-imaging distance can be determined by looking at the resulting phase difference term, $(\beta_v - \beta_{vp})z$. The self-imaging is defined as the distance, $z_{self-imaging}$, that corresponds to a phase difference between these two guided radial modes being an integer multiple of 2π. Therefore, under the asymptotic assumption for the lateral propagation constants, the self-imaging distance can be calculated by formulating and expression for the phase difference between the v^{th} and v_p modes as done in Eq. (21).

$$\left(\beta_v - \beta_{v_p}\right) z = \frac{\pi^2\left[2\left(v^2 - v_p^2\right) + (v_p - v)\right]}{4ka^2 n_{core}} z = 2\pi p, \qquad with\ p\ as\ integer \tag{22}$$

Thus, the distance that the two modes must propagate to satisfy the self-imaging conditions can be expressed as

$$z_{self-imaging} = \frac{8n_{core}ka^2}{\pi} \tag{23}$$

If we substitute in Eq. (23) the value of the wavevector $k = 2\pi/\lambda$, and express the radius a in terms of the diameter D, we obtain the following equation for the self-imaging position,

$$z_{self-imaging} = L = \frac{4n_{core}D^2}{\lambda} \tag{24}$$

where n_{core} and D corresponds respectively to the effective refractive index and diameter of the fundamental mode of the MMF, and λ is the free space wavelength.

The process behind the formation of such self-images can be more easily observed by using a commercially available beam propagation software package (BeamPROP from RSoft) as shown in Fig. 8. As shown in Fig. 8, we are interested in every fourth self-image since they have minimum losses as compared to other

images. We can also notice the periodicity of the self-imaging process, but other self-images exhibit higher losses.

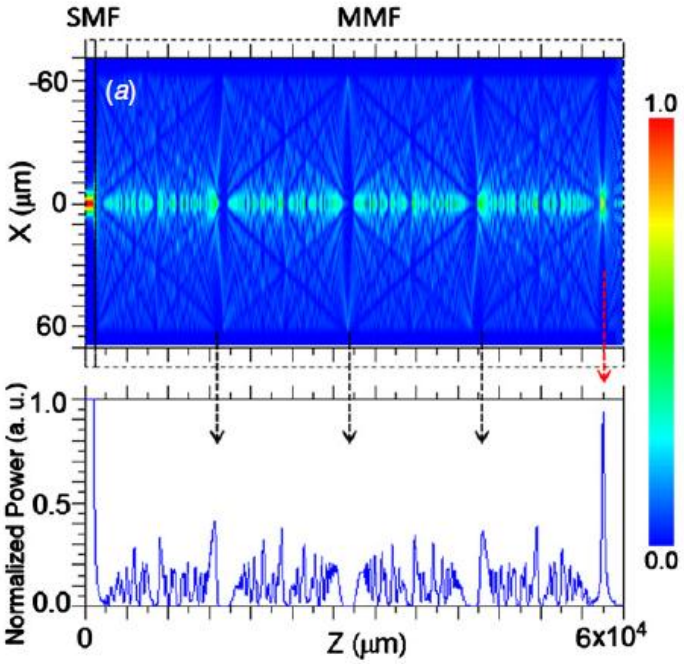

Fig. 8. Intensity distribution of the light inside the MMF (top), and normalized power along the optical axis of the MMF (down).

The self-images with higher losses are correlated with bigger phase errors between the propagating modes as compared to the required phase difference of 2π to reproduce the input field, and thus the intensity of the self-image is reduced. After the MMF is cleaved at the length dictated by equation (24), light with wavelength λ will be transmitted with minimum loss through the MMI structure. However, when the devices are detuned from this design wavelength, the image will be formed either before or after the facet of the output SMF and the transmitted intensity will have higher losses. Therefore, the response of the MMI sensor under a wide spectrum source will be similar to a band-pass filter as shown in Fig. 9.

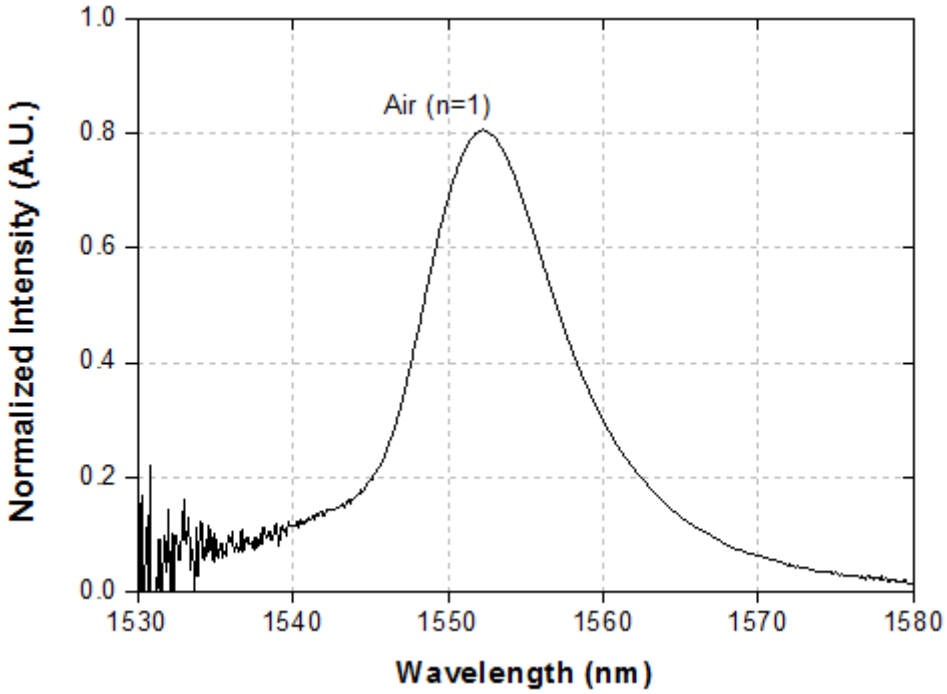

Figure 9.- MMI spectral response in air.

According to equation (24), by modifying the effective RI and the diameter of the MMF the MMI peak wavelength can be spectrally shifted

REFERENCES

1. M.D. Marazuela, M.C. Moreno-Bondi, Fiber-optic biosensors-an overview, *Anal. Bioanal. Chem.* vol. 87, 2002, pp. 289-295.
2. B. Lee, Review of the present status of optical fiber sensors. *Opt. Fiber Technol.* vol. 9, 2003, pp. 57-59.
3. R.J. Bates, Optical Switching and Networking Handbook. New York, McGraw.Hill, 2001, p. 10.
4. S. Koji, N. Naoya, S. Masato, Y. Ren'chi and S. Hirokazu, Evaluation of High-power Endurance in Optical Fiber Links, Furukawa Review, vol. 24, 2003.
5. D.D. Davis, S.C. Mettler and D.J. DiGiovanni, " A comparative evaluation of fiber fuse models", SPIE 2966, 1997, pp. 592-606.
6. I.R. Matias, F.J. Arregui, R.O. Claus, Optical Fiber Sensors, Encyclopedia of SENSORS, vol. X, pp.1-19, 2006.
7. G.F. Fernando, D.J. Webb, P. Ferdinand, Optical-Fiber Sensors, MRS BULLETIN, 2012.
8. Y.Shizhuo, P.B. Ruffin, F.T.S. Yu, Fiber optic sensors Second edition, Taylor & Francis Group, USA, 2008.
9. P.E.Tippens, Física.Conceptos y aplicaciones. Ed. McGraw Hill, séptima edición, 2007.
10. J. Dakin and B. Culshaw, "Fiber Sensors: Principals and Components", Vol. 1, Artech, Boston, Mass, USA, 1988.
11. B. Culshaw and J. Dakin, "Optical Fiber Sensors: Systems and Applications", Vol.2, Artech, Norwood, Mass, USA, 1989.
12. A. Krohn, "Fiber Optic Sensors: Fundamental and Applications", Instrument Society of America, Research Triangle Park, NC, USA, 1988.
13. B. Culshaw, Optical Fibre Sensing and Signal Processing, P. Pergrnus, London, UK, pp.36-45, 1984

14. G.D. Pitt, P. Extance, R.C. Near et al., “Optical-fibre sensors”, IEEE Technical Review, vol.3, no.8, pp. 379-417, 1986.
15. C. Pérez Conde, Sensores ópticos, Servei de Publicacions Universitat de València, 1996.
16. P. Koudelka et al., Optical fiber distributed sensing system applied in cement concrete commixture research, Radioengineering, vol. 19 (1), 2010, pp. 172-177.
17. V.A. Marquez-Cruz and J. hernandez-Cordero, “Surface tension measurements with a Fiber Optic Fabry-Perot Interferometer”, in Workshop on Specialty Fibers and their Applications, (Optical Society of America, 2013), paper, F2:33
18. A. R. Bahrampour, S. Tofighi, M. Bathaee and F. Farman, “Optical Fiber Interferometers and Their Applications”, Interferometry-Research and Applications in Science and Technology, Edited by Dr. Ivan Padron, InTech Europe, 2013, pp. 1-27.
19. J.L. Wu and Y.T. Wang, “A Fluorescence Optic-Fiber Temperature Sensor Using Phase-Locked Detection with Pulse Modulation Single Reference”, Journal of Pshysics; Conference Series 48, 2006, pp. 101-105.
20. C.H. Lee and J. Lee, “Characteristics of a Fiber Bragg Grating Temperature Sensor Using the Thermal Strain of an External Tube”, Journal of the Korean Physical Society, vol. 59 (5), 2011, pp.3188-3191.
21. A. Kumar Agraval, “Fiber-Optic Laser Doppler Velocimeter for Microcirculatory Flow Measurements”, A thesis sumnitted to the faculty of The University of Utha, 2005.
22. B. H. Lee, Y. H. Kim, K. S. Park, J.B. Eom, M. J. Kim, B.S. Rho and H. Y. Choi, “Interferometric Fiber Optic Sensors”, Sensors, vol. 12, 2013, pp. 2467-2486.
23. O. S. Wolfbels, “Fiber-optic Chemical Sensors and Biosensors”, Anal. Chem. Vol. 76, 2004, pp. 3269-3284.

24. Y. Huang et al., “Large-strain optical fiber sensing and real-time FEM updating of steel structures under the high temperature effect”, vol. 22 (1), 2013.
25. K. Bohnert, “Optical Fiber sensors for the electric power industry”, Optics and Lasers in Engineering, vol. 43, issues 3-5, 2005, pp. 511-526.
26. F. Baldini, A. Giannetti, A.A. Mencaglia, and C. Trono, “Fiber Optic sensors for Biomedical Applications”, Curr. Anal. Chem. vol. 4, 2008, pp.378-390.
27. P. Bhatia, B.D. Gupta, “Surface Plasmon Resonance Based Fiber Optic Ammonia Sensor Utilizing Bromocresol Purple”, Plasmonics, vol. 8(2), 2013.
28. J. Bravo, “Arquitecturas opticas de sensado basadas en nano-recubrimientos sobre fibra optica,”, tesis doctoral, Universidad Publica de Navarra, pp. 46-51, 2008.
29. U. Gunasilan, “Operative factors contributing to the selection of fiber-optic techniques for remote measurement of strain/stress”, in Proceedings of the IEEE 9th International Conference on Computer and Information Technology, Middlesex University Dubai, 2009.
30. S.M. Chamdiani, A.F. Jaeger, “Fiber optic Temperature sensor using Evanescent Field in D. Fibers, “IEEE Phot. Tech. Let. Vol 17, pp 2706-2708, 2005
31. A. Gaston, I. Lozano, “Evanescent Waves optical Fiber Sensing (temperature, PH, Relative Humidity sensors)”, IEEE Sensors Vol 3(6), pp. 296-298, 2000.
32. J.D. Love, “Tapered Single-mode Fibers and Devices, Part 1: Adiabatic Criteria,” IEEE Procededings-j, vol. 138 (5), pp. 343-354, 1991.
33. J.M. Corres, F.J. Arregui, I. Matias, “Design of humidity sensor Based on Tapered Optical Fiber”, Joruanl of Light, Tech, vol 24(11), pp. 4347-4358, 2006

34. K. Q. Kieu, M. Mansuripim, “Bionical Fiber Taper sensors”, IEEE Phot. Vol. 18, 2006
35. U. Willer, “Fiber optic Evanescent Field Laser sensor for In-situ gas diagnostics”, Spectrochim. Acta, part A 58, pp. 2427-2442, 2002.
36. R.A. Yoter, L. A Lee, “Sensor Technologies for Monitoring Metabolic Activity in Single cells”, IEEE sensors Vol 4(4), pp. 395-411, 2004
37. M. Othman, J.I. Clemente, “Spectroscopic Studies and Evanescent Optical Fiber Waves Sensing of Cu Based on Activated Mesostructured Silica Matrix”, J. of Mat. Sci, Vol. 40(17), pp. 4523-4530, 2005.
38. M. Ahmad, L.L. Hench, “Effect of Taper Geometries and Launch Angle on evanescent Wave Penetration Depth in optical Fibers”, Biosens. And Bioelectr., vol 20. Pp 1312-1319, 2005.
39. Y. Rodriguez Garcia, “Contribucion al desarrollo de sensores utilizando fibra optica y nanostructuras”, tesis doctoral, Universidad Publica de Navarra, pp. 26-28, 2013.
40. S. Silva, E.G. P. Pachon, M.A.R. Franco, J.G. Hayashi, F.X. Malcata, O. Frazao, P. Jorge, and C.M.B. Cordeiro, “Ultrahigh-sensitivity temperature fiber sensor based on multimode interference”, Appl. Opt. 51(16), 3236-3242 (2012).
41. P. Yeh, A. Yariv, and E. Marom, “Theory of Bragg fiber”, J. Opt. Soc. Am. 68(9), 1196-1201, 1978.
42. A. B. Socorro, I. del Villar, J. M. Corres, F.J. Arregui, and I.R. Matias, “Mode transition in complex refractive index coated single-mode-multimode-single-mode-structure”, Optics Express, vol. 21(10), 2013.
43. T. Erdogan, “Cladding-mode resonances in short and long period fiber gratings filters”, J. Opt. Soc. Am. A. vol. 14(8), 1997, pp. 1760-1773.
44. G. Decher, “Fuzzy nanoassemblies:toward layered polymeric multicomposites”, Science 277 (5330), 1997, pp. 1232-1237.

45. E. A. Lopez, D. Lopez Cortes, M.A. Basurto Pensado, D.A. May Arrioja, J.J. Sanchez Mondragon, “All-fiber multimode interference refractometer sensor”, Proc. SPIE 7316, 7316F, 2009.
46. D. Marcuse, “Mode conversion in optical fibers with monolithically increasing core radius”, J. Lightwave Technol., vol. LT5, pp. 125-133, 1987.
47. J.E. Antonio López, “Design and Fabrication of Photonic Devices Based on Multimode Interference”, tesis doctoral, Instituto Nacional de Astrofísica, Óptica y Electrónica, pp. 27-33, 2012.

CHAPTER III. OPTICAL FIBER SENSORS FOR THE DETECTION OF AMMONIA GAS

ABSTRACT

In this chapter, it is described the fabrication of two different optical fiber sensors for the detection of ammonia gas at low level concentrations. These sensors have been obtained by means of the utilization of colourimetric pH indicators, Bromocresol Green (BCG) and Universal indicator, attached to the multimode optical fiber core. These colourimetric pH indicators are, each one, immersed into a hydrophobic and gas permeable polyurethane film named Tecoflex® that acts as a ttraping matrix. Highly reproducible and reversible fiber optical sensors have been obtained employing a simple and quick dip-coating fabrication process. The sensors based on BCG pH indicator exhibit a wide spectral response (500 nm-750 nm) while showing recovery times of less than 15 s. Sensors based on universal pH indicator exhibit also a high sensitivity (10ppm) to ammonia over a broad wavelength range providing a differential response, with a valley around 500 nm and a peak around 650 nm, which allows to perform ratiometric measurements. The ratiometric measurements provide not only an enhanced signal, but can also help to eliminate any external disturbance due to humidity or temperature fluctuations. On the other hand, the hydrophobicity of the Tecoflex® film provides additional advantages, such as-operation even in extremely dry environments, efficient transport and leakage or detachment of the pH indicator prevention. The combination of the colourimetric pH indicators (BCG and Universal) with Tecoflex® provides reliable and robust optical fiber ammonia gas sensors suitable to be used in real applications.

3.1. INTRODUCTION

Ammonia is a coluorless gas produced by humans and by nature, is readily biodegradable and has a characteristic penetrating odour. This chemical substance is used in smelling salts, many household and industrial cleaners; for the manufacture of fertilizers for agricultural crops, lawns and plants; is a highly corrosive substance and the main effects of exposure occur in the skin, eyes, mouth, respiratory and digestive systems; found in at least 137 of the 1,647 sites on the National Priorities List identified by the Environmental Protection Agency (EPA) [1, 2]. Due to its potential hazard to human beings, even at small concentrations, real time evironmental monitoring of ammonia is a crital issue in closed environments. Optical fibers sensors (OFS) are an attractive option due to their inherent characteristics above mentioned in Chapter 2 [3, 4]. The key concept for employing OFS to detect ammonia is to take advantage of the basicity of ammonia. Therefore, by emploting either a colourimetric pH indicator which undergoes a suitable fluorescence or colour change when exposed to ammonium ions [5-21], ammonia gas can be measured by tracking absorption changes.

3.2. PRINCIPLE OF OPERATION

3.2.1. Therorically description

Based on the *Lambert-Beer* law, it is possible to obtain an approximation of the absorbed power by the sensitive pH coating [22]. Starting therefore:

$$P_l = P_0 . exp(-C\varepsilon AL) \quad (1)$$

where P_l is the power at the end of the absorber section, P_0 is the power before the absorption section, C is the concentration of the absorbing sustance, ε is the molar absorption coefficient, A is the coefficient depending on the geometry of the medium and L is the length of the optical fiber exposed to the absorbent material. Absorbance can be expressed as:

$$Abs_{d\beta} = -\left(\frac{10}{\ln 10}\right).\varepsilon ALC \tag{2}$$

Eq. 2 shows that the absorbance is linearly dependent on the concentration C. As our evanescent field sensor is concerned, the pH sensitive solution is linearly related to the concentration of ammonia gas, since the optical fiber sensor is an indirect sensor of ammonia gas, which measures the concentration of gas through of a pH change in the environment in which a pH indicator is.deposited on the fiber core. The coefficient A of Eq. 2. can be calculated from the evanescent absorption coefficient γ, for each of the angles of incidence of the modes travelling along the fiber θ_i

$$A\theta_i = \frac{\lambda.n_{coat}.\cos\theta\,.\cot\theta}{2\pi\rho e.n_{core}.\cos\theta_{crc}\sqrt{sen^2\theta - sen^2\theta_{crc}}} \tag{3}$$

$$\theta = cos^{-1}\left[sen\left(\frac{\theta_i}{n_{core}}\right)\right] \tag{4}$$

where n_{core} is the refractive index of the core, n_{coat} is the refractive index of the pH sensitive coating, θ_{crc} is the critical angle of incidence of the waveguide formed by the core and coating and ρe is the effective diameter of the core of the optical fiber. The last two parameters are defined as:

$$\theta_{crc} = sen^{-1}\left(\frac{n_{coat}}{n_{core}}\right) \tag{5}$$

$$\rho e = \rho + d_p \tag{6}$$

where ρ is the radius of the core of the optical fiber and d_p is the evanescent field penetration defined above in Eq. (4) in Chapter II. To obtain A, only the power needed for each mode, namely:

$$P_i(\theta_i) = \frac{sen\ \theta_i}{cos^3\theta_i} \tag{7}$$

$$A = \int_0^{\theta_c} \frac{P_i(\theta_i).A(\theta_i).d\theta_i}{\int_0^{\theta_c} P_i(\theta_i).d\theta_i} \tag{8}$$

where $\theta_c = sen^{-1}\left\{n_{core}.\cos\left[sen^{-1}\left(\frac{n_{coat}}{n_{core}}\right)\right]\right\}$ is the critical angle of the optical fiber.

The ammonia sensor studied in this chapter is develop from a pH sensor, thus, when inserting the sensor into solutions of different pH, the indicator changes its colour depending on the pH of the medium and the light guided by the optical fiber undergoes a change in the spectrum, as result from the induced absorption by colour change of the pH indicator. Detection of ammonia gas is based on a reversible reaction involving the deprotonation of the pH indicator (Bromocresol green and universal indicator) in the presence of ammonia. The first step is the

reaction of gaseous ammonia with water vapor to give ammonium hydroxide [22, 23]:

$$NH_3(g) + H_2O \leftrightarrow NH_4^+OH^- \quad (9)$$

The second step is the deprotonization of the indicator due to ammonium hydroxide, to give a modified form of the indicator and water, which causes the change in the indicator, that is:

$$NH_4^+OH^- + H^+Indicator^- \leftrightarrow NH_4^+Indicator^- + H_2O \quad (10)$$

Finally, the reverse reaction resulting in the initial form of the indicator and gas ammonia, from the indicator to its original colour is produced, that is:

$$NH_4^+OH^- + H^+Indicator^- \leftrightarrow NH_4^+Indicator^- + H_2O \quad (11)$$

These reactions cause a reversible colour change when the sensor is exposed to gaseous ammonia.

3.2.2. Tecoflex® membranes

Different materials, ranging from sol-gel glasses to polymers, have been used as a trapping matrix in order to attach the pH dependent material to the optical fiber. The immobilization of the indicator by means of a traditional sol-gel technique [24-27] requires a cycle of several hours for the deposition of the sensitive films on the substrates. The electrostatic self-assembly method has been

an efficient method to keep sensitive reagent immobilized in the fiber optic [28, 29], however, this method may result in the indicator film deterioration or wear, shortening its working life. The PVC [30] polymer is the most commonly used in the manufacture of optical fiber sensors. Nevertheless, this polymer has certain limitation as it can be for example the short lifetime caused for pollution with biological components. Moreover, another problem which often have these polymers is that they typically require admixture with plasticizers to be used in the manufacture of sensors. In recent years some types of polyurethanes are attracting the attention of researchers because they possess interesting properties for their use in the fabrication of optical fiber sensors: they are highly transparent and highly adherent, have a greater life span than other polymers such as PVC, are chemically stable and have good electrochemical properties, better than those of PVC, are low cost and can be prepared easily for their use in sensors without incorporating plasticizers. Here, we propose the use of commercial aliphatic thermoplastic polyurethane hydrophobic gas permeable membrane called Tecoflex® purchased from Thermedics [31] as reagent immobilizing matrix providing satisfying sensing results in aqueous or even extremely dry environments [32, 33]. These films are gas permeable and hydrophobic which means that is not necessary to soak the sensors in water, which allows the operation in drier environments as well as enhance the lifetime of the sensor by preventing the leaking of the indicator.

As it occurs with most of the gas sensors based on pH indicators, it is required an indicator, which is sensitive to ammonia gas without the need for water in the environment of the indicator. This is because the indicator directly reacts with the gas, without the occurrence of a change of pH in the environment where the indicator is embedded. Therefore, the characteristics of the chosen indicators are very important, since their interaction with the matrix Tecoflex® determine if the indicator is in an appropiate state of protonation to react with ammonia.

3.2.3. Bromocresol green (BCG) pH indicator

BCG pH indicator is a compound of the family of the triphenylmethanes, used in various laboratory activities as a tracking dye for DNA agarose gel electrophoresis, in protein determinations and in charge-transfer complexation processes among others [34-37]. The BCG pH indicator employed [38] to develop the optical fiber sensor described in this work is anionic and hydrophilic, and has been used in other studies as an indicator for the measurement of ammonia [39].

3.2.4. pH Universal Indicator

The universal pH indicator [40] is made of a mixture of the indicators Methyl Red, Methyl Yellow, Bromothymol Blue, Thymol Blue and Phenolphthale in an ethanolic solution, allowing the indicator to exhibit a wide wavelength operating range. Thus, when the sensor proposed in this Chapter is exposed to ammonia we obtain absorption changes with opposite responses at different wavelengths. This means that the absorption spectrum exhibits a peak and a valley with opposite behaviour, as the ammonia concentration is increased. Such behavior is ideal to perform ratiometric measurements that not only enhance the sensor response, but allow us to make the sensor immune to external disturbances such as humidity and temperature [41].

3.3. EXPERIMENTAL PROCEDURE

3.3.1. pH Sensitive solutions

3.3.1.1. BCG pH indicator sensitive solution

The pH sensitive solution was elaborated from a 120 ml ethanol solution containing 120mg of BCG pH indicator provided by Sigma-Aldrich [39] and 4.32 g of thermoplastic polyurethane (TPU) Tecoflex® provided by the company Thermedics. The sensitive solution was stirred for 3 h at 100 °C in a sealed container until it got a homogenous appearance before starting the coating process.

3.3.1.2. Universal pH indicator sensitive solution

The universal pH indicator is provided by the company PANREAC, and is made of a mixture of various indicators such as methyl red (40 mg), *p*-dimethylaminoazobenzene (60 mg), bromothymol blue (80 mg), thymol blue (100 mg) and phenolphthalein (20 mg) [40]. The pH sensitive solution was prepared by mixing 120 ml of ethanol, 120 ml of pH universal indicator, and 4.32 g of thermoplastic polyurethane (TPU), Tecoflex® .The sensitive film solution was stirred for 80 min at 100° C in a sealed container before starting the coating process.

3.2.2. Sensor head fabrication

The sensor was fabricated using FT-200-EMT from Thorlabs Inc. (Newton, NJ, USA), which is a multimode fiber (MMF) with core and cladding diameters of 200 and 225 µm respectively. The advantage of this MMF is that the cladding is made of polymer which facilitates its removal in a specific section of the MMF. The sensor head (Fig. 1) is fabricated by removing the outer protective plastic jacket of the fiber. First, the MMF was cleaved and the end facet is silver coated using a sputtering system (K675XD Quorum Technologies Ltd.), (Sacramento, CA, USA).

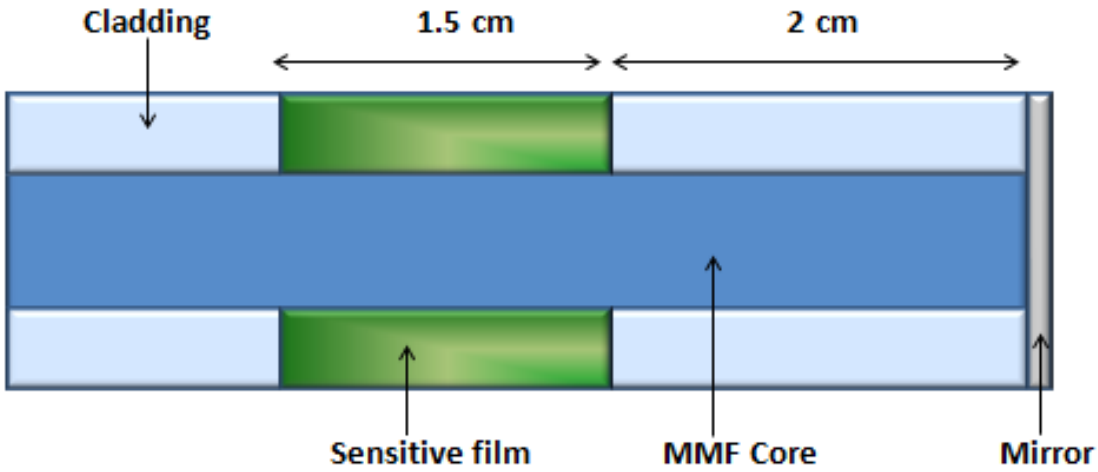

Fig.1. Schematic representation of the sensor head.

After this, a segment of 1.5 cm of the MMF cladding was carefully removed and cleaned with acetone to remove any remaining polymer waste. This section is located 2 cm away from the tip of the MMF. Finally, the un-cladded region was coated with the pH sensitive solution using a standard dip-coating technique and fully automated deposition system from Nadetech, Inc ® (Pamplona, Spain). The fiber was inserted and pulled out of the solution at a rate of 150 mm/min while the temperature was maintained at 100° C during the whole process. The coated MMF sensor head was kept at room temperature during 20 min, and then placed into an oven for thermally curing at 85° C for 15 min. The sensing head was always kept at room temperature for a day before any measurement. The reflection configuration setup (Fig.2) with the silver coated end facet reduces the size of the sensor and improves the performance of the sensor because the incident light passes twice through the sensitive region.

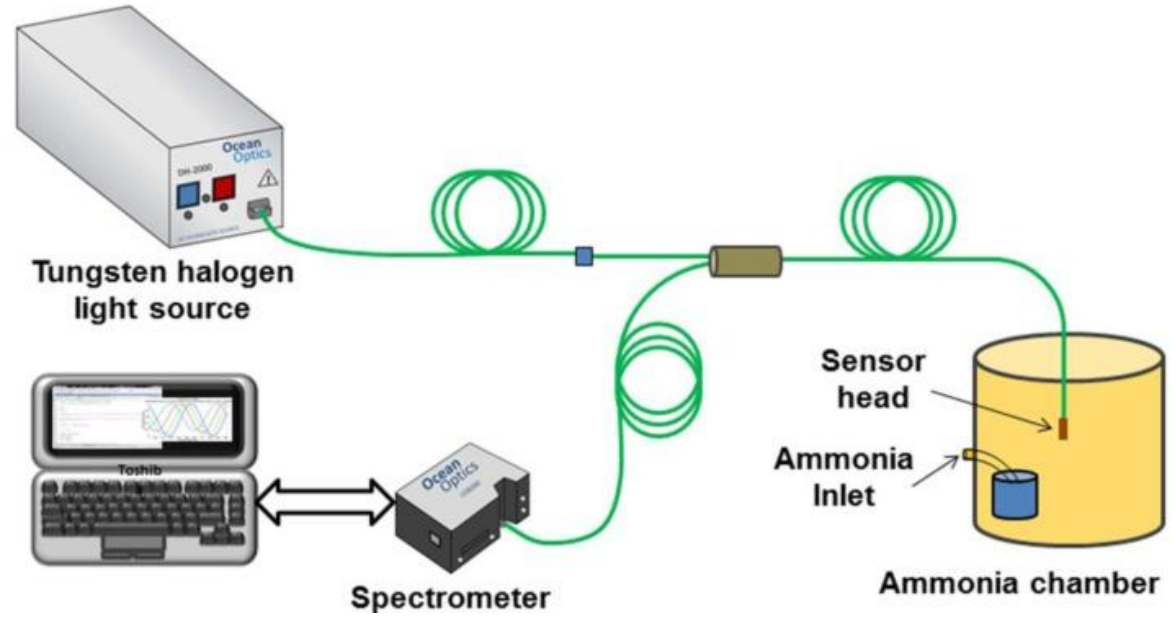

Fig. 2. Experimental setup for testing the ammonia sensor.

3.3.3. Experimental setup

The sensor heads were characterized using the experimental setup shown in Fig. 2. The optical source is a DH-2000-S tungsten halogen light source (Spectral Products, Puntnam, CT, USA), with an emission spectrum covering a wavelength range of 215 - 2,000 nm. The optical source is connected to a bifurcated assembly, UV-200-2 from Ocean Optics®. The response of the sensors was characterized using a sealed chamber of 300 mL in order to create a controlled gaseous ammonia environment. We used aqueous solution of ammonia (1 mo/L density od 0.73 g/L) to obtain concentrations of 10, 25, 50, 75 and 100 ppm into the chamber as it is shown in Fig. 2. These concentrations were used to evaluate the performance of the sensor within the permissible levels described before. The sensing head was inserted in the chamber without any contact with the aqueous solution of ammonia.

3.4. Experimental results

3.4.1. BCG pH indicator sensor characterization

In order to obtain the sensor response in the presence of different ammonia concentrations and the recovery time when ammonia is removed, the sensor was operated in several consecutive cycles at different concentrations of ammonia gas. First, a background reference was recorded when the sensor was exposed to air without ammonia gas. The ammonia concentration was modified from 0 to 100 ppm and the sensor was exposed to ammonia vapor during 20 min in each case. The BCG pH indicator has initially a green colour that changes to blue colour after the exposure to ammonia gas. As it has been mentioned before, ammonia acts as an acceptor of protons from the BCG pH indicator and increases the pH. The spectral response of the sensor is shown in Fig. 3.

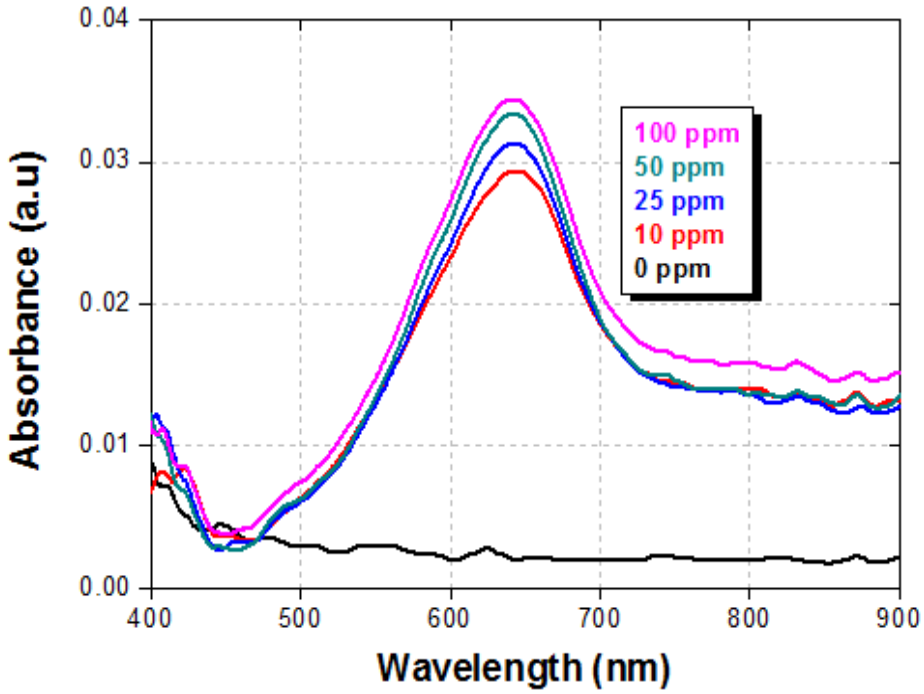

Fig. 3. Spectral response of the sensor based on BCG pH indicator subjected to different ammonia gas concentrations and air.

It is possible to see a single absorption peak around 640 nm, caused by the bluish colour that the pH sensitive film acquires under ammonia gas environment. It is important to say that this colour change is observed even by eye inspection. The spectral response from Fig. 3 is then integrated within the spectral range of 500 - 750 nm as a function of time. The dynamic response of the device at the four different ammonia concentrations is shown in Fig. 4.

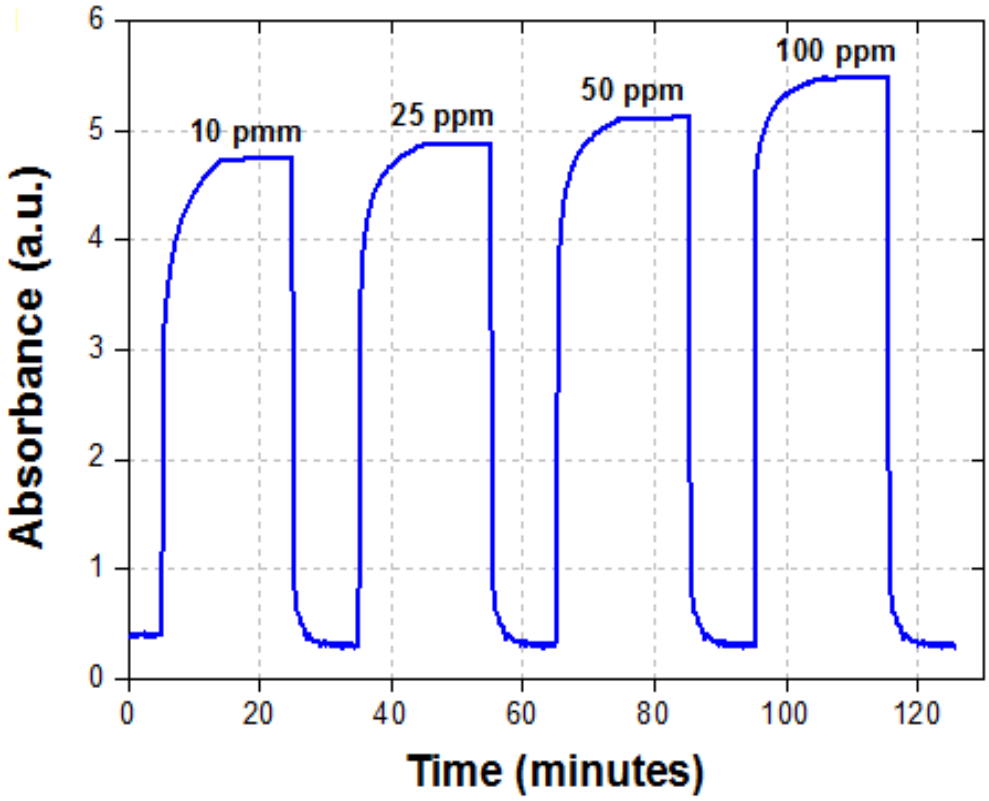

Fig.4. Dynamic response of the optical fiber sensor based on BCG pH indicator submitted to different ammonia gas concentrations.

We can observe that the absorption changes due to the presence of ammonia gas are reversible and the response returns to the original point in absence of ammonia in all cases. As shown in Fig. 4, the sensor exhibits a response time of 4 min for the measured value to rise at 90% of the maximum achievable value for each measured concentration. In contrast, the fall time in all

cases is quite fast with a maximum average duration of 15 s. Fig. 5 shows the curve obtained from this test, which shows a non-linear response of the device with the ammonia gas concentration. The maximum absorbance signal as a function of ammonia concentration is shown in Fig.5. Although the response is not linear, which is typical in this type of sensors, the response exhibits an R^2 value of 0.9964.

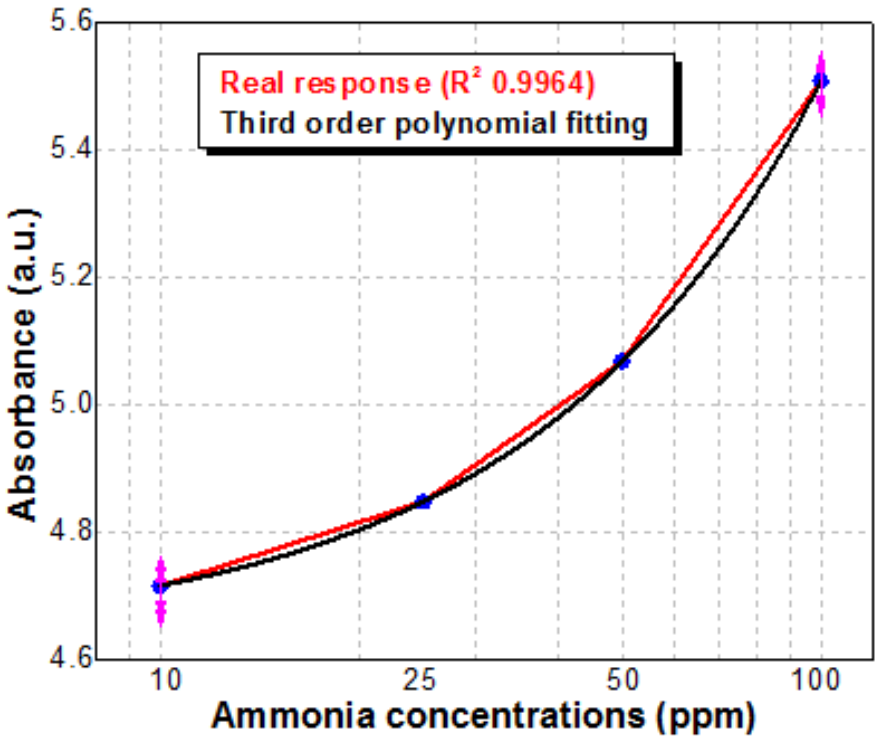

Fig. 5. Average response curve of the sensor based on BCG pH indicator for different concentrations of ammonia.

In order to test the repeatability and reversibility the sensor was exposed to three consecutive cycles of 20 min in the presence of 25 ppm of ammonia gas and 10 min in air; the results are plotted in Fig. 6, where it is easy to infer the highly repetitive and reversible optical fiber sensors response.

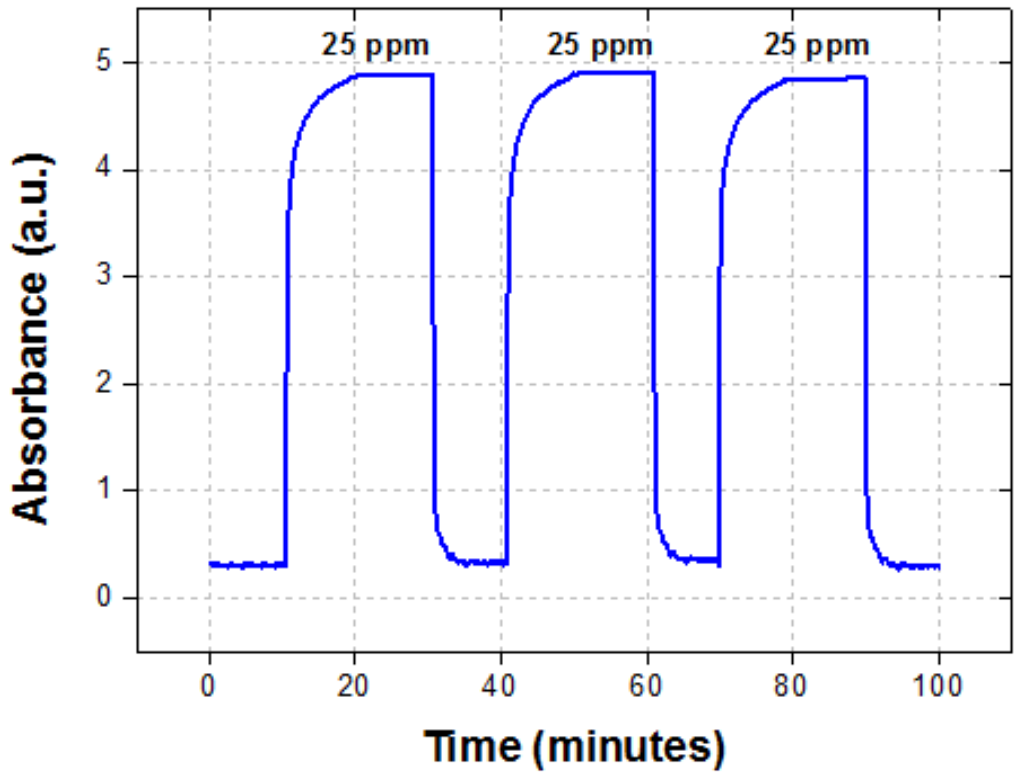

Fig.6. Dynamic response of the sensor based on BCG pH indicator when it is submitted to 25 ppm and air alternatively.

Since the maximum absorbance change occurs below 10ppm we believe that the sensor could be capable of detecting smaller ammonia concentrations, but this was not possible due to the sealed chamber conditions.

3.4.2. Universal pH indicator sensor characterization

The sensor was first characterized to determine its spectral response under the presence of 100 ppm ammonia. Prior to filling the chamber with ammonia, a background reference is recorded by taking the response of the sensor when exposed to air. This background is removed from any further measurement in order to observe the spectral changes resulting only from changes in the chamber atmosphere. As a result, a flat response should be obtained when the sensor is

again exposed to air, which confirms that the sensor performance has not been degraded. This is shown by the black line in Fig. 7.

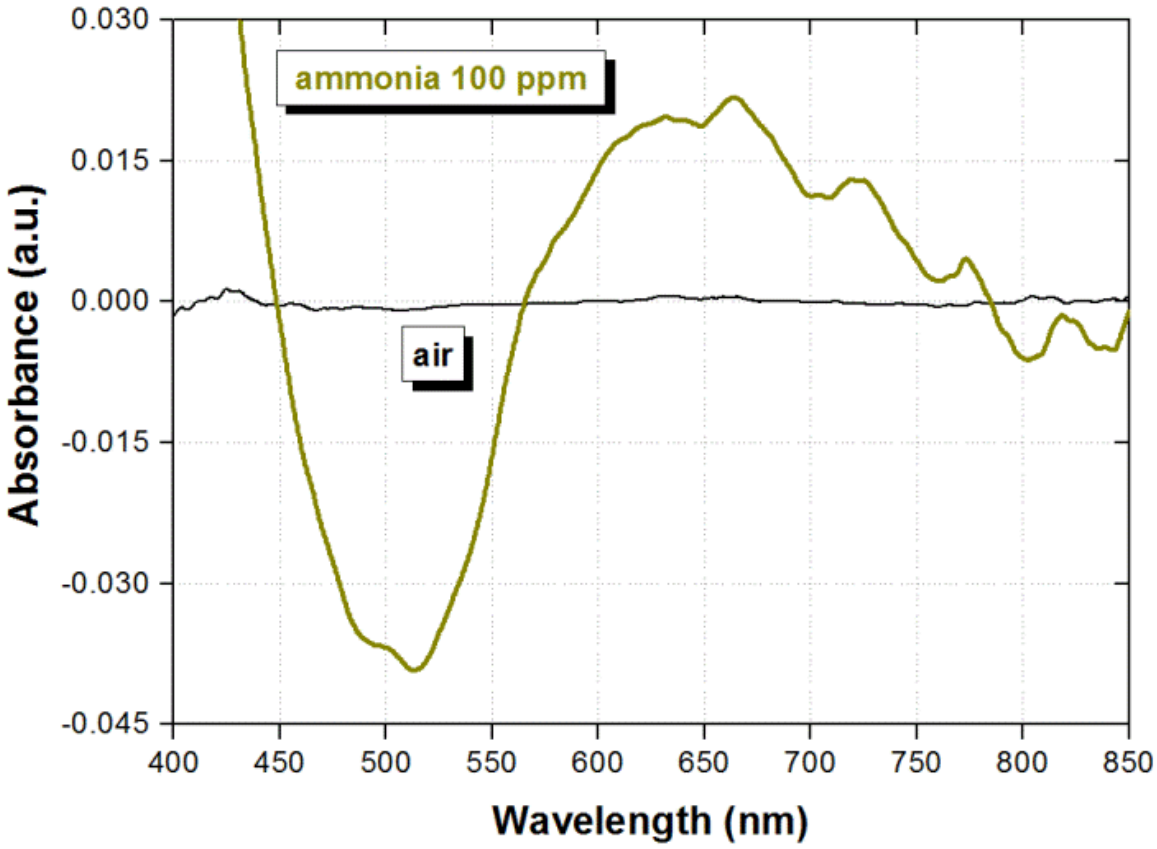

Fig. 7. Spectral response of the sensor based on Universal pH indicator subjected to air and 100 ppm of ammonia.

The spectral response of the sensor in the presence of 100 ppm of ammonia, after an exposure time of 20 min, is shown by the green line in Fig. 7. It is possible to observe two suitable measurement wavelength ranges in Fig. 7, where the sensor exhibits maximum absorption changes. A valley is formed around 500 nm as a result of the absorbance reduction, while a peak is formed around 650 nm as a result of the absorbance increase. Such differential response of the sensor is very convenient because, as it has been described earlier and will be shown in the next paragraphs, it enables perform ratiometric measurements as well as remove external disturbances not related to ammonia. The majority of the sensitive

films and dyes are susceptible to variations in temperature and humidity, which can interfere with the detected signal.

The feasibility of eliminating fluctuations in the sensor response due to external disturbances is better observed by exposing the sensor to different values of temperature and humidty. As shown in Fig. 8, when the temperature and humidity are modified, tha absorbance is increased around the wavelengths of 500 nm and 600 nm. In this case, the background was taken at a temperature of 21°C and humidity of 44%.

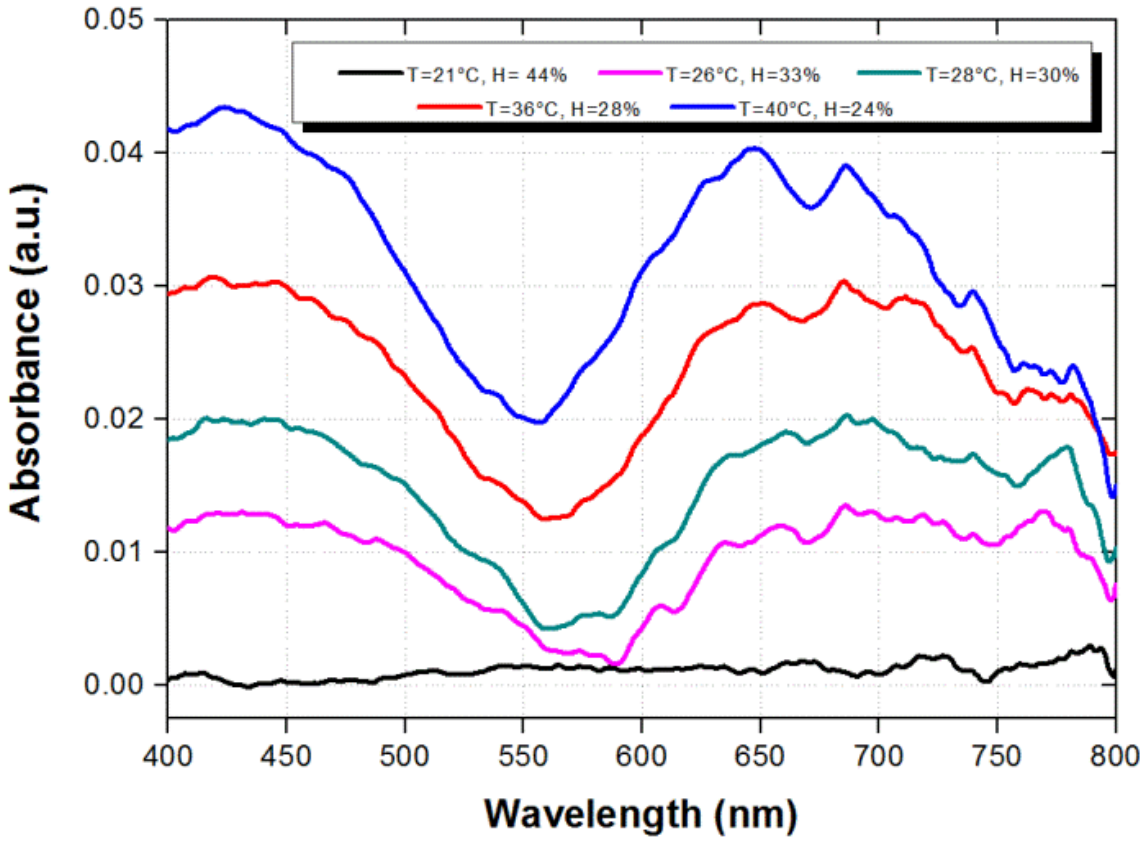

Fig. 8. Spectral response of the sensor based on Universal pH indicator for different values of temperature and humidity.

Since the sensor exhibits opposite response around the wavelength range of 500 nm when ammonia is detected, as compared to temperature and humidity changes, thus by taking the difference between the signals around 500 nm and 600 nm (ratiometric signal) we can eliminate such disturbances due to temperature and humidity while detecting the presence of ammonia. Although not critical under normal operation conditions, temperature and partial pressure, commonly associated to gas adsorption, should be also taking into account because they will also play an import role in the sensitivity of the device. In order to evaluate both, the sensor response in the presence of different ammonia concentrations and the recovery time when ammonia is removed, the sensor was operated in several consecutive cycles within the absence and presence of ammonia. The ammonia concentration was modified from 0 to 100 ppm and the sensor was exposed to ammonia vapor during 20 min in each case. A recovery time in the absence of ammonia (air atmosphere) of 10 min was also allowed between each ammonia concentration. The spectral response of the sensor under the different ammonia concentrations is shown in Fig. 9.

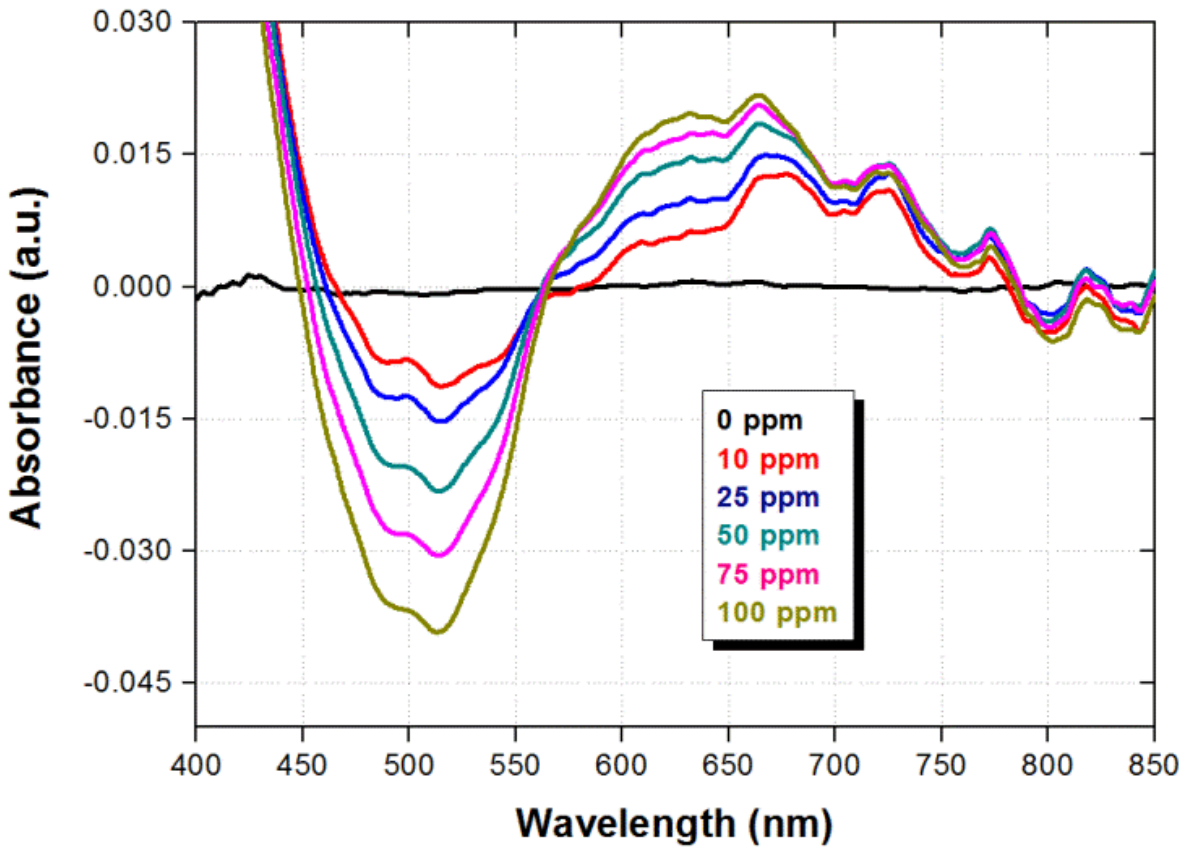

Fig. 9. Spectral response of the optical fiber sensor based on Universal pH indicator subjected to different ammonia concentrations where ratio is the difference between both signals.

It can be observed that the spectral response is modified in a similar way for all concentrations, and only the absorption is decreased/increased around the wavelengths of 500/650 nm as the ammonia concentration is increased. The absorbance variation as function of the pH/ammonia concentrations can be attributed to the utilization of different pH dyes that undergo colour changes at different pH/ammonia concentration values. The spectral response from Fig. 9 is then integrated within the spectral ranges of 450 – 550 nm and 600 – 700 nm and the difference between both signals is taken to obtain a ratiometric signal (ratio). The dynamic response of the three signals is shown in Fig. 10.

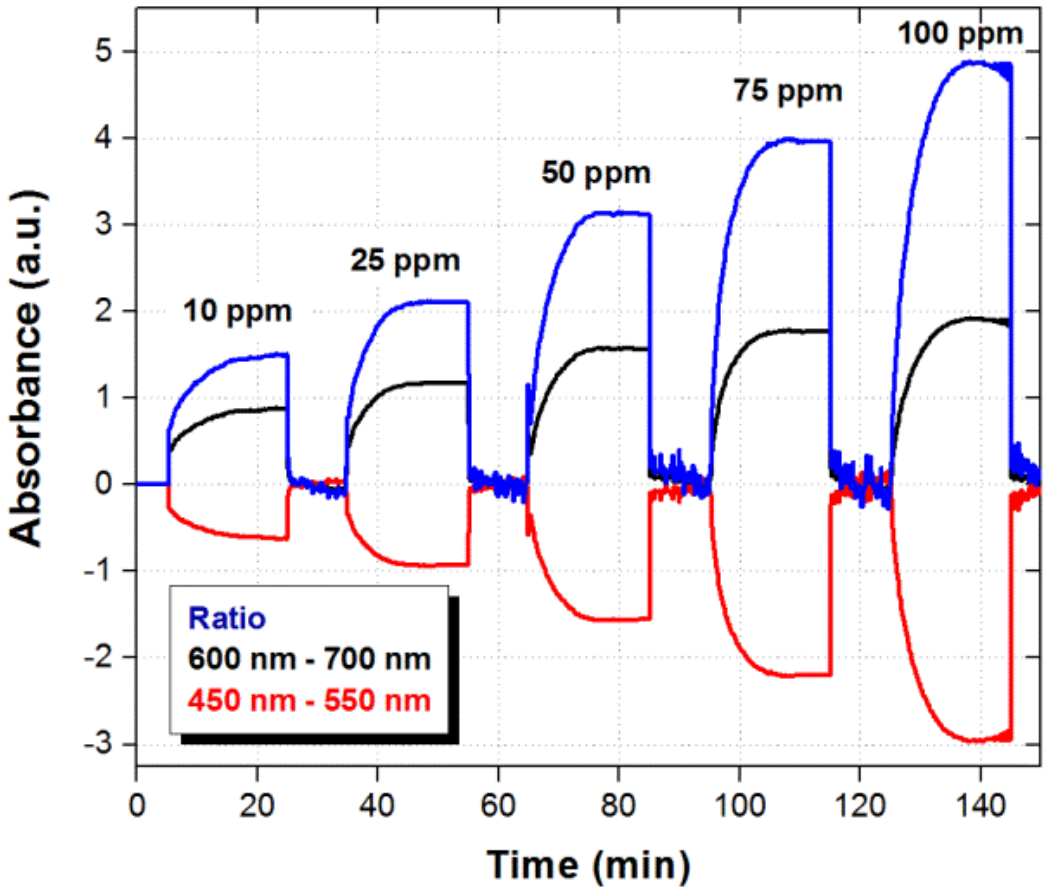

Fig. 10. Dynamic response of the optical fiber sensor based on Universal pH indicator subject to different ammonia concentrations where ratio is the difference between both signals.

As explained before, we can observe that the integrated signals also show opposite response, and the ratio of the signals provide an enhanced and robust response with a good dynamic range. We can also observe that the absorption changes due to the presence of ammonia are fully reversible and the signal returns to its original value after the ammonia is removed. As shown in Figure 10, the sensor exhibits a response time of five min for the measured value to rise at 80% of the maximum achievable value for each measured concentration. The fall time in all cases is quite fast with an average duration of 18 s.

In addition to an enhanced response, the ratiometric signal also allows us to discriminate signal fluctuations due to external factors. It is well known that pH indicators are sensitive to humidity and temperature, and this should also occur in our pH universal indicator. The sensor response to humidity and temperature was evaluated using a climatic chamber model Challenge 250 from Angelantoni Industry (Angelantoni Induestie, Massa Martana, Italy). As shown in Figure 11, the sensor was exposed to variations from 10% to 85% relative humidity (RH) and a temperature increment from 10°C to 30°C which falls outside the humidity changes. The optical absorbance as a function of the time was measured at the selected wavelengths ranges and the result are also shown in Fig. 11.

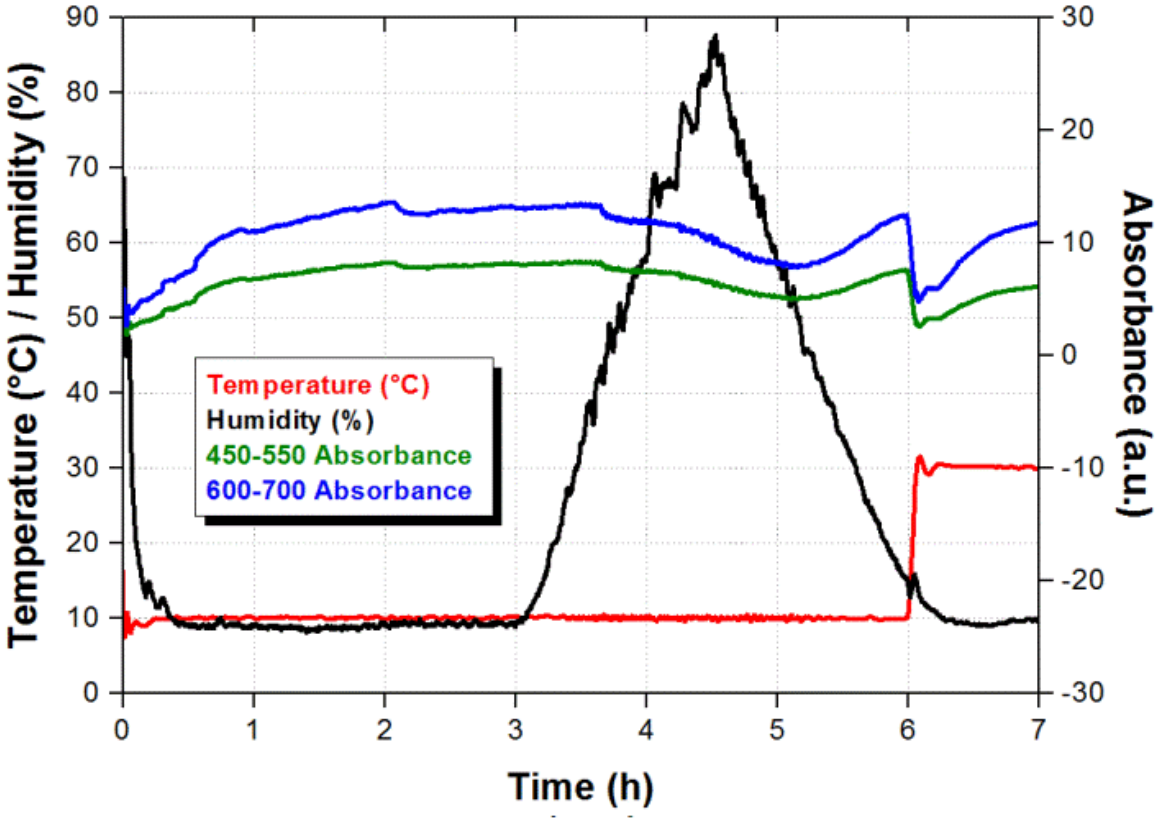

Fig. 11. Integrated signals as a function of time during humidity and temperature variations.

We can observe that the sensor response is slow and the absorbance is reduced as the humidity is increased. In the case of the temperature increment we notice an instantaneous reduction of the absorbance, which slowly recovers the

absorbance value at the beginning of the temperature increment. However, the most important result is that both integrated signals change not only in the same direction but also with similar proportion. Therefore, when we take the ratiometric measurement we obtain a correction factor that can be applied to the sensor response and eliminate the contributions due to humidity and temperature. As shown in Fig. 12, when the correction factor is not applied the ratiometric signal exhibits small variations as a result from humidity and temperature changes. Nevertheless, a flat response is obtained when the correction factor is taken into account. Since both integrated signals move to opposite directions in the presence of ammonia, the corrected ratiometric signal should be exhibit a clear step during the exposure to ammonia.

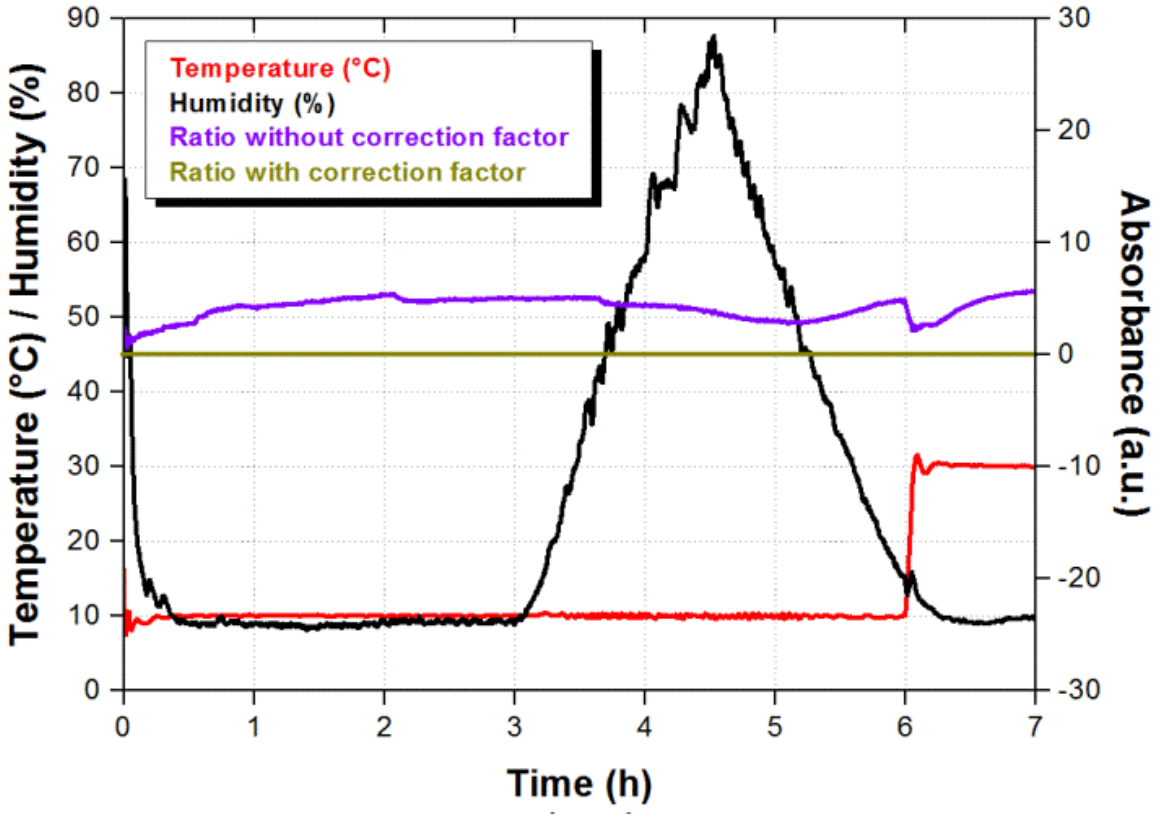

Fig.12. Ratiometric signal with and without correction factor.

The maximum ratiometric signal as a function of ammonia concentration is shown in Fig. 13. Although the response is not linear, which is typical in this type of sensors, the response exhibits an R^2 value of 0.9963.

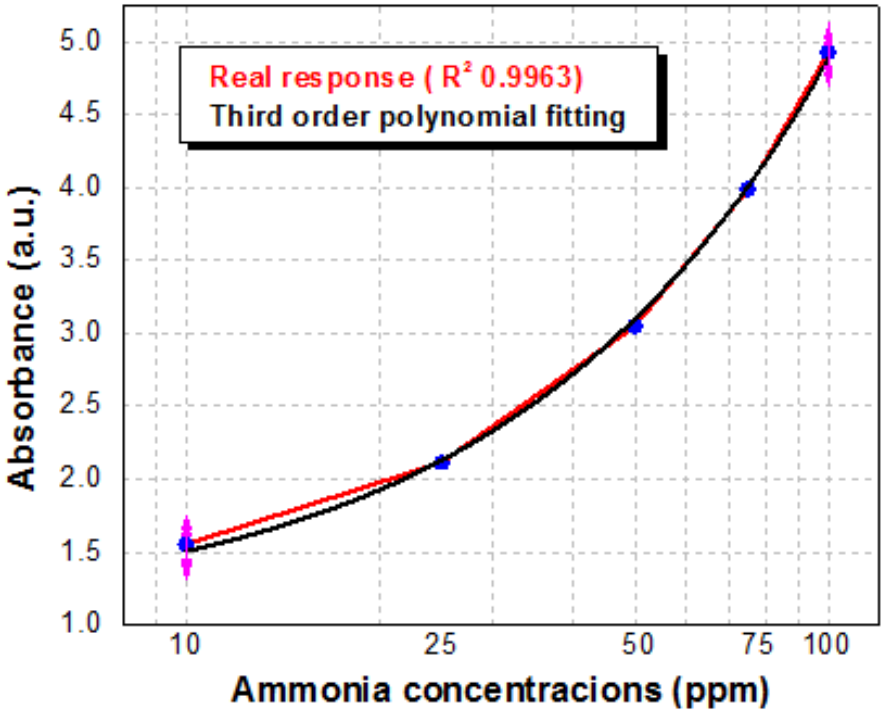

Fig. 13. Maximum ratiometric signal as a function of ammonia concentration.

The repeatability of the sensor was also evaluated by subjecting the sensor to consecutive cycles of 20 min in the presence of 25 ppm of ammonia and 15 min in air. As it is shown in Fig. 14, the signal reaches the same maximum value every time that the sensor is exposed to the 25 ppm of ammonia.

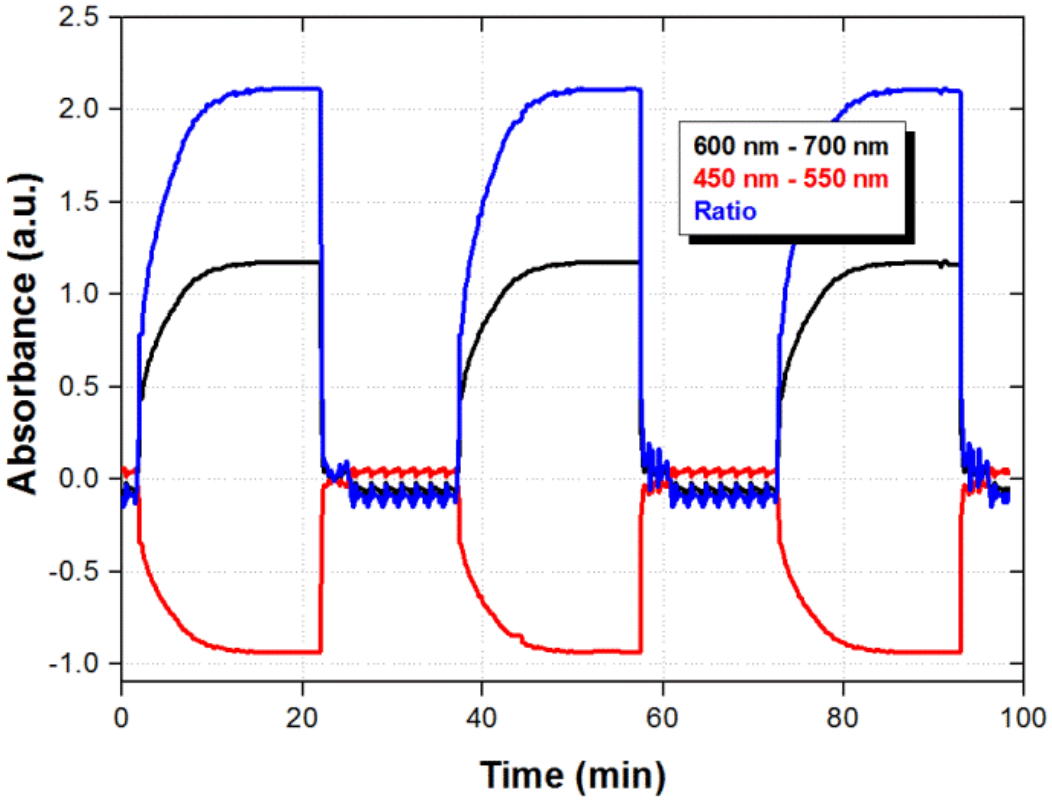

Fig. 14. Dynamic response of the sensor based on Universal pH indicator when submitted to consecutive cycles at 25 ppm of ammonia.

We can also notice that the fast recovery is preserved after different ammonia measurements. The results demonstrate a highly repetitive behavior of the sensor which is convenient for long term of operation. We should also highlight that the minimum ammonia concentrations of 10 ppm detected by the sensor is well below the recommended detection limit of 25 ppm. Based on the experimental dynamic range we believe the sensor should be capable od detecting smaller ammonia concentrations. Finally, considering the sensor configuration, we have in general three paramters that could be modified in order to improve sensitivity: film thickness, interaction length and MMF diameter. Ideally the film thickness could be increased in order to enhance the sensitivity, as long as the optical field interacts with the film. However the sensor response becomes slower since the gas has to penetrate a thicker film. Therefore, a thinner film with a longer interaction length is

preferred in this case. We could also reduce the diameter of the MMF in order to allow stronger interactions of the optical mode with the film. Such improvements should also increase the limit of detection of the sensor and will be the subject of future work.

3.5. CONCLUSIONS

We have fabricated sensitive optical fiber gas ammonia sensors using a BCG pH indicator and a mixture of pH indicators in a universal indicator. These sensors present a fast response time to different ammonia gas concentration and a fast recovery time. The indicators were also embedded in a Tecoflex® film that enables a more efficient operation of the sensor under different humidity conditions. The advantages of these sensors consist of a straightforward fabrication as well as good reproducibility and reversibility with ammonia exposure limits. The main difference between the pH BCG indicator and the pH Universal indicator is the spectral response to the presence of ammonia gas; that is, while the pH Universal indicator shows a valley around 500 nm as result of the absorbance reduction, while a peak is formed around 650 nm as result of the absorbance increase; the pH BCG indicator shows only a single absorption peak around 640 nm. The broadwavelength response of the pH Universal indicator provides a differential response that allows us to obtain ratiometric measurements of ammonia concentrations. The ratiometric measurements provide not only an enhanced output signal, but they also eliminate any external disturbances due to humidity or temperature fluctuations. Based on the experimental dynamic range we believe that the sensor could be capable of detecting smaller ammonia concentrations. We can also mention that the combination of the colourimetric pH indicators and Tecoflex® films as immobilizing matrix results in highly sensitive and robust ammonia gas fiber optic sensing devices. The sensors response could be

easily optimized attending to three parameters: film thickness, interaction length, and MMF diameter.

REFERENCES

1. B. Timmer, W. Olthuis, A. van den Berg, “Ammonia sensors and their applications-A review”, Sens. Actuators B Chem., vol. 107,pp. 666-67, 2005.
2. United States Environmental Protection Agency (EPA). Ammonia. Available online: http://www.epa.gov/caddis/ssr_amm_int.html. (Accessed on: 24 June 2014).
3. B. Lee, “Review of the present status of optical fiber sensors. Opt. Fiber Technol., vol. 9, pp. 57–59, 2003.
4. M.D. Marazuela, M.C. Moreno-Bondi, “Fiber-optic biosensors-an overview”, Anal. Bioanal. Chem., vol. 372, pp. 664–682, 2002.
5. F.J. Arregui, M. Otano, C. Fernandez, I.R. Matias, “An experimental study about the utilization of Liquicoat® solutions for the fabrication of pH optical fiber sensors”, Sens. Actuators B Chem, vol. 87, pp. 289–295, 2002.
6. C. Wenquing, D. Yixiang, “Optical fiber-based evanescent ammonia sensor”, Sens. Actuators B Chem, vol. 100, pp. 252–259, 2002.
7. P. Bhatia, B.D. Gupta, “Surface plasmon resonance based fiber optic ammonia sensor utilizing bromocresol purple”, Plasmonics, vol. 8, pp. 779–784, 2013.
8. M. Ahmad, N. Mohammad, “Sensing material for oxygen gas prepared by doping sol-gel film with tris (2,2- bipyridyl) dichlororuthenium complex”, J. Non Cristaline Solids, vol. 209, pp. 86–91, 2001.
9. S. Tao, L. Xu, J.C. Fanguy, “Optical fiber ammonia sensing probes using reagent immobilized porous silica coating as transducers”, Sens. Actuators B Chem., vol. 115, pp. 158–163, 2006.
10. F.J. Arregui, D. Galbarra, I.R. Matias, K.L. Cooper, R.O. Claus, ZrO2 thin films deposited by the electrostatic self-assembly method on optical fibers for ammonia detection. In Proceedings of the 15th Optical Fiber Sensors

Conference Technical Digest, Portland, OR, USA, pp. 265–268, 10 May 2002.

11. C.R. Zamarreño, J. Bravo, J. Goicoechea, I.R. Matias, F.J. Arregui, “Response time enhancement of pH sensing films by means of hydrophilic nanostructured coatings”, Sens. Actuators B Chem., vol. 128, pp. 138–144, 2007.
12. T. Werner, I. Klimant, O.S. Wolfbeis, “Ammonia-sensitive polymer matrix employing immobilized indicator ion pairs”, Analyst, vol. 120, pp. 1627–1631, 1995.
13. A. Mills, L. Wild, Q. Chang, “Plastic colourimetric film sensors for gaseous ammonia”, Mikrochim, vol. 121, pp. 225–236, 1995
14. C. Malins, M. Landl, P. Simon, B.D. MacCraith, “Fibre optic ammonia sensing employing novel near infrared dyes”, Sens. Actuators B Chem., vol. 51, pp. 359–367, 1998.
15. J. Goicoechea, C.R. Zamarreño, I.R. Matias, F.J. Arregui, “Optical fiber pH sensors based on layer-by-layer electrostatic self-assembled Neutral Red”, Sens. Actuators B Chem., vol.132, pp. 305–311, 2008.
16. J. Moreno, F.J. Arregui, I.R. Matias, “Fiber optic ammonia sensing employing novel thermoplastic polyurethane membranes”, Sens. Actuators B Chem., vol. 105, pp. 419–424, 2005.
17. T.D. Rhines, M.A. Arnold, “Simplex optimization of a fiber-optic ammonia sensor based on multiple indicators”, Anal. Chem., vol. 60, pp. 76–81, 1988.
18. P. Çaglar, R. Narayanaswamy, “Ammonia-sensitive fibre optic probe utilising an immobilised spectrophotometric indicator”, Analyst, vol. 112, pp. 1285–1288, 1987.
19. M. Trinkel, W. Trettnak, F. Reininger, R. Benes, P. O’Leary, O.S. Wolfbeis, “Optochemical sensor for ammonia based on a lipophilized pH indicator in a hydrophobic matrix”, Int. J. Environ. Anal. Chem, vol. 67, pp. 237–251, 1997.

20. A. Lobnik, O.S. Wolfbeis, “Sol-gel based optical sensor for dissolved ammonia”, Sens. Actuators B Chem., vol. 51, pp. 203–207, 1998.
21. M. Trinkel, W. Trettnak, F. Reininger, R. Benes, P. O’Leary, O.S. Wolfbeis, “Study of the performance of an optochemical sensor for ammonia”, Anal. Chim. Acta, vol. 320, pp. 235–243, 1996.
22. A. Goñi Soto, “Estudio de nuevos materiales para su aplicación en la fabricación de sensores de fibra óptica”, Tesis de Ingeniería, Universidad Pública de Navarra, 2003.
23. J. Moreno, “Medicion de variables químicas mediante un sensor de fibra óptica”, Proyecto Final de Carrera, Universidad Pública de Navarra, 2002.
24. C. Wenquing, D. Yixiang, “Optical fiber-based evanescent ammonia sensor”, Sens. Actuators B Chem., vol. 110, pp, 252-259, 2005.
25. J.B. Kuo, T.L. Chou, “Optical Waveguide Sensors using Evanescent Wave Excitation of fluorescent Dye in Sol Gel Glass”, Electronic Letters, vol. 27 (14), pp. 1247-1249, 1991.
26. M. Ahmad, N. Mohammad, “Sensing material for oxygen gas prepared by doping sol-gel film with tris (2,2- bipyridyl) dichlororuthenium complex”, Journal of Non Cristaline Solids, vol. 290, pp. 86-91, 2001.
27. V. Chernyak, R. Reisfeld, R. Gvishi, D. Venezky, “Oxazine-170 in sol-gel glass and PMMA films as a reversible optical waveguide sensor for ammonia and acids”, Sensors Mater (Japan), vol. 2, p.117, 2002.
28. F.J. Arregui, D. Galbarra, I.R. Matias, K.L. Cooper, R.O. Claus, ZrO_2 thin films deposited by the electrostatic self-assembly method on optical fibers for ammonia detection, in: The 15th Optical Fiber Sensors Conference Technical Digest, Portland, OR, pp. 265-268, 2002.
29. D.A. Chang-Yen, Yuri Lvov, M.J. McShane, Electrostatic self-assembly of a ruthenium-based oxygen sensitive dye using polyion-dye interpolyelectrolite formation, Sensors Actuators B Chem. vol. 87, pp. 336-345, 2002.

30. C. Malins, M. Landl, P. Simon, B.D. MacCraith, “Fibre optic ammonia sensing employing novel near infrared dyes”, Sens. Actuators B Chem. vol.51, pp. 359-367, 1998.
31. Lubrizol Corporation. Material Data Center Datasheets. Available online: http://www.materialdatacenter.com/ms/en/Tecoflex/The+Lubrizol+Corporation/Tecoflex%C2%AE+SG-80A/5bf9ca76/2418 (accessed on 25 October 2013).
32. J. Moreno, F. J. Arregui, I.R. Matias, “Fiber optic ammonia sensing employing novel thermoplastic polyurethane membranes”, Sens. Actuators B Chem. vol. 105, pp. 419-424, 2004.
33. R. Raghuvir, Fibre-optic probe for the measurement of fluid parameters, patent No. WO9410553, 1994.
34. M.A. Raggi et al., “A calorimetric assay for dicyclomine hydrochloride using bromocresol green”, Journal of Pharmaceutical and Biomedical Analysis, vol. 3(3), pp. 287-291, 1995.
35. D.N. Agbaba, D. Radovic, “Spectrophotometric determination of molsidomine in pharmaceutical formulations using bromocresol green”, Journal of Pharmaceutical and Biomedial Analysis, vol. 11(3), pp. 247-249, 1993.
36. J.A. Breland and R.H. Byrne, “Spectrophotometric procedures for determination of sea water alkalinity using bromocresol green”, Deepsea Research Part I Oceanographic Research Papers, vol. 40 (3), pp. 629-641, 1993.
37. D. Webster et al., “An assessment of the suitability of bromocresol green for the determination of serum albumin”, Clinica Chimica Acta, vol. 53 (1), pp.101-108, 1974.
38. Sigma-Aldrich, Bromocresol Green. Available online: http://www.sigmaaldrich.com/catalog/product/sial/114359?lang=es&region=MX (Accesed on: 28 June 2014).

39. A. Mills, L. Wild, Q. Chang, “Plastic Colourimetric Film Sensors for Gaseous Ammonia”, Mikrochim. Acta 121, pp. 225-236, 1995.
40. Indicador Universal de pH. Available online: http://www.patacake.net/panreac/spanish/catalogo/fichastec/281370ES.HTM (accessed on 25 October 2013).
41. F. J. Arregui, M. Otano, C. Fernandez-Valdivielso, I. R. Matias, “An experimental study about the utilization of Liquicoat ® solutions for the fabrication of pH optical fibers sensors”, Sens. Actuators B Chem., vol. 87, pp. 289-295, 2002.

CHAPTER IV. FIBER OPTIC SENSOR APPLIED IN ETHANOL INDUSTRY

ABSTRACT

In this chapter, we propose and demonstrate the fabrication of an optical fiber sensor based on multimode interference effects (MMI) with applications in two of the most important areas in ethanol industry: alcoholic beverages (Rum) and combustibles (Gasohol). The operation of the MMI rum sensor relies on the fact that when rum is adulterated, which can be done either with ethanol or ethylene glycol, the refractive index (RI) of the adulterated rum will be different as compared to the original rum. Since the white rum (Bacardi®) has a RI close to 1.345 and the highest RI of the contaminant is 1.412 (ethylene glycol), the RI of the adulterated rum will increase as the volume of the contaminant is increased. Therefore, considering that the MMI sensor exhibits a sensitivity of 258.06 nm /RIU for liquids with RI ranging from 1.318 to 1.4203, we can accurately determine if a rum sample is free of contaminants or adulterated with other liquid, which is typically performed using ethanol or toxic elements like ethylene glycol. Although the sensor cannot determine which kind of liquid is altering the rum, it can easily detect when the original rum has been adulterated, even with small amounts of liquid. The sensor also provides high repeatability and reversibility while using a fast and simple fabrication process. The operational principle of the MMI gasohol sensor relies on the fact that the addition of ethanol to the gasohol blend reduces the refractive index (RI) of the gasoline. Since MMI sensors are capable of detecting small RI changes, the ethanol content of the gasohol blend is easily determined by tracking the MMI peak wavelength response. Gasohol blends with ethanol content from 0% to 50% have been clearly identified using these devices obtaining a linear response with a maximum sensitivity of 0.270 nm/%ETOH. The sensor can also

distinguish when water incorporated in the blend has exceeded the maximum volume tolerated by the gasohol blend, which is responsible for phase separation of the ethanol and gasoline and could cause serious engine failures. Since the MMI gasohol sensor is straightforward to fabricate and does not require any special coating it is a cost effective solution for real time and in-situ monitoring the quality of gasohol blends.

4.1. INTRODUCTION

Ethanol comes from corn and sugar cane as well as from cellulosic biomass, trees and grasses. At room temperature and pressure is a colorless volatile liquid; widely used in the elaboration of alcoholic beverages and in the pharmaceutical sector, as an active ingredient of some medicines and cosmetics; also employed as industrial and domestic fuel; as a good solvent, and can be also used as antifreeze [1, 2]. Ethanol industry provided a significant contribution to the economy of United States in 2005 adding $17,700 billion of dollars; make expenditures by approximately $5, billion in inputs (mainly corn) and $2,400 million to expand production capacity, that is, expansion and construction of new refineries [3].

In this chapter, the design and development of a fiber optic sensor based on MMI effects for monitoring the quality of two products based on Ethanol are presented: Rum as alcoholic beverage and Gasohol blends based on ethanol and ordinary gasoline.

4.1.1. Ethanol for the preparation of rum alcoholic beverage

Depending on the type of alcoholic beverage, ethanol appears accompanied by various chemicals that give it color, taste, and smell, among other features. A standard practice in most countries, which is required by law, is to specify how

much ethanol is contained in an alcoholic beverage. This is typically done by displacing on the bottle label the percentage of alcohol by volume. The key objective of such regulations is to maintain the quality of the beverage, but mainly to prevent harm to human beings due to alcohol intoxication. Meanwhile, ethylene glycol (EG) is used in the adulteration of alcoholic beverages as a solvent and antifreeze, and the toxicity is due to the accumulation of metabolites [4, 5].

Among the variety of commercial alcoholic beverages, rum is the most consumed worldwide [6], which makes it an easy target for adulteration. As a result, instruments that could accurately detect contaminants in alcoholic beverages are highly desirable. In optical fiber sensors area, some approaches have been investigated using optofluidic Bragg fiber array [7], plastic optical fibers [8], optical fiber sensors arrays [9] has been reported. Additionally, other works incorporate thin films around the fiber [10] and quantum dots [11] attached to the optical fiber. However, the main inconvenient in these systems is the need for special preparation of the fiber or the deposition of a sensitive material. A fiber sensor that can be suited for the detection of adulterated alcoholic beverages is the one based on multimode interference (MMI) effects. MMI devices can be very sensitive to RI changes of liquids [12-14] and, since this is a parameter that is modified when ethanol and EG is added to an alcoholic beverage, they are well suited for this work. In this chapter, is demonstrate the application of a MMI fiber sensor as a tool to monitor the adulteration of rum with another liquid, which is typically performed using either ethanol or ethylene glycol. Although the sensor cannot determine which kind of liquid is altering the rum, it can easily detect when the original rum has been adulterated, even with small amounts of liquid. The sensor can be operated by following either spectral shifts or intensity changes as long as external intensity fluctuations are removed from the experimental setup. The advantages of the sensor are that its fabrication is straightforward, and

exhibits great reproducibility and reversibility, with no significant interference against temperature or humidity.

4.1.2. Ethanol for the preparation of gasohol combustible

As a consequence of the growing demand of petroleum and green combustible, some alternatives have been proposed as renewable fuel sources. In this sense, methanol and ethanol are also used as fuel, especially when mixed with gasoline. However, methanol has received less attention than ethanol because it is highly toxic, extremely volatile and therefore would increase the risk of fire or explosion [15]. Ethanol has become a very popular choice as fuel (E100) in markets such as Brazil, USA, Sweden, Thailand and others, with the advantage that combustion is less polluting and highly oxygenated. The resulting fuel mixture of ethanol and gasoline is called gasohol [16, 17]. Two common blends are E10 and E85, with ethanol content of 10% and 85%, respectively. Since alcohol has corrosive properties, special adaptations to conventional engine vehicles that employ ordinary gasoline are required; otherwise the engine is at risk of degradation in some component materials as well in the fuel system [18]. Since ethanol has lower price (about 60%) than gasoline, a common malpractice is to increase ethanol concentration in the mixture that is sold to car owners. Therefore, the gasohol blend and their water content should be monitored not only when the blend is distributed, but also in real time when gasohol is being used. Optical fibers sensors are an attractive option due to their inherent characteristics mentioned above in last chapters. Some approaches have been investigated using Long Period Gratings [19], Fiber Brag Gratings [20] and incorporating sensitive polymer around the fiber [21-25]. However, the main inconvenient in these systems is the need for a special preparation of the fiber or the deposition of a sensitive material. A fiber sensor that can be suited for the detection and identification is the one based on multimode interference effects (MMI). In this Chapter, is demonstrate efficient quality control of a variety of gasohol blends using MMI fiber sensors. As we

previously explained a particular gasohol blend is defined by the volume concentration of ethanol incorporated into the blend. Considering that ethanol has a smaller refractive index than gasoline, we expect that gasohol blends with higher ethanol content will exhibit a smaller RI than gasoline. Since MMI sensors are capable of detecting small RI changes, accurate control of gasohol blends is realized in a simple way. Additionally the sensor is capable of detecting when water incorporated in the blend has exceeded the maximum volume tolerated by the gasohol blend, which is responsible for phase separation of the ethanol and gasoline. We should highlight that since the sensor does not require any particular coating its fabrication is rather simple and inexpensive.

4.2. PRINCIPLE OF OPERATION

As shown in Eq. (24) in Chapter II, the peak wavelength can be shifted when the effective RI and diameter are modified, which can be achieved via the evanescent field of the propagating modes. In order to allow the modes to interact with the surrounding media we use a MMF known as No-Core fiber, which is a MMF without cladding (i.e. air is the cladding). Therefore, when the MMI device is immersed in a liquid, such ethanol, rum, gasohol, gasoline or ethylene glycol, the index contrast between core and liquid cladding will be reduced which increases the effective diameter and RI of the fundamental mode. The net result is that the MMI peak wavelength will be shifted to longer wavelengths as the RI of the liquid is increased.

In order to discriminate the liquid mixtures, the spectral separation between the transmitted MMI peaks when the No-core fiber is surrounded by ethanol and gasoline has to be clearly identified. Using finite element method software (COMSOL multiphysics) we can obtain the effective diameter and RI of the fundamental mode, when the MMI is immersed in two different liquids, and these values are the used in Eq. (24) in Chapter II to obtain the transmitted MMI peak

wavelength for a fixed MMF length. The no-Core MMF parameters used in the simulations are a core RI of 1.444 and a diameter of $125\ \mu m$. We consider the RI at 1550 nm of a liquid substance with RI of 1.3622 and a liquid substance of RI 1.4223 respectively [26]. The length of the No-Core fiber was taken as 58.98 mm, which corresponds to a better curve. As shown in Fig. 1 in the case of ethanol the transmitted peak is located at 1560.75 nm whilst for gasoline is located at 1582 .08 nm. The peak-to-peak difference of 21 nm should be enough to identify different gasohol mixtures whose MMI peak wavelength will within this range. Nevertheless, as will be shown later, we can slightly increase the sensitivity by reducing the diameter of the No-Core fiber.

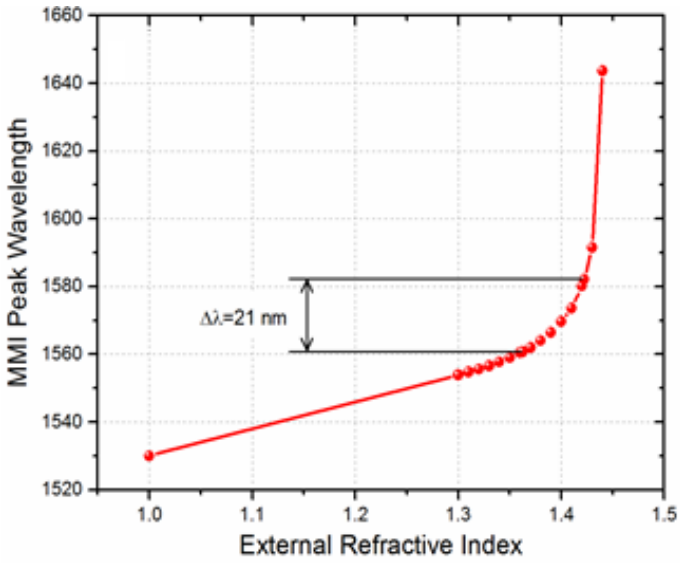

Fig.1. MMI peak wavelength response as a function of the RI of the external media.

4.3. RUM ADULTERATION DETECTION USING AN OPTICAL FIBER SENSOR BASED ON MULTIMODAL INTERFERENCE EFFECT (MMI)

4.3.1. Experimental procedure.

The No Core-MMF used in our experiments is provided by Prime Optical Fiber Corporation. Prior to fabricate the MMI sensor we need to obtain the exact

length of the No Core-MMF that will provide the desired MMI peak wavelength. The length of the No Core-MMF is calculated using Eq. (24) in Chapter II for a wavelength of 1550 nm. The effective RI and diameter correspond to values of $n_{MMF} = 1.444$ and $D_{MMF} = 125\ \mu m$. Using these values in Eq. (24) in Chapter II, for the case of the fourth self-image $(p = 4)$, we obtain a length of $58.22\ mm$ for the No Core-MMF. The MMI sensor is fabricated by first splicing the No Core-MMF to a SMF using standard splicing procedures. It is important to mention that the polymer cladding around the No Core-MMF is entirely removed. In fact, after mechanically stripping the polymer, the No Core-MMF is immersed in acetone to eliminate any residue. Using a micrometer, we can then control the length of the No Core-MMF to be cleaved with a length of 58.22 mm. After cleaving, this end is spliced to the output SMF and the MMI sensor is ready for testing. The experimental setup for testing the MMI sensors is shown in Fig. 2. The broadband optical source was a superluminiscent diode (SLD) centered at 1550 nm. The SLD is connected to the input SMF of the device, and the output SMF is then connected to an optical spectrum analyzer (OSA) Anritsu MS9740A to capture the transmitted spectrum. The SLD was operated using current and temperature controllers, Thorlabs LDC220C and TED200C respectively, in order to avoid intensity fluctuations from the optical source. Sharp radius of curvature was also eliminated and the remaining fiber was fixed to the optical table to prevent intensity variations from the optical fiber itself.

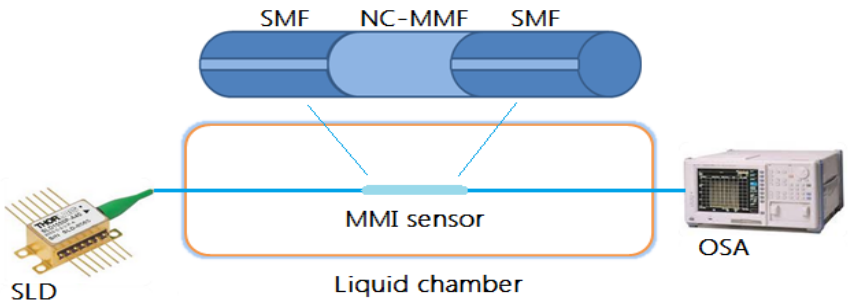

Fig. 2. Experimental setup.

As shown in Fig. 2 the sensor was fixed in a channel which was then covered to form small chamber. The chamber included input and output plastic tubes to facilitate insertion and removal of the liquids. We should also mention that when a MMI device is bent the MMI spectral response could be also shifted [27]. However, such effect is observed for small radius of curvature (i.e. large bending) which is not the case in our experimental setup. Nevertheless, in the case of intensity measurements, the MMI sensor is tensioned using a weight of 25 gr to minimize any bending due to surface tension in the channel. In the case of spectral measurement a weight of 5 gr is used, which guarantees that no spectral shifts are observed while maintaining the fiber with small tension. Since both optical fibers and liquids are sensitive to temperature, the measurements were performed at a controlled temperature of 25°C.

Regarding the rum used in our experiments, although we have a wide range of brands available in the market, we selected Bacardi® White Rum (750 ml bottle) because it is well known worldwide. Certified rum was used in order to guarantee that it was not adulterated prior to our experiments, and the percentage of alcohol by volume was 40% as indicated in the rum label. We should also mention that in the market we can also find other rum presentations ranging from 375 ml, 750 ml, 980 ml, 1750 ml, 2000 ml, and 3 liters, all of them having 40% of alcohol by volume. However, changes on the optical properties of the rum due to the presentation are not expected as long as they belong to the same batch. In the case of different production batches, slight changes could be expected due to slight fluctuation during the fabrication processes.

The response of a MMI sensor immersed in liquids with different refractive indexes was evaluated to obtain the sensitivity of the sensor. Mixtures of water and glycerin were prepared at different proportions to obtain a range of liquids with refractive indexes ranging from $n = 1.318$ (100% water) to $n = 1.4203$ (30% water /

70% glycerin) [28, 29]. As shown in Fig. 3, the peak wavelength is red shifted as the RI of the liquid is being increased.

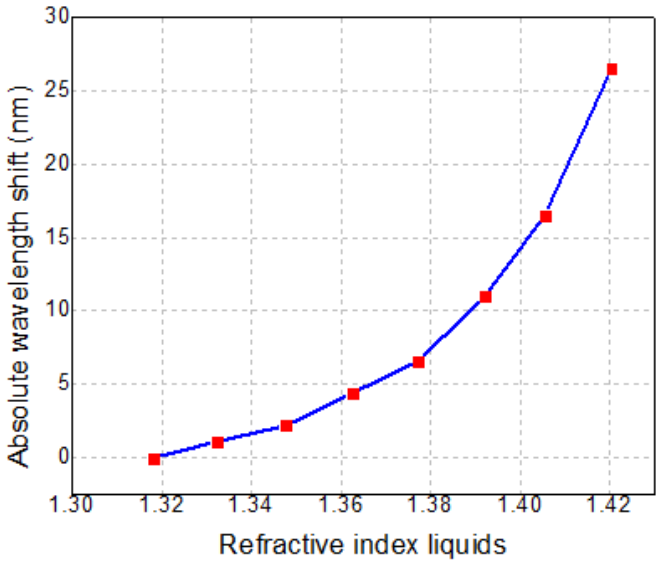

Fig. 3. MMI peak wavelength shift as a function of the liquid RI.

While both effective RI and diameter of the No Core-MMF are being altered, the quadratic behavior of the plot in Fig. 3 means that the diameter is the dominating factor associated to its square dependence. Since adulteration of rum will basically modify the RI of the rum, the sensor is well suited for such application. A sensitivity of 258.06 nm/RIU can be estimated from Fig.3. This device is also used to obtain the RI of rum, anhydrous ethanol, and ethylene glycol. This is performed by correlating the MMI peak wavelength shift that is experimentally observed with their corresponding refractive index obtained in Fig.3, and their values are shown below.

4.3.2. Experimental results

The spectral response of the MMI sensor for the liquids involved in our experiments is shown in Fig. 4.

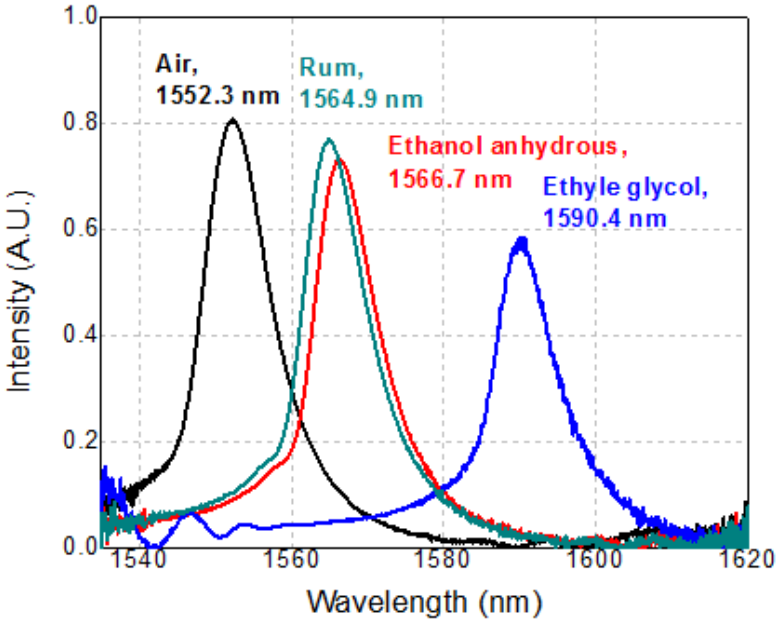

Fig. 4. Spectral response of the MMI sensor for different liquids.

As shown in Fig. 4 (black line) the peak wavelength in air is at 1552.3 nm which is very close to the design wavelength of 1550 nm. The difference can be attributed to slight differences in RI diameter, as well as to the errors in the No Core-MMF length due to our cleaving stage. Nevertheless, MMI devices fabricated afterwards exhibit the same peak wavelength and the error can be easily eliminated. When a sample of rum ($n{\sim}1.345, \lambda = 1550\, nm, T = 25°C$) is inserted in the channel we can observe a wavelength shift of 12.67 nm, with the peak wavelength at 1564.9 nm. This peak wavelength is our reference when the rum has not been adulterated. When the sensor is exposed to anhydrous ethanol ($n{\sim}1.3464, \lambda = 1550\, nm, T = 25°C$) provided by Sigma-Aldrich®, the peak wavelength is shifted to 1566.7 nm. Although the shift is relatively small ($\sim 1.8\, nm$) it can be easily resolved by the OSA. The largest wavelength shift is observed when EG (($n{\sim}1.412,\ \lambda = 1550\, nm, T = 25°C$) provided by Sigma-Aldrich® is covering the sensor and exhibiting a wavelength shift of 25.5 nm. Taking into

account previous results we should be able to identify when a rum sample has been adulterated by comparing the measured peak with that of our pure rum reference. As we mentioned before, this sensor does not determine if the liquid in the mixture is anhydrous ethanol, EG or both but it is capable of resolving if the original rum has been altered even for small amounts of liquid. We should highlight that we are using anhydrous ethanol, rather than standard ethanol, because ethanol has a tendency to adsorb water and this can alter his RI value. It is also important to notice that, the peak intensity should increase as the RI is being increased due to the reduction of scattering losses. However, in the experimental test the signal is reduced due to small bending of the fiber which does not affect the peak wavelength at all. Since industrial ethanol is relative inexpensive, the addition of certain amounts of ethanol to rum is the simplest way of adulteration. We prepared solutions of rum with different volumes of anhydrous ethanol. The starting point is 10 ml of pure rum, and we replace certain volumes with anhydrous ethanol. As shown in Fig. 5, as the volume of anhydrous ethanol is increased the spectral response is shifted to longer wavelengths.

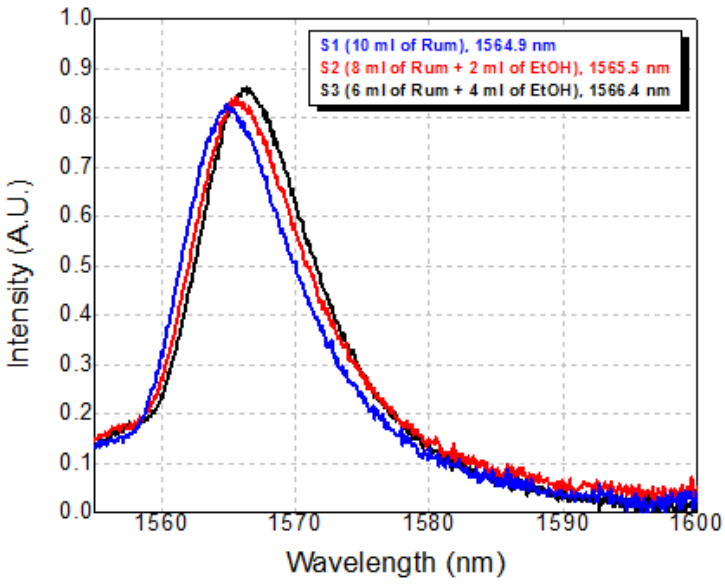

Fig. 5. Spectral response of the MMI sensor for different concentrations of Rum with anhydrous ethanol.

Although this shift is relatively small ($\sim 1.5\ nm$), it provides a clear indication that the rum has been adulterated when compared to pure rum. Despite the fact that this shift is easily resolved by the OSA, a simpler way to measure this small shift is by monitoring intensity changes at one of the steepest walls of the spectrum. In order to avoid intensity fluctuations we applied enough tension to the device to keep the fiber straight during liquid insertion and removal. As shown in Fig.5, we have two options to measure intensity changes, for instance, we tracked the intensity changes at 1570 nm by using the spectrums obtained from the OSA and the results are shown in Fig. 6.

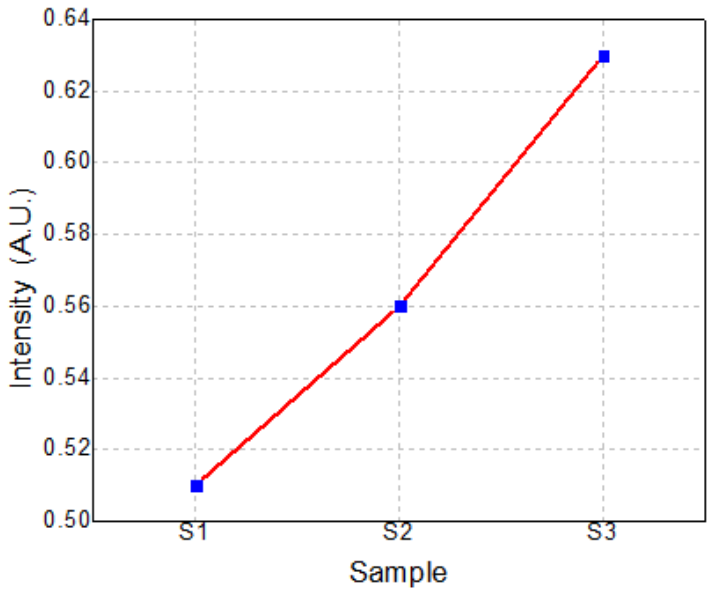

Fig. 6. Intensity as a function of the ethanol concentration (sample number).

We can observe that the contamination with ethanol can be clearly identified and the response is quite linear. The advantage of this approach is that we eliminate the need of an OSA and can operate with a single diode laser and a photo-detector.

The use of EG as an adulterant has also been detected in different alcoholic beverages. In fact, in 1985 there was a well-known case in Europe due to the adulteration of Italian and German wines with EG. Based on the large spectral shift between rum and EG shown in Fig. 4, we should be able to detect quite easily small quantities of EG in rum. Taking 10 ml of rum as the starting volume, we prepared different solutions where the EG was increased in volumes of 1 ml while the same amount of rum was reduced. As shown in Fig. 7, a spectral shift of 1.3 nm is easily observed even for 1 ml of EG, while awavelengths shift of 7.7 nm is observed when the volume of rum has been replaced with EG by 50%.

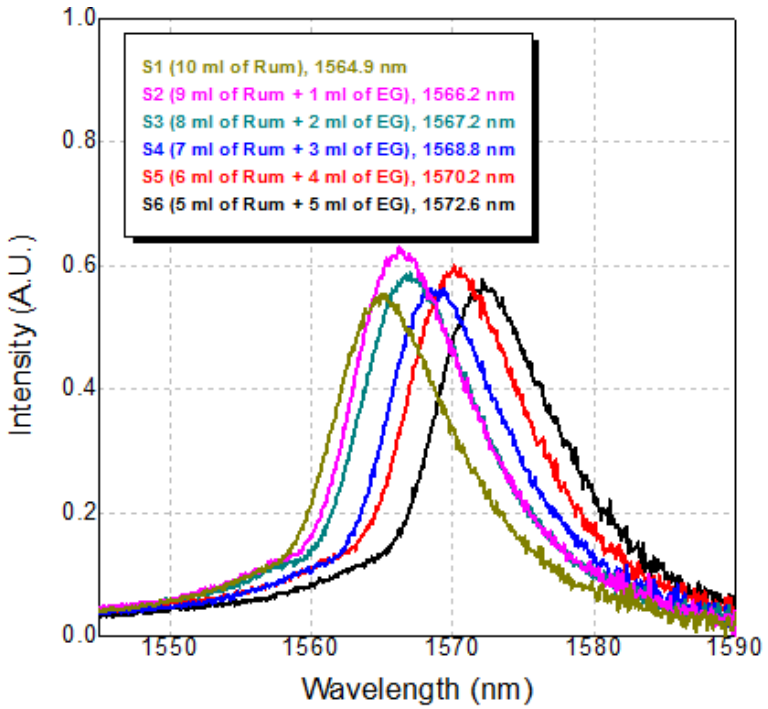

Fig. 7. Spectral response of the MMI sensor for different concentrations of Rum with ethylene glycol.

As it was mentioned before, the intensity variations that we observe in Fig. 7 are related to slight movement (bending) of the No Core-MMF, which can be solved by applying more tension to the fiber when it is glued to the channel. A

similar approach to follow intensity changes can be also applied as long as such external intensity variations are eliminated as explained before.

It is well known that the sensitivity of MMI sensors can be increased by reducing the diameter of the No Core-MM [21]. According to Eq. (24) in Chapter II, if the diameter of the No Core-MMF length has to be reduced to obtain the same MMI peak wavelength. Therefore, using Eq. (24) we can calculate the required No Core-MMF length for a diameter of $80\ \mu m$ nd peak wavelength of 1552.5 nm, which result in a No Core-MMF length of 23.81 mm. A second MMI sensor with a No Core-MMF length of 23.81 mm was fabricated and the diameter of the No Core-MMF was reduced by immersing the fiber in buffered oxide etching (BOE) solution, which is a mixture of hydrofluoric acid and ammonium fluoride as the buffer agent. Since the etching rate is relatively slow ($\sim 130\ nm/min$), we can monitor the transmitted spectrum in real time. After a total time 170 min we can observe that the MMI peak wavelength is at $\lambda = 1552.5\ nm$. The new MMI sensor with reduced diameter was tested again for the rum, anhydrous ethanol and EG. As shown in Fig. 8, the peak wavelength shift is increased for all the liquids, but it is more significant at higher RI of the liquids.

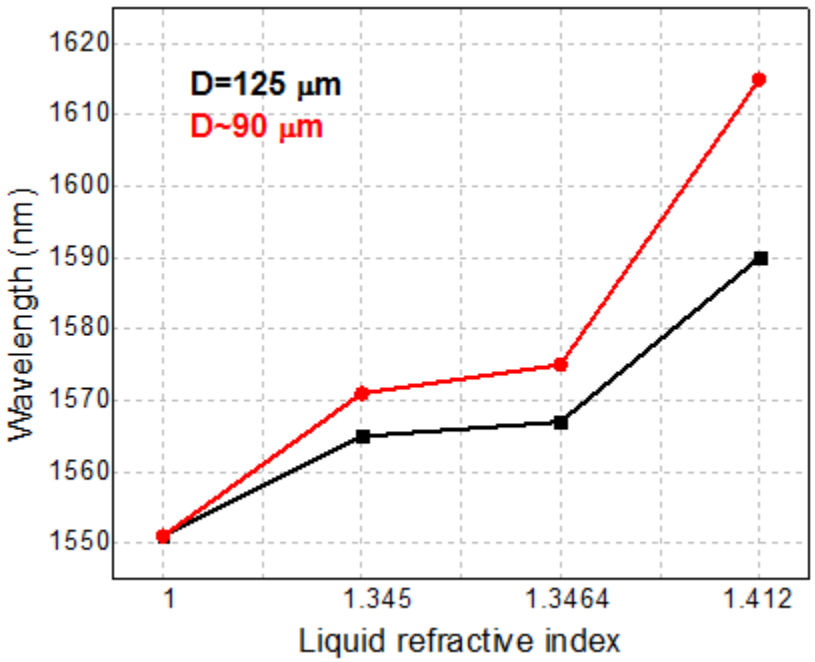

Fig. 8. MMI peak wavelength shift as a function of the liquid RI for different No Core-MMF diameters.

In particular, we can notice that the peak wavelength separation between rum and anhydrous ethanol has been increased to 3.7 nm (105.55 % improvement). The main issue when the No CoreMMF diameter is reduced is related to the fact that the band-pass response gets broader, which difficults the identification of the exact peak within the band-pass response and imposes a limit in the final diameter that can be reduced. Therefore, intensity monitoring is better than wavelength to small spectral changes and spectral monitoring is better for higher spectral changes.

4.4. GASOHOL QUALITY CONTROL FOR REAL TIME APPLICATIONS BY MEANS OF MULTIMODE INTERFERENCE (MMI) FIBER SENSOR.

4.4.1. Experimental procedure

The No-Core fiber used in our next experiments was the same type described in the above section. The MMI sensor was fabricated by first splicing the SMF to one end of the No-Core MMF. Using a microscope and a micrometer stage we align the splicing point with the edge of the cleaver knife, and the fiber is then moved away a distance of 59.58 mm. The No-Core MMF length is slightly larger as estimated from Eq. (24) in Chapter II for peak wavelength transmission at 1530 nm and air as the surrounding medium, which could be related to slight variations of the RI and diameter of the NO-Core MMF. The No-Core MMF is finally cleaved and spliced to another SMF, and at this stage the sensor is ready for testing. We should highlight that the surface of the No-Core fiber should be free of any polymer that could interfere with the measurements. Therefore, after fabrication, the MMI device was cleaned using a sulfuric acid solution (1M) to remove any residual polymer. The experimental setup for testing the MMI gasohol sensors is the same shown in Fig 2. The MMI structure was fixed into a channel engraved in a Delrin plate with integrated liquid inlet and outlet channels. During the measurements we monitored the temperature (~23°C) and humidity (~26%), and small variations of less than 4% were observed during the experiments. Such small variation does not significantly alter the response of the sensor. It is important to mention that in Mexico we have two different kinds of gasoline with 87 and 92 octanes, named G87 and G92 respectively, and both are free of ethanol. Therefore, in order to obtain different gasohol blends, we prepared different mixtures of G87 diluted with anhydrous ethanol (AE) as shown in Table 1.

Solution	G87 (ml)	Anhydrous Ethanol (ml)	G87 /AE (%)
G87	10	0	100/0
E10	9	1	90/10
E20	8	2	80/20
E30	7	3	70/30
E40	6	4	60/40
E50	5	5	50/50

Table 1. Gasohol blends were prepared using anhydrous ethanol and G87 gasoline. The blends are labeled following standard convention.

The mixtures were selected according to the different gasohol blends that are commonly used in several countries [16-30, 31]. We should also highlight that AE was used to guarantee that the gasohol blends do not contain or will absorb water. Although the results reported here were performed using the G87 type, similar results could be obtained with the G92 type. We also believe that similar results could be obtained for other types of gasoline used worldwide.

4.4.2. Experimental results.

We first measured the spectral response of the MMI sensor when it is covered with AE and G87 gasoline. As shown in Fig. 9, we have a separation of 15.2 nm between the transmitted peak wavelengths, which is smaller than the expected values obtained from Fig. 9.

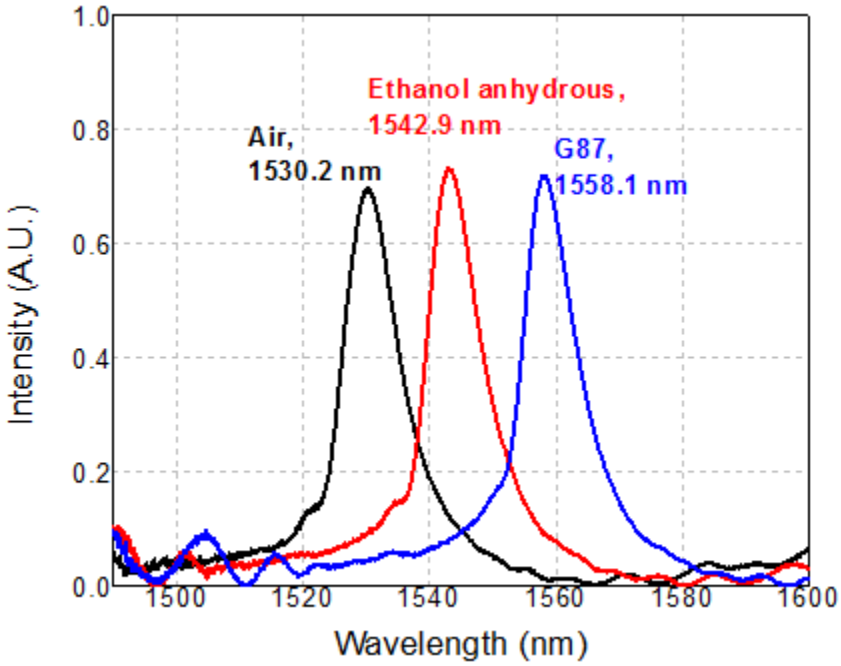

Fig. 9. Spectral response of the MMI sensor for anhydrous ethanol and G87 gasoline.

Such difference is related to the fact that the RI of ethanol and gasoline are very similar that both RI liquids substances used in the simulations. Nevertheless, the peak wavelength separation between AE and G87 gasoline should be enough to monitor the different gasohol blends. Gasohol measurements were performed by first mixing the gasohol blends for a period of 2 min. After mixing, the gasohol was inserted into the channel and the spectral response of the MMI sensor was acquired with the OSA. Before a new measurement the MMI sensor is rinsed with pure ethanol and, after filling the channel with a new gasohol blend, the spectral response is measured again. The spectral response of the MMI sensor for each one of the gasohol blends, as listed in Table 1, is shown in Fig. 10.

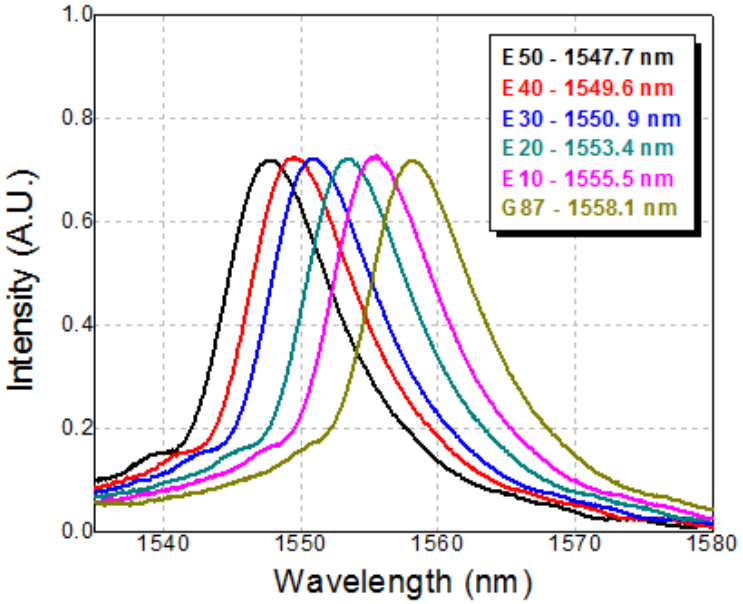

Fig. 10. Gasohol blends from Table 1 (MMF diameter of 125 µm).

We can observe that the spectral response of the MMI sensor is shifted to longer wavelengths as the amount of AE is reduced from the gasohol blend. Such response is correlated with the fact that the G87 gasoline has a higher RI than the AE.

As shown in Fig.10, the sensor can clearly identify the different gasohol blends. However, a simple way to slightly enhance the sensitivity of the MMI sensor is by reducing the diameter of No-Core fiber, which effectively increases the interaction between the evanescent field and the gasohol. Using a buffered oxide etching (BOE) solution, which is a mixture of ammonium fluoride and hydrofluoric acid (6:1 volume ratio), the external diameter of the No-Core fiber (originally 125 µm) was reduced to approximately 90 µm by applying an etching time of 130 minutes. In order to achieve a specific peak wavelength after the etching, the length of the No-Core fiber is calculated using Eq. (2.20) with the target diameter of 90 µm. In this particular case the length of the No-Core fiber was 31.35 mm for a peak wavelength close to 1530 nm. We should highlight that, before etching, the

transmitted spectra does not show any noticeable peak related to the image. As the fiber is being etched, we can observe a well-defined peak appearing from the long wavelength edge of the transmitted spectra. As the etching continues, the whole spectrum is shifted to shorter wavelengths until we reach the desired peak wavelength value. As shown in Fig.11 the peak wavelength is very close to the design peak wavelength of 1530 nm. Also shown in Fig. 11 is the spectral response of the modified MMI sensor when it is covered with AE and G87 gasoline.

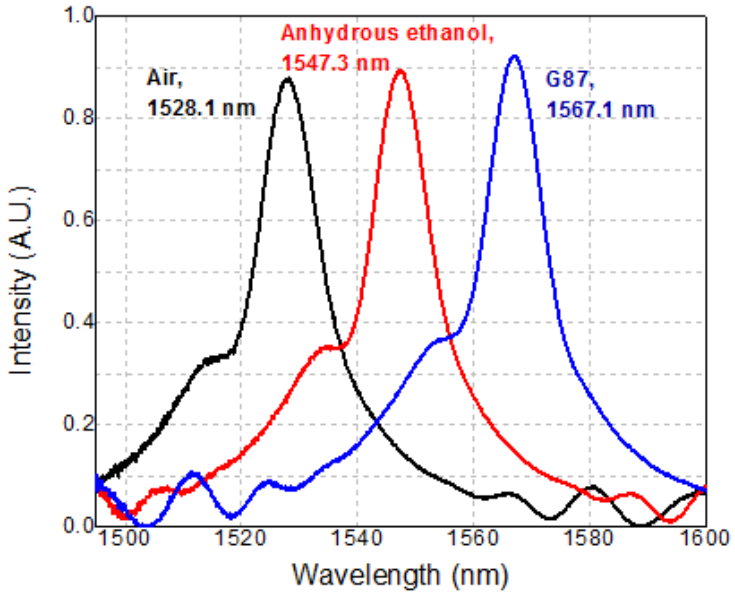

Fig. 11. Spectral response of the MMI sensor for E and G87 gasoline (No-Core MMF diameter of 90 μm).

Here we observe an increment in the peak wavelength difference between AE and G87 gasoline of 19.8 nm (30.26% improvement). We measured the gasohol blends using this sensor and, as shown in Fig. 12, a sensitivity of 0.270 nm/%AE is obtained as compared to a sensitivity of 0.208 nm/%AE from the original MMI sensor without etching. We should also highlight that the response of both sensors are highly linear.

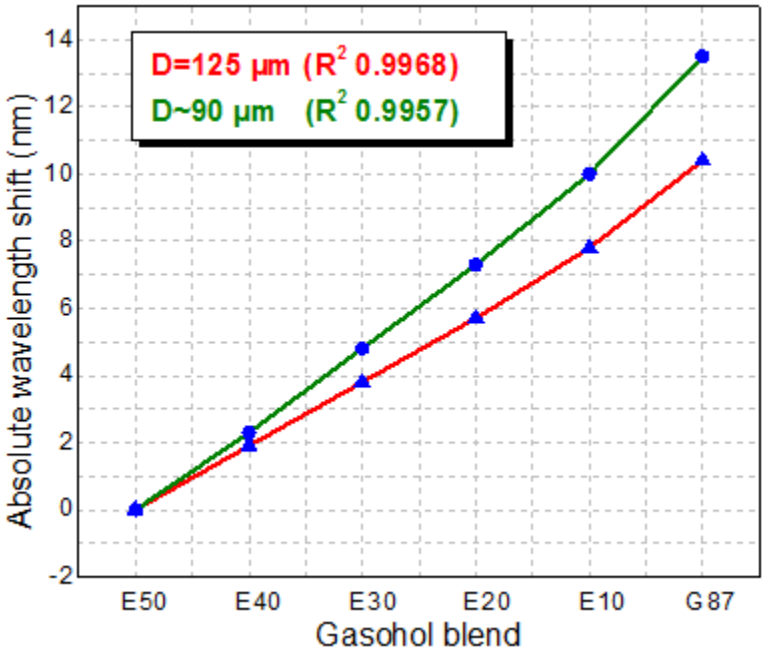

Fig. 12. Absolute peak wavelength shift of both MMI sensors as a function of the gasohol blends.

A more critical issue when monitoring gasohol blends is related to the capability of ethanol to absorb water. As we previously described, there is a maximum amount of water that the blend can hold before having phase separation issues. This limit is at 4% of water volume with respect to the ethanol volume that will be mixed with gasoline. This effect can be easily observed in Fig.13 (a)-(d). The gasohol blend in this case is E10 that corresponds to 90% of gasoline and 10% of AE. The bottles shown in each figure, going from left to right, have a water volume of 1%, 5%, and 10% with respect to the AE volume. Fig. 13 (a) shows the gasohol blend when the water/AE mixture is gently added to the G87 gasoline. We can notice that the bottle with 1% of water volume is well mixed with the gasoline, whilst the one with 10% of water volume exhibits immediately a phase separation process. The bottle with 5% water volume does not experience a drastic phase separation process, but the liquids are not homogeneously mixed, instead a slightly cloudy colloidal suspension is obtained. Fig. 13(b), (c) and (d), correspond to snap

shots taken every three second after the bottles have been shook for one minute. We can easily observe that the E10 blend with 1% water volume remains practically unaltered. However, the E10 blends with water volumes of 5% and 10% become cloudy due to the inability of the ternary constituents to be mixed. We can also notice that the blend with 10% water volume goes into phase separation very rapidly, while the 5% water volume takes a longer time on the order of 2 minutes.

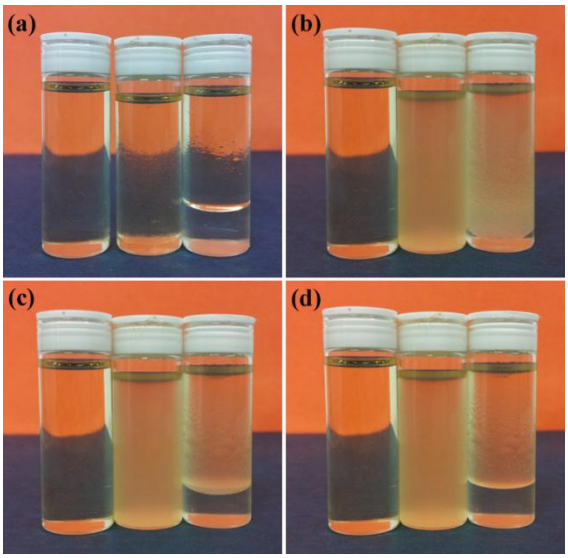

Fig. 13. Gasohol samples with different water percentage of 1%, 5%, and 10% (left to right) with **(a)** After adding AE/water to G87, **(b)** After shaking the samples, **(c)** Three seconds after shaking and **(d)** Six seconds after shaking.

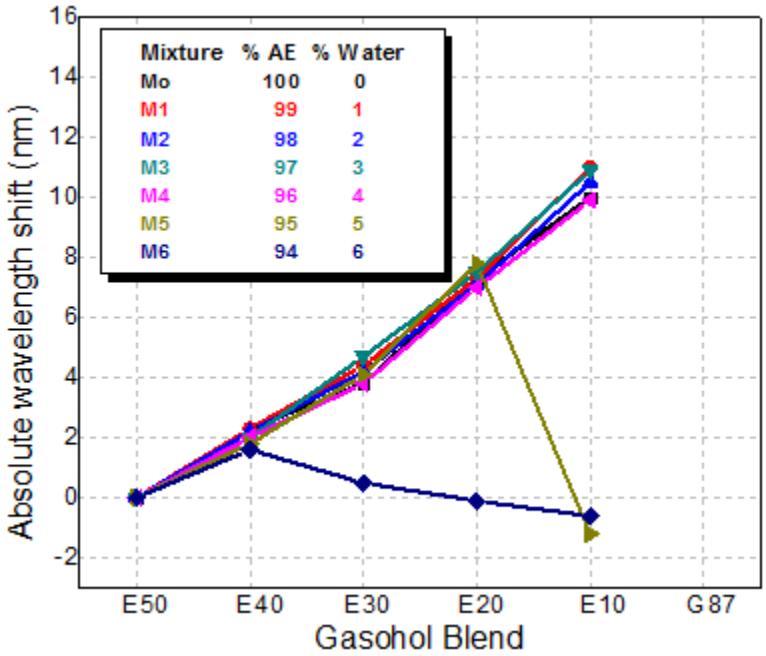

Fig. 14. Absolute peak wavelength response of the MMI sensor as function of gasohol blends with different water volumes.

We evaluated the ability of the etched MMI sensor (90 µm diameter) to detect water content in the different gasohol blends shown in Table 1. For each gasohol blend we prepared a set of samples with different water content from 0% to 6% with increments of 1% (labeled M0 to M6), with respect to the total AE volume. The gasohol blend-water mixture was vigorously shaken before every measurement, then it was introduced into the channel, and the transmitted spectrum is immediately acquired. As shown in Fig.14, all gasohol blends with water content from 0% to 4% exhibit a similar response as before.

We only notice a slight change in the sensitivity which can be related to the different water content. Nevertheless, when the water content increases to 5% we observe a significant deviation of more than 10 nm from the linear response for the E10 gasohol blend. We can also notice that the as the water content increases to 6%, a similar effect is observed for the E30 and E20 gasohol blends. This behavior is related with the formation of small droplets of gasoline and AE with water due to

the phase separation, which effectively reduces the RI for the gasohol blend. This also reduces the effective RI and diameter of the fundamental mode in the MMI device, and the peak wavelength is also reduced. At higher water volume the effect is seen by all the gasohol blends. In fact, since complete phase separation occurs in a matter of seconds for high water volumes, in a real application the sensor can be placed close to the bottom of the gasohol container. In this scenario the RI seen by the MMI sensor under complete phase separation will be that of the AE with water, which should be very close to that of the AE, and a larger peak wavelength deviation from linearity should be observed. The results demonstrate the feasibility of employing the MMI sensor as a reliable system for gasohol quality control that is not only a simple but also a cost effective system.

4.5. CONCLUSIONS

We demonstrated the application of an MMI optical fiber sensor as a tool for monitoring the quality control of rum. The sensor can detect the adulteration of rum due to presence of ethylene glycol and anhydrous ethanol. The sensor can be spectrally or intensity interrogated when fluctuations are removed from the experimental setup. The advantages of the sensor are that the fabrication is straightforward, and exhibits great reproducibility and reversibility, while the response has no significant interference against temperature or humidity. We also explore the feasibility of enhancing the sensor response by reducing the diameter of the No Core-MMF.

A novel gasohol fuel detection system based on MMI fiber sensors was also demonstrated. The MMI sensor relies on the fact that the RI of the gasohol blend is reduced as the ethanol content is increased. Since MMI sensors are capable of detecting small RI changes, accurate control of gasohol blends is achieved by tracking the peak spectral response of the MMI sensor. Gasohol blends with

ethanol content from 0% to 50% are clearly identified with a maximum sensitivity of 0.270 nm/%AE. The sensor is also capable of detecting when the water content of the gasohol blend exceeds the maximum volume that induces phase separation effects. When this occurs the liquids are not homogeneously mixed and a slightly cloudy colloidal suspension is obtained. Since the effective RI of the suspension is lower than the homogeneous mixture, we obtain a shorter peak wavelength response that the deviates from the linear response of the MMI sensor. Since the MMI sensor is straightforward to fabricate and does not require any special coating it is a cost effective solution for monitoring the quality of gasohol blends.

REFERENCES

1. M.A. Nogueira Cesar, “Chemicals from Ethanol,” Process Economics Program Report 235, SRI consulting, 2007.
2. L. Kaphalia, N. Borounmand, J. Hyunsu, B.S. Kaphalia, W.J. Calhoun, “Ethanol metabolism, ocidative stress, and endoplasmic reticulum stress responses in the lung of hepatic alcohol dehydrogenase deficient deer mice after chronic ethanol feeding”, Toxic Appl. Pharmacol,vol. 277(2), pp. 109-17, 2014.
3. The economic feasibility of ethanol production from sugar in the United States. [(Accessed on 22 July 2014)].
   Available online: http://www.usda.gov/oce/reports/energy/EthanolSugarFeasibilityReport3.pdf .
4. .J. Roldan, C. Frauca, A. Duenas, “Intoxicación por alcoholes”, Anales Sis. San Navarra, vol. 26, pp. 129-139, 2003.
5. J. Brent, “Current management of ethylene glycol poisoning”, Drugs vol. 61, pp. 979-988, 2001.
6. A. Smith, “Spice keeps rum moving in Europe”, The International Wine & Spirit Research Magazine pp. 10-12, 2012.
7. A. Yildirim, F. E. Ozturk, M. Bayindir, “Smelling in chemically complex environments: An optofluidic Bragg fiber array for differentiation of methanol adulterated beverages”, Anal. Chem. vol. 85, pp. 6384−639, 2013.
8. M. Morisawa, S. Muto, “Plastic optical fiber sensing of alcohol concentration in liquors”, J. Sensors 709849, 2012.
9. C. Elosua, C. Bariain, A. Luquin, M. Laguna, I. R. Matias, “Optical fiber sensors array to identify beverages by their odor”, IEEE Sens. J. vol. 12, pp. 3156-3162, 2012.

10. Y. Kurauchi, T. Yanal, N. Egashira, K. Ohga, “Fiber-optic sensor with chitosan/poly(vinyl alcohol) cladding for determination of ethanol in alcoholic beverages”, Anal. Sci. vol. 10, pp. 213-217, 1984.
11. Z. H. Zhang, R. Lockwood, J. G. C. Veinot, A. Meldrumb, “Detection of ethanol and water vapor with silicon quantum dots coupled to an optical fiber”, Sens. Actuators B Chem., vol. 181, pp. 523– 528, 2013.
12. Q. Wang, G. Farrell, “All-fiber multimode-interference-based refractometer sensor: proposal and design”, Opt. Lett. vol. 31, pp. 317-319, 2006.
13. J. E. Antonio López, D. López Cortes, M. A. Basurto Pensado, D. A. May Arrioja, J. J. Sánchez Mondragón, “All-fiber multimode interference refractometer sensor”, Proc. SPIE 7316, 73161F 2009.
14. Q. Wu, Y. Semenova, P. Wang, G. Farrell, “High sensitivity SMS fiber structure based refractometer –Analysis and experiment”, Opt. Express, vol. 19, pp. 7937-7944, 2011.
15. Frequently Asked Questions about Methanol. Available online: http://www.methanex.com/products/faqs.html (Accessed on 25 May 2014).
16. Fuel Economy and Emissions of the Ethanol Optimized Saab 9-5 Biopower. Available online: https://www1.eere.energy.gov/bioenergy/pdfs/analysis_saab2007.pdf (Accessed on 25 May 2014).
17. The Brazilian biofuels industry. Available online: http://www.biotechnologyforbiofuels.com/content/1/1/6 (Accessed 25 May 2014).
18. Ethanol fuel and cars. Available online: http://interestingenergyfacts.blogspot.mx/2008/09/ethanol-fuel-and-cars.html (Accessed on 25 May 2014).

19. R. Felate, M. Müller, J.L.Fabris, H.J. Kalinowski, “Long Period Gratings in Standard Telecommunication Optical Fibers for Fuel Quality Control”, Annals of Optics. vol.5, 2003.

20. V.V. Spirin, M.G. Shlyagin, S.V. Miridonov, F.J. Mendieta Jiménez, R.M. López Gutiérrez, Fiber Bragg grating sensor for petroleum hydrocarbon leak detection. Opt. Lass.Eng. vol. 32 (5), pp. 497-503, 1999.

21. R.M. López, V.V. Spirin, S.V. Miridonov, M.G. Shlyagin, G. Beltrán, E.A. Kuzin, “Sensor de fibra óptica distribuido para la localización de fugas de hidrocarburo basado en mediciones de transmisión/reflexión”, Revista Mexicana de Física, vol. 48 (5), pp. 457-462, 2002.

22. A. MacLean, C. Moran, W. Johnstone, B. Culshaw, D. Marsh, P. Walker, “Detection of hydrocarbon fuel spills using a distributed fibre optic sensor”,Sens. Actuators A. vol. 109, pp. 60-67, 2003.

23. A. Treviño Santoyo, M.G. Shlyagin, F.J. Mendieta, V.V. Spirin, L. Niño de Rivera, “Variación del espectro de transmitancia de una fibra óptica con recubrimiento de polímero por influencia de hidrocarburos y cambios de temperatura”, Revista Mexicana de Física, vol. 51 (6), 600-604, 2005.

24. E. Sensfelder, J. Bürck. H. J Ache, Characterization of a Fiber Optic System for the Distributed Measurement of Leakages in Tanks and Pipelines. Applied Spectroscopy, vol. 52, pp. 1283-1298, 1998.

25. Y. Zhao, J. Yang, J. Q. Wang, F. X. Gui, High-accuracy low-water-content measurement of crudle oil based on a near-infrared spectral absorption method. Optical Engineering, vol. 43 (10), pp.2216-2217, 2004.

26. G.R.C. Possetti , L.C. Cocco , C. I., Yamamoto,de L. V. R.Arruda, R., Falate, M. Muller, “Application of a long-period fibre grating-based transducer in the fuel industry”, Meas. Sci. Technol., p. 20, 2009.
27. T. Walbaum, C. Fallnich, “Multimode interference filter for tuning of a mode-locked all-fiber erbium laser”, Opt. Lett. vol. 36, pp. 2459-2461, 2011.
28. .F. Hoytt, “New table of the refractive index of pure glycerol at 20°C”, Ind. Eng. Chem. vol. 26, pp. 329–332, 1934.
29. S. Kedenburg, M. Vieweg, T. Gissibl, H. Giessen, “Linear refractive index and absorption measurements of nonlinear optical liquids in the visible and near-infrared spectral region”, Opt.Mater. Express vol. 2, pp. 1588-1611, 2012.

Effects of Intermediate Ethanol Blends on Legacy Vehicles and Small Non-Road Engines, Report 1- Updated. Available online: http://www.nrel.gov/docs/fy09osti/43543.pdf
(Accessed on 17 December 2013).

30. J.Goettemoeller , A. Goettemoeller , Sustainable Ethanol: Biofuels, Biorefineries, Cellulosic, Biomass, Flex-Fuel Vehicles, and Sustainable Farming for Energy Independence; Prairie Oak Publishing; USA, pp. 56-61, 2007.

CHAPTER V. SENSITIVITY OPTIMIZATION OF MULTIMODAL INTERFEROMETERS (MMI) BY MEANS OF THIN INDIUM TIN OXIDE (ITO) COATINGS

ABSTRACT

In this chapter we propose and experimentally demonstrate the fabrication of novel sensitivity enhanced multimodal interferometers (MMI) by means of the utilization of high refractive index Indium Tin Oxide (ITO) thin films coatings. ITO coating has been described and characterized regarding optical properties. In particular, experimental results showed that a MMI coated with an ITO thin film with thickness of ~36 nm shows a sensitivity of 354.10 nm/RIU for RI measurements within the range of 1.318–1.391, which represents a factor 2 sensitivity enhancement when compared with the MMI without coating. The advantages of these multimodal interferometers are that the fabrication is straightforward, and exhibits great reproducibility and reversibility. They also serve as a simple and cost effective platform for development of optical fiber sensors with no significant interference with temperature or humidity.

5.1. INTRODUCTION

Interferometers are measuring instruments that use the wave properties of light as well as the phenomenon of interference to identify the refractive index (RI) of solids, liquids and gasses. Some application areas of the interferometers are: agriculture, materials science, cosmetics, textile, biotechnology, medicine, food technology, environmental real time monitoring, earth sciences, atmospheric and mineralogy, forensics, clinical chemistry, military research, oil industry, pharmaceutical industry, among others [1-3].

Structures in optical fibers to develop interferometers and refractometers have attracted considerable attention for the last years due their inherent properties, such as good sensitivity, light weight, remote monitoring capability, immunity to electromagnetic interference, high resolution, small size, portability, low cost, easy multiplexing of different signals and good corrosion resistance [4-8]. Some approaches have been reported to measure the refractive index (RI) of liquids employing long period gratings (LPG) and Bragg gratings [9,10], macro-bend single-mode fiber (SMF) [11], D-type fiber optic based on total internal reflection heterodyne interferometry [12], Fabry-Perot interferometer [13], Mach Zehnder Interferometry with waist-enlarged fusion bitaper [14], surface plasmon resonance [15], micro-sphere resonator [16], microfiber coil resonator [17], narrowband cladding-mode resonance shifts [18], optical ring resonator [19], among others. Although these refractometers/interferometers devices have reported a good sensitivity, they usually require complex equipment for special preparation of the fiber and require the use of additional material and instrumentation inside-outside of the fiber that could impact the cost of the final developed device.

There is a particular phenomenon applied to SMF-MMF-SMF structures (SMS), which is called multimodal interference (MMI) effect. This phenomenon has been traditionally explored for the design and development of optical fiber interferometers and satisfactorily meets good sensitivity to measure changes in refractive index of liquids substances [20-23]. The advantages of these MMI structures are that their fabrication is straightforward, and exhibits great reproducibility and reversibility, with no significant interference against temperature or humidity. The effective diameter and refractive index of the MMF are responsible for the sensitivity of the SMS devices. Thus, their sensitivity can be improved by means of etching processes on the MMF section [25], taper processes on the MMF section [26] and incorporating high refractive index thin films coatings [27-29] on

the MMF section as it will be described in this chapter. However, in etching and taper process are additional problems such as MMF misalignment, adequate splicing of the MMF to the SMF, also require an extremely careful handling to avoid breaking the MMF. A reason to justify the application of an additional coating in optical fiber interferometer/refractometer is the possibility to use coatings that are sensitive to a humidity [30], specific gas [31], pH [32], chemical [33] or biological species [34], and temperature [27, 29], which permits to increase the number of applications of the optical fiber interferometers as sensing devices. In view of the previous success combining thin-films with optical structures that are inherently sensitive to the surrounding medium, the application of a thin-film to a MMF section of SMS structure should lead to interesting results.

Novel applications have been recently described by manufacturing optical fiber refractometers based in materials with unique optical and electrical properties, such as Titanium Dioxide (TiO_2) [35], Indium Oxide (In_2O_3) [36] or Indium Tin Oxide (ITO) [36]. ITO electrochemical stability, compared to traditional gold and silver, offers multiple possibilities, such as: easier processible surfaces or simpler surface chemistries; ITO can operate at temperatures up to 1400 °C and can be used in harsh environments, such as gas turbines, aircraft engines and rocket motors; another benefit of ITO is that if moisture does penetrate, ITO will degrade less than compared to a common choice of transparent conducting oxide [37-39].

In this chapter, we have employed a high refractive index ITO film to change the effective diameter and refractive index of the fundamental mode of a SMS structure, and hence, enhance the sensitivity of MMI interferometers in the near infra-red region by means of the utilization of different ITO coating thickness values. To our knowledge, this is the first time that ITO coated SMS structures have been studied for the fabrication of tunable optical fiber interferometers as a simple and cost effective platform for development of optical fiber sensors with no

significant interference against temperature or humidity and a straightforward fabrication process.

5.2. PRINCIPLE OF OPERATION

As we explained before, a SMS structure is fabricated by splicing a segment of MMF between two SMF segments. In our device the SMS structure is able to see the liquid surrounding the fiber because the MMF does not have a cladding. A simple way to enhance the sensitivity of the SMS structure is to coat the MMF with a very thin high RI film. This has been used on other fiber structures, but to our knowledge, this is the first time that it is used in a SMS sensor. The only restriction we have in order to coat the high RI film on the MMF surface is that we need to control the film thickness to very thin values. If the film is too thick, it will start guiding and all the light from the MMF will be coupled into the high RI film.

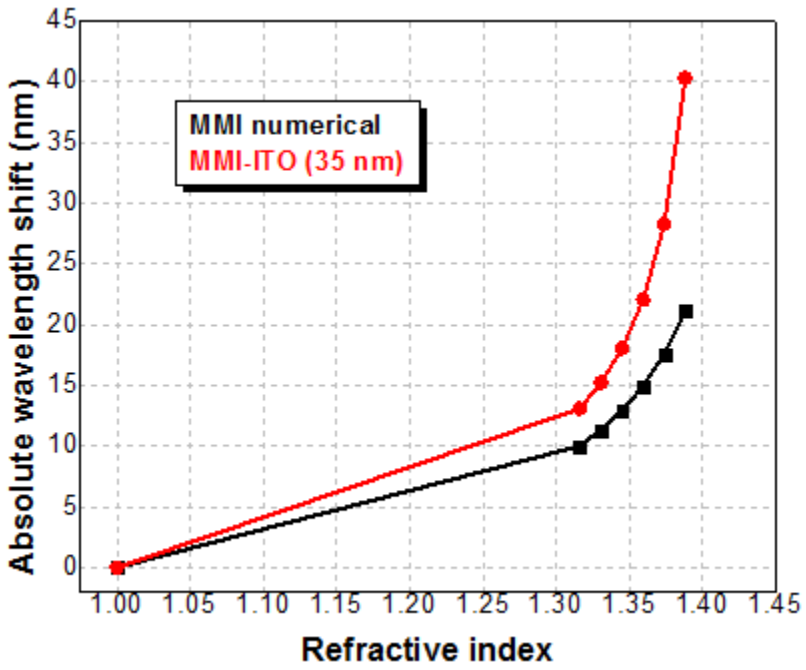

Fig 1. Simulation results of MMI and MMI+ITO interferometers for different external medium RI

The peak wavelength of the SMS sensor after it has been coated with a high RI film is still dictated by Eq. (24) in Chapter II. In this case we need to find the effective RI and effective diameter of the fundamental mode including the thin film. COMSOL Multiphysics was used in order to numerically calculate both effective values. According to our simulations, when the SMS device with high RI film is covered with liquid, the effective diameter of the fundamental mode is increased as compared to a SMS structure without film under the presence of the same liquid. In terms of the effective RI we observed changes on the order of 10^{-5}, which can be easily neglected. Thus, we can obtain the SMS peak wavelength for a coated SMS sensor as a function of the surrounding liquids by using Eq. (24) in Chapter II. All the values are the same as before, except for the effective diameter of the fundamental mode which is calculated for a film of 35 nm and RI of 2.13 at 1550 nm. As shown in Fig. 1, the SMS without film exhibits the typical wavelength shift for the RI of the liquids. Nevertheless, the SMS structure coated with the high RI film exhibits a larger wavelength shift and hence a higher sensitivity. We can also notice that the sensitivity is even higher when the thickness of the film is increased.

5.3. EXPERIMENTAL PROCEDURE

5.3.1. SMS ordinary structure fabrication

Prior to the fabrication of the MMI structures we need to obtain the exact length of the NC-MMF that will provide the desired MMI peak wavelength. First we prepare the ordinary SMS structure, so from Eq. (24) in Chapter II, we employ a NC-MMF segment of 60.57 mm spliced between two segments of SMF-28 (core diameter of 125 μm) for a wavelength of 1490 nm for the case of the fourth self-

image $p = 4$. The NC-MMF cladding was removed with acetone to clean any remaining residue.

5.3.2. Experimental setup

The experimental set-up for testing the MMI refractometer is the same that was described in Fig. 2 of Chapter IV.

5.3.3. Indium Tin Oxide as thin film coating

Indium Oxide is an n-type (gap 3.7 eV) semiconductor and as such is currently used in integrated circuits to form heterojunctions with p-lnP, n-GaAs. However, Indium Oxide shows its best properties when it is doped with Tin Dioxide, thereby forming ITO (Indium Tin Oxide) (gap 4 eV) [40, 41]. The ITO films (90% ln_2O_3 and 10% SnO_2) works as a transparent electrical conductor, may reflect a portion of the infrared region of the spectrum and it is also opaque in the near infrared region, because of free carrier absorption. ITO acts as a transparent conducting film, meanwhile increasing the thickness and increasing the concentration of charge carriers will increase its conductivity but will decrease its transparency [42]. ITO properties may vary during the ITO sputtering process attending to several fabrication parameters such as oxygen flow, sputter time, current intensity, partial pressure and temperature. The adjustment of ITO fabrication parameters can help to define the final properties of the film such as strength, thickness, roughness, as well as the two major properties of ITO: resistivity and transparency. The ITO film resistivity initially decreases with an increase in the ITO film thickness of 50 to 100 nm and remains nearly constant for thicknesses up to 300 nm, to subsequently increase its value. The ITO film thicknesses between 10 and 50 nm provide resistivities in a range between 10.10^{-4} and $9.10^{-4}\ \Omega.cm$. The optical transmittance decreases when the thickness of the film is increased, which can be attributed to increased absorption, interference

phenomena, minimum and maximum reflection achieved for different combinations of wavelengths and thicknesses [43].

5.3.4. SMS ITO coating structure fabrication

We employ two NC-MMF segments of 58.97 mm and 58.60 nm for a wavelength of 1530 nm and 1540 respectively, both for the case of the fourth self-image $(p = 4)$. The NC-MMF cladding was removed with acetone to clean any remaining residue. For the manufacture of coatings of ITO sputtering equipment (K675XD Quorum Technologies Ldt.) was used with a partial pressure of argon between 9.6^{-3} and $6.10^{-3}\, mbar$ and current intensity of $150\, mA$, which allowed to achieve deposition rates of $0.3\, nm/s$ [39]. Since this fabrication technique is designed to be used on flat substrates it was necessary to introduce into the vacuum chamber a rotation mechanism based on a DC motor which is adapted to clamp and rotate the fiber throughout the whole deposition process. The NC-MMF segment of 58.60 nm and NC-MMF segment of 58.97 mm were prepared by stopping the deposition process after 1 and 2 minutes, obtaining ITO thicknesses of $d{\sim}18\, nm$ and $d{\sim}36\, nm$ respectively. Fig. 2 shows the section of the sensitive region. Next, we repeat the process described in section 2.1.to finish the ITO coated SMS structures.

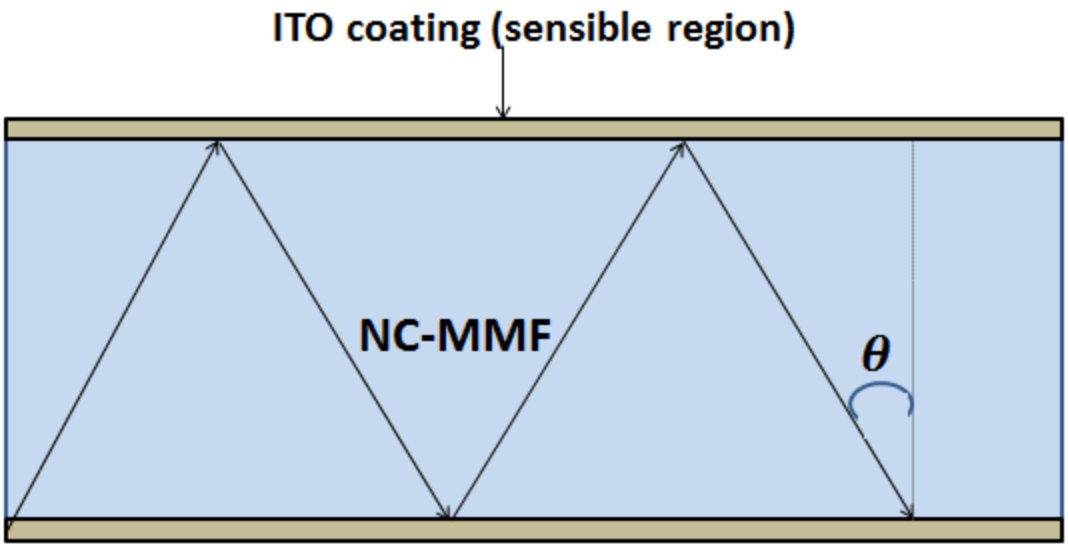

Fig. 2. Longitudinal section of the sensitive region.

5.4. RESULTS AND DISCUSSION

Mixtures of water and glycerin were prepared at different concentration solution to obtain a range of RI from 1.318 (100% water) to 1.408 (40% water / 60% glycerin) [49, 50] in order to study the utility of the MMI structures as refractometers. As shown in Fig. 3(a), the peak wavelength is red shifted as the RI of the liquid is being increased.

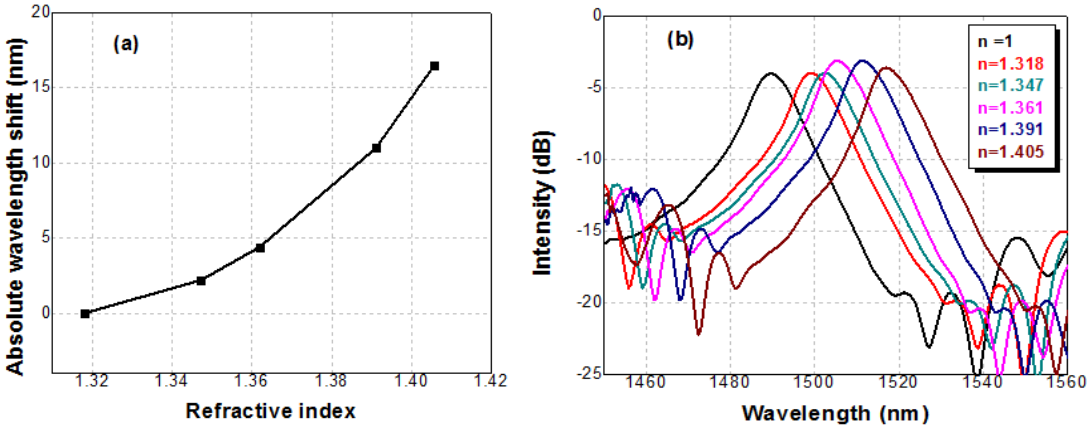

Fig. 3. (a) MMI interferometer peak wavelength shift as a function of the water/glycerin solutions RI, and (b) MMI spectral response for water/glycerin solutions.

Since both effective RI and diameter of the NC-MMF are being altered, the quadratic behavior means that the diameter is the dominating factor since it has a square dependence. A sensitivity of 183.333 nm/RIU can be estimated from Fig. 3(a). The spectral response of the MMI ordinary interferometer for the solutions described above is shown in Fig. 3(b). As it is shown in Fig 3(b), a spectral shift of 2.4 nm is easily observed between water (red line) and the solution of 80% water/20% of glycerin (dark cyan line). As it is shown in Fig. 3(b), a spectral shift of 16.5 nm is observed when the volume of water has been replaced with glycerin by 40%. (brown line).

In Fig. 4, we can observe the real and imaginary parts of the ITO refractive index between 1200-1900 nm (obtained with the ellipsometer UVISEL Horiba Jobin Yvon).

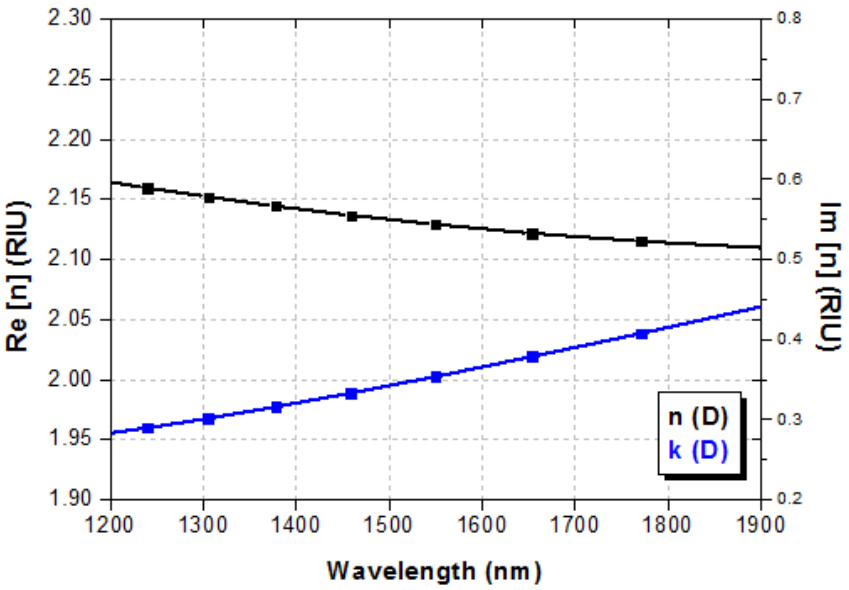

Fig. 4. ITO refractive index and absorption coefficient at Near Infrared region

We can appreciate a high RI of ITO at 1500 nm (n~2.13), therefore it is expected an increase in the sensitivity of the MMI interferometers if this material is deposited on the surface of the NC-MMF. The complex refractive index part is high in the same region, so the presence of remarkable absorption is also possible.

The spectral response of both ITO coated MMI interferometers for each one of the water/glycerin solutions is represented in Fig. 5. We can observe that the spectral response in both devices is shifted to longer wavelengths as the amount of water is reduced from the solution blend. Such responses are correlated with the fact that the glycerin has a higher RI than the water. As it is shown in Fig 5(a), a spectral shift of 5 nm is easily observed between water (red line) and the solution of 80% water/20% of glycerin (dark cyan line) while a spectral shift of 27.5 nm is observed when the volume of water has been replaced with glycerin by 40%. (brown line).

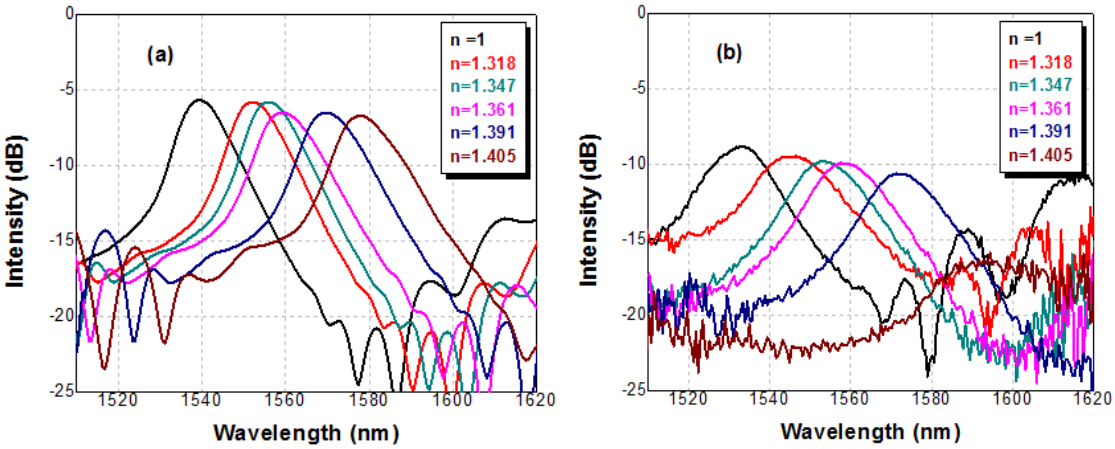

Fig. 5. MMI spectral response for different ITO layer times sputtering deposition values: (a) 1 min and (b) 2 min when they are immersed in water/glycerin solutions with different RI.

We can see in Fig. 4 that the ITO refractive index high complex part makes the possible the presence of elevate absorption, that's why the intensity of both responses tends to decrease as the thickness of ITO deposited on the NC-MMF increases. In particular, the signal intensity is almost vanished in the MMI ITO coating structure of 2 minutes [Fig. 5(b)] for the solution of water 60%/ glycerin 40%. (brown line). As it is shown in Fig. 6, the peak wavelength shift is increased for all the liquids, but it is more significant when the RI of the surrounding medium is higher.

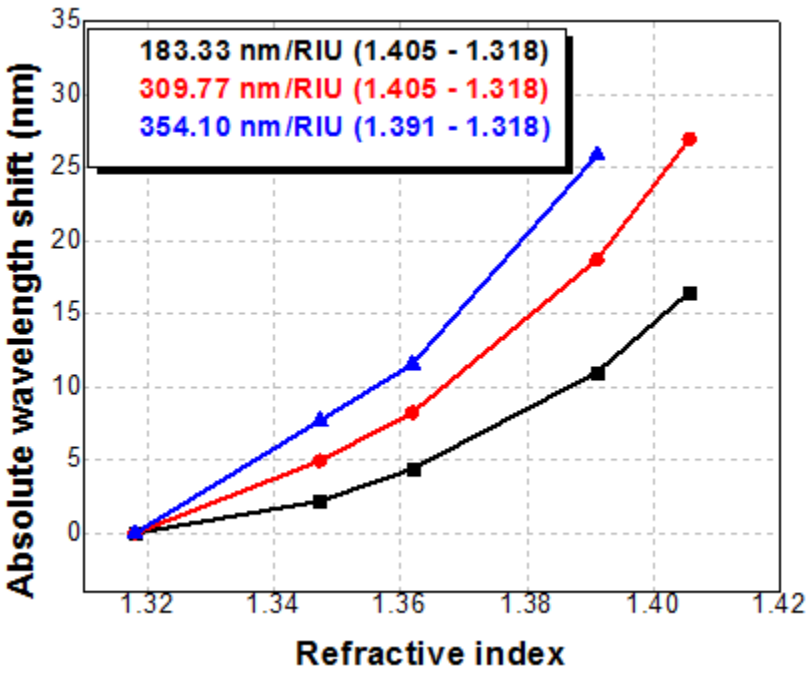

Fig. 6. MMI interferometer peak wavelength shift as a function of the water/glycerin solutions RI for the MMI without ITO (black), MMI+ITO:1min (red line) and MMI+ITO:2 min (blue line).

In particular, we can notice that the peak wavelength separation between RI of 1.318 and 1.391 is increased to 19 nm in MMI interferometer 1 min ITO coating ($d{\sim}18\,nm$) while the peak wavelength separation between the same RI is increased to 26 nm in MMI interferometer 2 min deposition ITO coating ($d{\sim}36\,nm$). The main issue when the ITO coating in is increased is related to the fact the band-pass response gets shorter, which complicates the identification of the exact peak of the band-pass response and imposes a limit in the final ITO coating thickness that can be deposited on NC-MMF.

5.5. CONCLUSIONS.

We have presented the fabrication of MMI interferometers based on indium tin oxide (ITO) coatings with response in the near infrared region. We have explored the feasibility of enhancing the MMI interferometer sensitivity by means of the fabrication of smooth and homogeneous ITO coatings onto the NC-MMF.. Fabricated ITO coated MMI interferometers doubled the sensitivity of the devices without ITO. The sensitivity obtained for a MMI with an ITO coating of 36 nm thickness was 354.10 nm/RIU for RI measurements within the range of 1.318–1.391. The MMI+ITO fabricated devices are a simple and cost effective platform for development of optical fiber sensors with no significant interference against temperature or humidity as well as a straightforward fabrication process and the possibility to perform novel approaches on ITO devices technology.

REFERENCES

1. P. Hariharan, Basics of INTERFEROMETRY, Academic Press, Elsevier second edition, USA 2007.
2. W. Lauterborn, T. Kurz, Coherent Optics: Fundamentals and Applications, Springer, second edition, 2002.
3. P. Hariharan, Optical Interferometry, Academic Press, Sydney, 1985.
4. B. Lee, “Review of the present status of optical fiber sensors”, Opt Fiber Technol, vol.9, pp. 57-59, 2003.
5. M.D. Marazuela, M.C. Moreno-Bondi, “Fiber-optic biosensors-an overview”, Anal. Bioanal, Chem., vol. 372, pp. 664-682, 2002.
6. Y.Shizhuo, P.B. Ruffin, F.T.S. Yu, Fiber optic sensors Second edition, Taylor & Francis Group, USA, 2008.
7. I.R. Matias, F.J. Arregui, R.O. Claus, Optical Fiber Sensors, Encyclopedia of SENSORS, vol. X, pp.1-19, 2006.
8. G.F. Fernando, D.J. Webb, P. Ferdinand, Optical-Fiber Sensors, MRS BULLETIN, 2012.
9. G. R. C. Possetti, L. C. Cocco, C. I. Yamamoto, L. V. R. de Arruda, R. Falate, M. Muller, “Application of a long-period fibre grating-based transducer in the fuel industry”, Meas. Sci. Technol., vol. 20, 2009.
10. A. Yildirim, F. E. Ozturk, M. Bayindir, “Smelling in chemically complex environments: An optofluidic Bragg fiber array for differentiation of methanol adulterated beverages”, Anal. Chem., vol. 85, pp. 6384−639, 2013.
11. P. Wang, Y. Semenova, Q. Wu, G. Farrell, Y. Ti and J. Zheng, “Macrobending single-mode fiber-based refractometer”, Appl. Opt., vol. 48 (1), pp. 6044-6049, 2009.
12. C. Ming-Hung, H. Shao-Nan, Y. Hsiharng, “D-type optic sensor used as a refractometer based on total internal reflection heterodyne interferometry”, Sens. Actuators B Chem., vol. 101(3), p.322-327, 2004.

13. O. Frão, P. Caldas, J.L. Santos, P.V.S. Marques, C. Turck, D.J. Lougnot and O. Soppera, “Fabry-Perot refractometer based on an end-of-fiber polymer tip”, Opt. Lett., vol.34(16), 2474-2476 (2009).
14. K. Ni, X. Dong, C.C. Chan, T. Li, L. Hu, W. Qian, “Miniature refractometer based on Mach-Zehnder interferometer with waist-enlarged fusion bitaper”, Opt. Commun., Vol. 292, p.84-86, 2013.
15. B.D. Gupta, R.K. Verma, “Surface Plasmon Resonance-Based Fiber Optic Sensors: Principle, Probe Designs, and Some Applications”, Journal of sensors, vol. 2009.
16. N.M. Hanumegowda, I.M. White, H. Oveys, and X.Fan “Label-Free Protease Sensors Based on Optical Microsphere Resonators”, Sensors Lett. vol. 3, 315-319, 2005.
17. F. Xu, G. Brambilla, “Demonstration of a refractometric sensor based on optical microfiber coil resonator”, Appl. Phys. Lett, vol. 92, 2008.
18. C.F. Chan, C. Chen, A. Jafari, A. Laronche, D. Thompson and J. Albert, “Optical fiber refractometer using narrowband cladding-mode resonance shifts”, Applied Optics, vol. 46(7), pp.1142-1149, 2007.
19. X. Fan, I.M. White, H. Zhu, J.D. Suter and H.Oveys, “Overview of novel integrated optical ring resonator bio/chemical sensors”, Proc. SPIE, vol. 6452, 2007.
20. J. E. Antonio-Lopez, D. A. May-Arrioja, and P. LiKamWa, “Optofluidic tuning of multimode interference fiber filters”, Proc.of SPIE vol. 7339 73390D-1, 2009.
21. J.E. Antonio-Lopez, J.G. Aguilar Soto, D.A. May-Arrioja, P.Likamwa, J.J. Sanchez Mondragon. “Optofluidically tunable MMI filter”, CLEO/IQEC, 2009.
22. A. Castillo-Guzman, J.E. Antonio-Lopez, R. Selvas-Aguilar, D.A. May-Arrioja, J. Estudillo-Ayala. “Widelly tunable all erbium-doped fiber laser based on multimode interference effects”, CLEO/IQEC, 2009.

23. J.E. Antonio-Lopez, A. Castillo- Guzman, R. Selvas-Aguilar, D.A. May-Arrioja, P. liKamWa, “All-fiber tunable MMI fiber laser”, Proc. Of SPIE Vol. 7339 73390Q-1, 2009.
24. P.A.S. Jorge, S. O. Silva, C. Gouveia, P. Tafulo, L. Coelho, P. Caldas, D. Viegas, G. Rego, J. M. Baptista, J. L. Santos and O. Frazão, “Fiber Optic-Based Refractive Index Sensing at INESC Porto”, Sensors, vol.12, pp. 8371-8389, 2012.
25. A.J. Rodríguez Rodríguez, D.G. Martínez Camacho, K. González Gutiérrez, D.A. May-Arrioja, R.F. Domínguez Cruz, I.R. Matías Maestro, C. Ruíz Zamarreño, “Run adulteration detection using an optical fiber sensor based on multimodal interference (MMI)”, Opt. Pura Ap. 46(4), pp. 345-352, 2013.
26. Claudecir R Biazoli, Susana Silva, Marcos A R Franco, Orlando Frazão,Cristiano M B Cordeiro, “Multimode interference tapered fiber refractive index sensors”, Applied Optics, vol. 51(24), pp. 5941-5, 2012.
27. S. Silva, E. G. P. Pachon, M. A R Franco, J. G. Hayashi, F X. Malcata, O. Frazão, P. Jorge, C. M. B. Cordeiro, “Ultrahigh-sensitivity temperature fiber sensor based on multimode interference”, Applied Optics, vol. 51(16), pp. 3236-42, 2012.
28. A.B. Socorro, I. Del Villar, J. M. Corres, F.J. Arregui, and I.R. Matias, “Mode transition in complex refractive index coated single-mode-multimode-single-mode structure”, Opts.Exp.Lettr, vol 21(10), 2013.
29. H. Fukano, Y. Kushida, S. Taue, “Multimode-interference-structure optical-fiber temperature sensor with high sensitivity”, IEICE Electronic Express, vol. 10(24), 2013.
30. J. M. Corres, I. del Villar, I. R. Matias, and F. J. Arregui, “Fiber-optic pH-sensors in long-period fiber gratings using electrostatic self-assembly,” Opt. Lett. 32(1), pp. 29–31, 2007.
31. Z. Gu, Y. Xu, and K. Gao, “Optical fiber long-period grating with solgel coating for gas sensor,” Opt. Lett., vol. 31(16), pp. 2405–2407, 2006.

32. C. R. Zamarreño, M. Hernáez, I. Del Villar, I. R. Matías, and F. J. Arregui, “Optical fiber pH sensor based on lossy-mode resonances by means of thin polymeric coatings,” Sens. Actuators B Chem., vol. 155(1), pp. 290–297, 2011.
33. P. Pilla, A. Iadicicco, L. Contessa, S. Campopiano, A. Cutolo, M. Giordano, and A. Cusano, “Optical chemosensor based on long period fiber gratings coated with d form syndiotactic polystyrene,” IEEE Photon. Technol. Lett., vol. 17(8), pp. 1713–1715, 2005.
34. D. W. Kim, Y. Zhang, K. L. Cooper, and A. Wang, “Fibre-optic interferometric immuno-sensor using long period grating,” Electron. Lett. 42(6), 324–325 (2006).
35. M. Hernaez, I. Del Villar, C. R. Zamarreño, F. J. Arregui, and I. R. Matias, “TiO2 Optical fiber refractometers based on lossy mode resonances supported by TiO2 coatings,” App. Opt., vol. 49(20), pp. 3980-3985, 2010.
36. C. R. Zamarreño, P. Sanchez, M. Hernaez, I. Del Villar, C. Fernandez-Valdivielso, F. J. Arregui and I. R. Matias, “Dual-Peak Resonance-Based Optical Fiber Refractometers” Phot. Tech. Lett., vol. 22(24), pp. 1778-1780, 2010.
37. C. R. Zamarreño, M. Hernaez, I. Del Villar, F. J. Arregui, and I. R. Matias, “ITO coated optical fiber refractometers based on resonances in the infrared region,” IEEE Sensors Journal vol. 10(2), pp. 365-366, 2010.
38. H. Kim, C. M. Gilmore, "Electrical, optical, and structural properties of indium–tin–oxide thin films for organic light-emitting devices", J. Appl. Phys. 86 (11), 1999.
39. S. López, C.R. Zamarreño, M. Hernaez, I. Del Villar, I.R. Matias, F.J. Arregui, “Optical Fiber Refractometers with Response in the Visible Spectral Region by means of ITO Coatings”, 7ª Reunión Española de Optoelectrónica, OPTOEL’11.

40. “Indium tin oxide thin film strain gages for use at elevated temperatures.[Accesed on: 25-July-2014] Available online: http://search.proquest.com/docview/276304893
41. H. Kim and C.M. Gilmore, “Electrical, optical, and structural properties of indium-tin-oxide thin filmsfor organic light-emitting devices”, J.Appl.Phys, vol.86(11), 1999.
42. S.H. Mohamed, F.M. EL-Hossary, G-A- Gamal and M.M. Kahlid, “Properties of Indium Tin Oxide Thin Films Deposited on Polymer Substrates”, Acta Physica Polonica A, vol. 115(3), 2009.
43. C.H. Yang, S.C. Lee, T.C. Lin, S.C. Chen, “Electrical and optical properties of indium tin oxide films prepared on plastic substrates by radio frquency magnetron sputtering”, Thin Solid Films, vol.516, pp.1984-1991, 2008.
44. J. Homola, Surface Plasmon Resonance Based Sensors, Springer, Berlin 2006.
45. O.S. Wolfbeis, “Fiber-optic chemical sensors and biosensors”, Anal. Chem., vol. 76, pp.3269-3284, 2004.
46. B.D. Gupta, C.D. Singh, “Influence of skew rays on the sensitivity of signal-to-noise ratio of a fiberoptic surface-plasmon-resonance sensor”, Applied Optics, vol. 46, pp. 4563-4569, 2007.
47. A.K. Sharma, B.D. Gupta, “On the sensitivity and signal to noise ratio of a step-index fiber optic surface plasnon resonance sensor with bimetallic layers”, Opt. Comm., vol. 245, pp. 159-169, 2005.
48. R.C. Jorgenson, S.S. Yee, “A fiber-optic chemical sensor based on surface Plasmon resonance”, Sens. Actuators B Chem, vol. 12, pp. 213-220, 1993.
49. S. Kedenburg, M. Vieweg, T. Gissibl, H. Giessen, “Linear refractive index and absorption measurements of nonlinear optical liquids in the visible and near-infrared spectral region”, Opt. Mater. Express, vol. 2, pp. 1588-1611, 2012.

50. F. Hoytt, “New table of the refractive index of pure glycerol at 20°C”, Ind. Eng. Chem., vol. 26, pp. 329–332, 1934.

CHAPTER VI. CONCLUDING REMARKS.

The scope of this thesis work was the design, fabrication, deployment and verification of the correct operation of optical fiber structures for three industrial applications: gaseous ammonia detection, adulteration of alcoholic beverages and gasohol quality control; were the principle of operation of our sensor provides an advantage over other reported sensors. In general, the work done allowed fulfilling the objectives set at the beginning of the investigation. At first order the behaviour of the different sensing structures and its physical-mathematical fundaments was described. Then, these structures were physically implemented and practically demonstrated as useful tools for real applications.

For the gaseous ammonia detection at low level concentrations, we described two optical fiber sensors employing colourimetric pH indicators:Bromocresol Green (BCG) and Universal indicator, attached to the multimode optical fiber. These colourimetric pH indicators are each one immersed into a hydrophobic and gas permeable polyurethane film named Tecoflex® that acts as a ttraping matrix, providing additional advantages, such as-operation even in extremely dry environments, efficient transport and leakage or detachment of the colourimetric pH indicators prevention. BCG pH indicator exhibits a wide spectral response (500 nm-750 nm) while showing recovery times of less than 15 s. Universal pH indicator exhibits also a sensitivity to ammonia over a broad wavelength rangee providing a differential response, with a valley around 500 nm and a peak around 650 nm, which allows to perform ratiometric measurements, providing not only an enhanced signal, but can also eliminate any external disturbance due to humidity or temperature fluctuations. The combination of the colourimetric pH indicators (BCG and Universal) and Tecoflex® film provides reliable and robust optical fiber ammonia gas sensors suitable to be used in real applications. Based on the experimental dynamic range, sensors responses could

be easily optimized attending to three parameters: film thickness, interaction length, and MMF diameter; that the sensors could be capable of detecting smaller 10 ppm ammonia concentrations. The advantages of these sensors consist of a straightforward fabrication as well as good reproducibility and reversibility with ammonia exposure limits.

There is a particular phenomenon applied to SMF-MMF-SMF structures (SMS) and is explored for the design and development of optical fiber interferometers, which is called multimodal interference (MMI) effect and satisfactorily meet good sensitivity for adulteration detection in alcoholic beverages (particularly Rum) and gasohol quality control, providing high repeatability and reversibility while using a fast and simple fabrication without any special coating making it a cost effective solution for real time and in-situ monitoring with no significant interference against or humidity. A common feature during the adulteration of alcoholic beverages and the preparation of gasohol mixtures is that the refractive index of the original liquid is modified when is mixed with other liquid. Therefore, refractive index optical fiber sensor can be used to monitor when a liquid has been contaminated. Considering that the MMI sensor exhibits a sensitivity of 258.06 nm /RIU for liquids with RI ranging from 1.318 to 1.4203, we can accurately determine if a rum sample is free of contaminants or adulterated with other liquid, which is typically performed using ethanol or toxic elements like ethylene glycol. Gasohol blends with ethanol content from 0% to 50% have been clearly identified using these MMI devices obtaining a linear response with a maximum sensitivity of 0.270 nm/%ETOH. The sensor can also distinguish when water incorporated in the blend has exceeded the maximum volume tolerated by the gasohol blend. We also explore the feasibility of enhancing the sensors response by reducing the diameter of the No Core-MMF and can be operated by

following either spectral shifts or intensity changes, making these an attractive option to fabricate portable sensors devices.

Due to effective diameter and refractive index of the MMF are responsible for the sensitivity of the SMS devices, they can improve their sensitivity by incorporating high refractive index thin films coatings on the MMF section. A reason to justify the application of an additional coating in optical fiber interferometer/refractometer is to increase the number of applications of the optical fiber interferometers as sensing devices. In this thesis work, we used a high refractive index ITO film to change the effective diameter and refractive index of the fundamental mode of a SMS structure, and hence, the sensitivity optimization of MMI interferometers in the near infra-red region by different ITO coating thickness values. We explored the feasibility of enhancing the MMI interferometer response by smooth and homogeneous coatings onto the No-Core with ITO thin-films sputtered by employing a rotating mechanism. Fabricated ITO coated MMI interferometers enhanced their own sensitivity of 354.10 nm/RIU for RI measurements within the range of 1.318–1.391 for an ITO coating of 36 nm thickness approximately. This means a factor 2 sensitivity enhancement when compared with the MMI without ITO coating. These optical fiber interferometers are a simple and cost effective platform for development of optical fiber sensors with a straightforward fabrication process and the possibility to perform novel studies in ITO devices technology. This thesis work led to the design and build optical fiber sensors for measurements of different parameters as well as to improve the response of existing devices through the introduction of new techniques. The results obtained from this thesis turn it a useful work in the study of new materials applicable to optical fiber sensors, while opening new avenues of research in the field of optical fiber sensors for industrial applications.

ANNEXES

ANNEX A. PUBLICATIONS FROM RESEARCH

Rum adulteration detection using an optical fiber sensor based on multimodal interference (MMI), A.J. Rodríguez Rodríguez, D.G. Martínez Camacho, K. González Gutiérrez, D.A. May-Arrioja, R.F. Domínguez Cruz, I.R. Matías Maestro, C.Ruíz Zamarreño. Óptica Pura y Aplicada, Special Section: VIII Spanish Meeting on Optoelectronics 2013, DOI: http: //dx.doi.org/10.7149/OPA.46.4.345

Fiber Optic Sensor based on Multimode Interference Effects for Gasohol Detection and Quality Control, A.J. Rodríguez-Rodríguez, R.F. Domínguez-Cruz, O. Baldovino-Pantaleón and D. A. May-Arrioja. Proceedings of Mexican Optics and Photonics Meeting (MOPM) 2013. http://mopm.cicese.mx

Fiber Optic Leak Detection Sensor using MMI effects, A.J. Rodríguez-Rodríguez, D.A. May-Arrioja and R.F. Domínguez-Cruz. RIAO/OPTILAS' 2013, VIII Iberoamerican Optics Meeting and XI Latinamerican Meeting on Optics, Lasers and Applications, 2013, Porto, Portugal.

A Fiber Optic Ammonia Sensor Using a Universal pH Indicator, Adolfo J. Rodríguez, Carlos R. Zamarreño, Ignacio R. Matías, Francisco J. Arregui, Rene F. Domínguez Cruz and Daniel A. May-Arrioja. Sensors 2014, 14, 4060-4073; doi:10.3390/s140304060.

Fiber Optica Ammonia Sensor Using Bromocresol Green pH Indicator, Adolfo Josué Rodríguez Rodríguez, Daniel Alberto May-Arrioja, René Fernando Domínguez Cruz, Ignacio Raúl Matías Maestro, Francisco Javier Arregui San Martín, Carlos Ruíz Zamarreño. IEEE SENSORS 2014, Paper 1636 accepted as Poster.

Gasohol quality control for real time applications by means of multimode interference fiber sensor, A. J. Rodríguez Rodríguez, D.A. May-Arrioja, R.F. Domínguez Cruz, O. Baldovino Pantaleón, C.R. Zamarreño and I.R. Matías. Manuscript under review by *Sensors* (2014).

Sensitivity optimization of multimodal interferometers (MMI) by means of thin indium tin oxide (ITO) coatings, A. J. Rodríguez Rodríguez, D.A. May-Arrioja, C.R. Zamarreño and I.R. Matías. Manuscript under review by *Sensors Journal, IEEE* (2014).

ANNEX B. IMAGES TAKEN DURING THE MANUFACTURING OF THE OPTICAL FIBER SENSOR BASED ON MULTIMODE INTERFERENCE (MMI) EFFECTS.

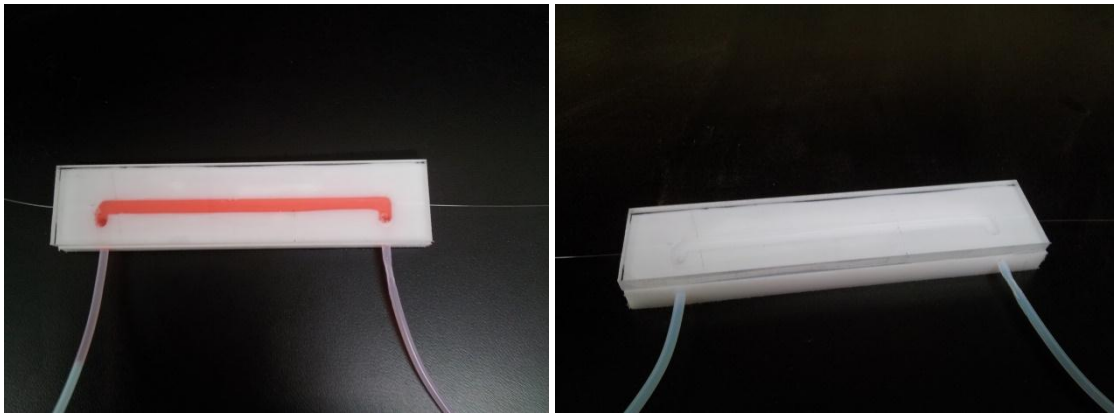

The SMS sensor was fixed in a channel which was then covered to form small chamber. The chamber included input and output plastic tubes to facilitate insertion (left) and removal (right) of the liquids.

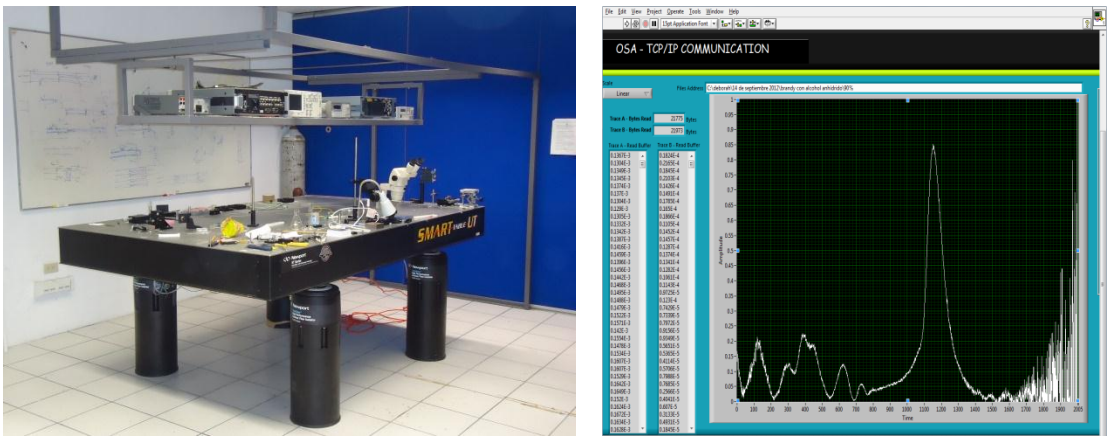

Fiber and Integrated (FIO) laboratory facilities UAT-UAMRR) (left); LabVIEW interface data acquisition (rigth).

ANNEX C. IMAGES TAKEN DURING THE MANUFACTURING OF THE OPTICAL FIBER SENSOR BASED ON COATINGS BY SPUTTERING.

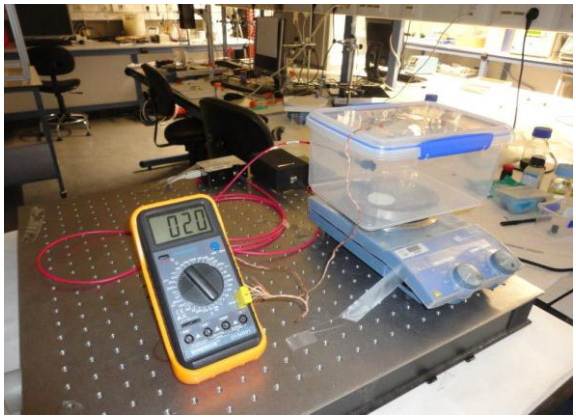

The ammonia gas sensor head was inserted in the chamber without any contact with the aqueous solution of ammonia (left); handout and computer equipment for the measurement reading (right).

Sensors laboratory facilities (UPNA) (left); the coated MMF sensor head was kept at room temperature during 20 min, and then placed into an oven for thermally curing at 85° C for 15 min (right).

ANNEX D. IMAGES TAKEN DURING LECTURES ABOUT OPTICAL FIBERS SENSORS IN INDUSTRY.

Lecture “Optical fiber sensors for the detection of toxic substances in the industry” in the *First Forum of Electronics, Computing and Job security* organized by the Universidad Autónoma de Tamaulipas-Unidad Académica Multidisciplinaria Reynosa Rodhe (UAT-UAMRR) (2014).


UNIVERSIDAD AUTÓNOMA DE TAMAULIPAS

LA GENERACIÓN del CONOCIMIENTO con VALORES

La Unidad Académica Multidisciplinaria Reynosa Rodhe otorga el presente reconocimiento al

M.C. Adolfo Josué Rodríguez Rodríguez

Por impartir la conferencia “Sensores en fibra óptica para la detección de sustancias tóxicas presentes en la Industria” en el Primer Foro de Electrónica, Computación, Informática y Seguridad Laboral celebrado en esta Unidad Académica.

Verdad Belleza Probidad

M.C. José Guadalupe Rivera Martínez
Director de la UAM Reynosa Rodhe

Ciudad Reynosa Tam. 29 de Abril de 2014